

Nonlinear Analysis of Chemical Processes with Material and Energy Recycles

Dissertation

zur Erlangung des akademischen Grades

**Doktoringenieur
(Dr.-Ing.)**

von Dipl.-Ing. Roland Waschler

geb. am 22. Mai 1971 in Stuttgart-Bad Cannstatt

genehmigt durch die Fakultät für Elektrotechnik und Informationstechnik
der Otto-von-Guericke-Universität Magdeburg

Gutachter: Prof. Dr.-Ing. Achim Kienle
Prof. Dr.-Ing. Subramaniam Pushpavanam

Promotionskolloquium am 09. Juni 2005

Forschungsberichte aus dem Max-Planck-Institut
für Dynamik komplexer technischer Systeme

Band 10

Roland Waschler

**Nonlinear Analysis of Chemical Processes
with Material and Energy Recycles**

Shaker Verlag
Aachen 2005

Bibliographic information published by Die Deutsche Bibliothek

Die Deutsche Bibliothek lists this publication in the Deutsche Nationalbibliografie; detailed bibliographic data is available in the internet at <http://dnb.ddb.de>.

Zugl.: Magdeburg, Univ., Diss., 2005

Copyright Shaker Verlag 2005

All rights reserved. No part of this publication may be reproduced, stored in a retrieval system, or transmitted, in any form or by any means, electronic, mechanical, photocopying, recording or otherwise, without the prior permission of the publishers.

Printed in Germany.

ISBN 3-8322-4273-2
ISSN 1439-4804

Shaker Verlag GmbH • P.O. BOX 101818 • D-52018 Aachen
Phone: 0049/2407/9596-0 • Telefax: 0049/2407/9596-9
Internet: www.shaker.de • eMail: info@shaker.de

Acknowledgements

A stimulating atmosphere both on a professional and a personal level significantly facilitates the work on a difficult research topic and generally makes life much easier – and I was lucky enough to find both while working on this thesis as research assistant at the Max-Planck-Institut für Dynamik komplexer technischer Systeme in Magdeburg.

This is why I want to thank the institute's founding director Prof. Dr.-Ing. Dr.h.c. mult. E.D. Gilles for the possibility to work at the Max-Planck-Institut and benefit from its marvellous working conditions.

Foremost, however, I wish to thank Prof. Dr.-Ing. Achim Kienle, not only for supervising my research but also for his continuous support and many helpful advices. Throughout, he has found a proper balance between setting the right direction and still allowing a great amount of 'scientific freedom'.

I am also indebted to Prof. Subramaniam Pushpavanam for acting as referee of this thesis and for many encouraging and fruitful discussions. It has always been great fun to work with him during his visits at the MPI.

All the colleagues at the MPI with their constant readiness to help contributed to creating the delightful atmosphere that made my time in Magdeburg so pleasant. In particular, I want to express my thanks to Martin Häfele and Martin Ginkel. Whenever I was close to desperation because of some apparently unsurmountable computer problem I could rely on their expertise and instantaneous help. They were also an integral part of innumerable inspiring scientific and non-scientific discussions in the institute's tea kitchen, along with Frank Klose, Malte Kaspereit, Michael Mangold, Henning Schramm, and Klaus-Peter Zeyer, to name just a few.

Without Prof. Dietrich Flockerzi, Martin Häfele and Klaus-Peter Zeyer, the countless hours on the road between Magdeburg and Stuttgart would have been pretty dull - thanks for having made these trips bearable owing to many interesting debates about everything and anything.

When I first came to Magdeburg I had a certain feeling that it might be difficult to find somebody with a similar mindset and enthusiasm for all kinds of sports, always ready for in-depth discussions of all the latest developments. At the end of my very first day at the

MPI, after having met my new colleague Steffen Klamt, these concerns had vanished into thin air. And needless to say, discussions soon went much further than 'only' sports.

A special thanks also goes out to Carsten Conradi, who shared my passion for philosophy and joined my escapes from the world of engineering problems by immersing in the fascinating realms of Aristotle, Kant and other great thinkers during many seminars at the Institut für Philosophie at the Otto-von-Guericke-Universität Magdeburg.

A big "Thank you" to all of you – it has truly been a most enjoyable and inspiring time!

Last, but by no means least, I want to thank my family, my girl-friend Anette, and all my friends at home for their patience, for sticking together and for being close during the six years, even when much too often I had made myself scarce. They always let me know where my heart belongs.

Sindelfingen, July 2005

Roland Waschler

Für meine Eltern,
in Liebe und Dankbarkeit.

Contents

1	Introduction	1
1.1	Process integration on the flowsheet level and the plantwide control problem	1
1.2	Acetic acid production: An industrial case study	4
1.3	Outline of the thesis	7
2	Mathematical model of the acetic acid production plant	9
2.1	Basic plantwide control structure	9
2.2	Models of the reaction system units	13
2.2.1	Hybrid reactor model	13
2.2.2	Condenser and flash models	17
2.3	Models of the separation system units	18
2.3.1	The distillation columns	19
2.3.2	The Decanter	20
2.4	Remarks on model implementation and simulation tools	23
2.5	Steady-state simulation results	23
2.6	Principle problems in simulating integrated processes	26
2.6.1	Sensitivity with respect to model inaccuracies	26
2.6.2	Effects of model inaccuracies on the existence of steady-state operating points in recycle systems	29

3	Nonlinear Analysis I: Isolated reactor	33
3.1	Classical results: Multiple steady states in isothermal and non-isothermal pure liquid-phase CSTRs	34
3.2	General evaporatively cooled reactor	37
3.3	Industrial case study of an evaporatively cooled reactor	47
3.4	Summary	52
4	Nonlinear Analysis II: Reactor-separator systems with one recycle	53
4.1	Isothermal, binary liquid-phase reactor with flash separator and liquid recycle	54
4.1.1	(p,T)-flash	58
4.1.2	Q_{fl} fixed	63
4.1.3	V_{fl} fixed	67
4.1.4	Summary and interpretation of the results for the ideal binary systems	69
4.2	Binary system with an evaporatively cooled reactor, flash separator and liquid recycle	72
4.2.1	Evaporatively cooled reactor and (p,T)-flash	72
4.2.2	Flash control strategies with Q_{fl} fixed and V_{fl} fixed	80
4.2.3	Summary for recycle systems involving a two-phase reactor	81
4.3	Industrial example	82
4.3.1	Control structure CS1	82
4.3.2	Control structure CS2	86
4.3.3	Control structure CS3	90
4.4	Summary: Nonlinear behavior of integrated systems with one recycle	97

5	Nonlinear Analysis III: Production plant with nested recycles	99
5.1	Steady-state characteristics	99
5.1.1	System with recycles from first column closed	99
5.1.2	Overall plant	100
5.1.3	Summary	101
5.2	Dynamic simulation studies	102
5.2.1	Feed disturbance	102
5.2.2	Load changes	105
5.3	Summary	108
6	Alternative plantwide control structures	109
6.1	Alternative control structure I	109
6.2	Alternative control structure II	112
6.2.1	Steady-state characteristics of the reaction system	113
6.2.2	Dynamics of the overall plant	115
6.3	Summary	117
7	Conclusions	119
A	Modeling details and parameter values	123
A.1	Kinetics of the methanol carbonylation reaction	123
A.2	Physical property correlations, parameter values, and operating data	126
A.2.1	Acetic acid system	126
A.2.2	Model Systems	131

B Mathematical supplements	133
B.1 Some facts on the stability of dynamical systems	133
B.1.1 First order systems and the concept of static stability	133
B.1.2 Static vs. dynamic stability and local bifurcations of second order systems	134
B.1.3 Stability of linear third order sytems	137
B.2 Uniqueness of the steady state for the system from Section 4.1.2	137
B.3 Stability of individual process units	138
 Bibliography	 141

Notation

A_W	heat transfer area	m^2
c	concentration	$kmol/m^3$
c_p	molar heat capacity	$kJ/kmol$
Da	Damkoehler number	
e	model error	
E	activation energy	$kJ/kmol$
F	feed flow rate	$kmol/s$
h	molar enthalpy	$kJ/kmol$
H	Henry coefficient	bar or Pa
Δh_R	molar enthalpy of reaction	$kJ/kmol$
Δh_V	molar enthalpy of vaporization	$kJ/kmol$
J	Jacobian matrix with elements J_{lm}	
k	reaction rate constant	
k_0	preexponential factor	
k_1	kinetic constant	
k_W	heat transfer coefficient	$kW/(m^2K)$
K	vapor-liquid equilibrium constant	
K^{eq}	equilibrium reaction constant	
K^*	shifting order reaction constant	
L	liquid flow rate	$kmol/s$
n	molar holdup	$kmol$
N	number of column stages	
NC	number of components	
p	pressure	bar or Pa
q	volumetric flow rate	m^3/s
Q	heating/cooling rate	kJ/s
Q_G	heat generation curve	
Q_R	heat removal line	
r_0	reaction rate	$kmol/(m^3s)$
R	recycle flow rate	$kmol/s$
R	ideal gas constant	$kJ/(kmol K)$

S	sidedraw flow rate, or sensitivity	kmol/s
t	time	s or h
T	temperature	K
v	molar volume	m ³ /kmol
V	vapor flow rate	kmol/s
\mathcal{V}	Volume	m ³
x	liquid mole fraction, or general state of a dynamic system	
y	vapor mole fraction	

Greek letters

α	ratio of activation energy to enthalpy of vaporization	
β	phase distribution in LLE, or function of boiling temperatures	
γ	activity coefficient	
δ	numerical factor	
η	separation factor	$\in [0, 1]$
ϑ	temperature	°C
κ	recycling factor	$\in [0, 1]$
λ	eigenvalue	
ν	stoichiometric coefficient	
ρ	density	kg/m ³
σ	general molar quantity	
$\bar{\sigma}$	general partial molar quantity	
φ	fugacity coefficient	
ψ	(real) vapor fraction	$\in [0, 1]$
ψ^*	(potentially fictitious) vapor fraction	$\in (-\infty, +\infty)$

Superscripts

'	related to liquid phase
"	related to vapor phase
(1)	liquid phase (1) in decanter
(2)	liquid phase (2) in decanter

Subscripts

0	pure component property, or reference state
<i>B</i>	bottoms (of a column)
<i>c</i>	coolant
<i>crit</i>	critical
<i>C</i>	condenser
<i>C1</i>	column 1
<i>C2</i>	column 2
<i>D</i>	decanter
<i>fl</i>	flash
<i>i</i>	component <i>i</i>
<i>j</i>	operating unit, $j \in \{\mathbf{R}, \text{fl}, \dots\}$
<i>k</i>	tray index
<i>r</i>	reduced quantity
<i>ref</i>	reference state
<i>R</i>	reactor
<i>S</i>	saturation conditions, or steady state
<i>SN</i>	standard (normal) saturation conditions
<i>V</i>	vaporization
<i>W</i>	wall

Abbreviations

CC	composition control
CO	carbon monoxide
CS	control structure
CSTR	continuous stirred tank reactor
DAE	differential algebraic equations
<i>det</i>	determinant (of a matrix)
FC	flow-control
<i>HAc</i>	acetic acid
<i>H₂O</i>	water
LC	level-control
LLE	liquid-liquid equilibrium
<i>MeI</i>	methyl iodide
<i>MeOH</i>	methanol
ProMoT	Process Modeling Tool
<i>Rh</i>	rhodium
<i>RC</i>	reaction (consumption) curve
SISO	single input, single output
SOC	standard operating conditions
<i>SL</i>	supply line
SP	controller setpoint
TC	Temperature control
<i>tr</i>	trace (of a matrix)
VLE	vapor-liquid equilibrium

Kurzfassung

Beim Betrieb und in der Entwicklung moderner chemischer Produktionsanlagen stehen heutzutage Fragen der Sicherheit, der Umweltverträglichkeit und der Wirtschaftlichkeit mehr denn je im Mittelpunkt. Vor allem in Anbetracht immer strengerer gesetzlicher Vorgaben zur Reduktion von Emissionen, sowie angesichts steigender Rohstoff- und Energiepreise und eines immens zunehmenden globalen Konkurrenzdrucks gewinnt der Ressourcen schonende Betrieb von Produktionsprozessen weiter an Bedeutung.

Um diesen stetig steigenden ökonomischen wie auch ökologischen Anforderungen gerecht zu werden, liegt das Hauptaugenmerk speziell bei der Entwicklung neuer Prozesse verstärkt auf der Rückgewinnung nicht umgesetzter Eingangsstoffe und der Wiederverwertung freiwerdender Energie. Dies erreicht man typischerweise mittels stofflicher und energetischer Rückführungen zwischen verschiedenen Anlagenteilen in Form von Recycle-Strömen.

Neben den erwähnten Vorteilen bringt eine solche Prozess-Integration auf der Fließbildebene jedoch auch eine ganze Reihe neuer Probleme mit sich. In erster Linie ist aufgrund der Recycle-Struktur die Komplexität im Verhalten eines integrierten Prozesses gegenüber einem konventionellen Prozess ohne Rückführungen um ein Vielfaches erhöht. Während das Verständnis für die verfahrenstechnischen Grundoperationen der Stoffumwandlung und Stofftrennung in den jeweiligen Grund-Apparaten wie beispielsweise chemischen Reaktoren oder Destillationskolonnen zum Standard-Repertoire eines jeden Verfahrenstechnikers gehört, so steckt doch andererseits die Erforschung potentiell auftretender Phänomene in Prozessen mit Rückführungen noch vergleichsweise in den Kinderschuhen.

Dies wiederum erschwert die Konzeption geeigneter anlagenweiter Regelungsstrategien für den optimalen Betrieb hoch integrierter Produktionsprozesse erheblich. Insbesondere ist die einfache Übertragung etablierter Regelungskonzepte für isolierte Grundoperationen auf gesamte Anlagen nicht ohne weiteres möglich.

Das Ziel der vorliegenden Arbeit besteht nun im wesentlichen darin, einen Beitrag zu einem besseren Verständnis des Verhaltens von chemischen Produktionsanlagen mit stofflichen und energetischen Rückführungen zu liefern und so auf lange Sicht zu einem effizienteren Entwurf anlagenweiter Regelungsstrukturen beizutragen. Besonderes Augenmerk liegt dabei auf der Untersuchung von Phänomenen, die speziell dem nichtlinearen Charakter integrierter chemischer Prozesse zuzuschreiben sind.

Dazu werden zum einen einfache, idealisierte Modellsysteme betrachtet. Diese lassen sich mit rein analytischen Methoden untersuchen und ermöglichen im Idealfall die Ableitung allgemeingültiger Ergebnisse unabhängig von einem konkreten Stoffsystem. Zum anderen steht als reales industrielles Anwendungsbeispiel der Monsanto-Prozess zur Herstellung von Essigsäure mittels Methanol-Carboxylierung im Mittelpunkt der Betrachtungen. Dieser eignet sich aufgrund der großen Zahl an internen Recycles besonders gut für Untersuchungen zur anlagenweiten Dynamik und erlaubt die Validierung analytischer Ergebnisse mittels numerischer Studien an einem realen Beispielprozess.

In einem ersten Schritt wird zunächst das nichtlineare Verhalten des Essigsäure-Synthese-Reaktors eingehend analysiert. Dabei wird erstmals ein physikalischer Mechanismus aufgedeckt, der die Möglichkeit des Auftretens mehrfacher stationärer Zustände in zweiphasigen und unter Siedebedingungen betriebenen Reaktionssystemen zeigt.

Die sich anschließende Untersuchung allgemeiner Reaktor-Separator-Systeme als den elementaren Bausteinen größerer integrierter Anlagen offenbart die Vielfalt an möglichen nichtlinearen Phänomenen, die auf die Auswirkungen der Recycle-Ströme auf das Verhalten des gekoppelten Gesamtsystems zurückzuführen sind. Diese reichen von der Existenz mehrfacher stationärer Zustände über das Auftreten von Grenzzyklen und Relaxationsoszillationen bis hin zu so komplexen Phänomenen wie deterministischem Chaos.

Im Hinblick auf Fragen der anlagenweiten Regelung steht bei allen Untersuchungen stets das Verhalten der Reaktor-Separator-Systeme für verschiedene unter praktischen Aspekten interessante Regelungsstrukturen besonders im Vordergrund. Unter der Beschränkung auf rein dezentrale Regelungsstrategien wird gezeigt, dass die Wahl einer geeigneten Regelungsstruktur, d.h. die Wahl geeigneter Stell- und Regelgrößen, das Systemverhalten maßgeblich beeinflusst.

Die Studien des nichtlinearen Verhaltens integrierter Systeme liefern damit auch Hinweise auf potentiell attraktive Regelungsstrukturen für das betrachtete Anwendungsbeispiel. So gelingt auf Basis der allgemeingültigen Untersuchungsergebnisse für die vereinfachten, idealisierten Reaktor-Separator-Systeme die Ableitung einer besonders geeigneten anlagenweiten Regelungsstruktur für den Monsanto-Prozess.

Obwohl dem Einsatz von Methoden der nichtlinearen Dynamik wie der Bifurkations- und der Singularitätstheorie durch die schiere Größe anlagenweiter Problemstellungen natürliche Grenzen gesetzt sind, zeigen die Untersuchungen im Rahmen dieser Arbeit somit, dass die Analyse des nichtlinearen Verhaltens auch einfacher und den erwähnten Methoden zugänglicher idealisierter Systeme wesentlich zu einem verbesserten Verständnis integrierter chemischer Produktionsprozesse beitragen können. In Kombination mit nichtlinearen dynamischen Simulationsstudien haben sie damit auch ein großes Potenzial, die anspruchsvolle Aufgabe der Wahl einer geeigneten anlagenweiten Regelungsstruktur erheblich zu erleichtern.

Chapter 1

Introduction

1.1 Process integration on the flowsheet level and the plantwide control problem

When, in 1993, Downs and Vogel from the Eastman Chemical Company confronted the process control community with what has become famous as the *Tennessee Eastman challenge process* [18], this breathed new life into academic research devoted to a topic that had been surprisingly subdued for several decades: The search for a suitable control structure for an entire chemical plant, better known as the **plantwide control problem**.

Probably the clearest formulation of this problem had been given by Foss as early as 1973, when he pointed out that the most important questions related to the structural nature of the plantwide control problem are: “*Which variables should be controlled, which variables should be measured, which inputs should be manipulated, and which links should be made between them?*” [19]. Clearly, these questions address the problem of finding a suitable decentralized control structure, corresponding to the search for suitable controlled and manipulated variables out of the huge set of process variables available in a large chemical plant, along with appropriate loop-pairings between them.

In spite of the obvious significance of the problem, since the early work of Buckley [11] back in 1964, and apart from some singular publications by Morari, Stephanopoulos and their respective coworkers in the early 1980s [4, 55], the topic has received little attention, such that in 2000 Stephanopoulos concluded that “*The synthesis of plant-wide control*

structures has **resurfaced** as the most important design problem in process control”[78].¹

The reasoning behind this statement emphasizing the importance of plantwide control problems is obvious: Given the ever-expanding competition between companies in a global market, and in order to comply with the constantly tightening legislative requirements in terms of environmental standards, more and more industrial production processes rely on **energy integration and material cycles** in order to reduce energy costs and loss of unconverted reactants, thus trying to meet the continuously increasing economical and ecological demands. Coming along with this tightening of process-integration via recycle structures on the flowsheet level is the requirement to design effective control structures for complete plants by explicitly taking into account the effects introduced by the higher degree of interconnection.²

Such key characteristics of coupled systems that are clearly attributable to the presence of recycles encompass e.g. the typical increase of an integrated system’s time constants when compared to the individual process units’ time constants. Another well-known and prominent feature of recycle systems is the so-called ‘snowball effect’. This notion was introduced by Luyben to denote the frequently encountered situation where a small change of an external stream results in large deviations of internal recycle streams within an integrated system, indicating a large steady-state sensitivity of recycle streams with respect to disturbances [45].

A more comprehensive treatment of recycle effects will be presented later on. Here the above examples do only illustrate the more general fact that recycles may completely change the characteristic behavior of a process unit when it is an integral part of a coupled system compared to the behavior of the individual unit in stand-alone operation. Vice versa, it is in general not possible to deduce the behavior of a system with recycles from knowledge about the individual units’ characteristics. Put in simple words: *‘The system is more than simply the sum of its parts’*.

A major consequence of this high complexity of an integrated system’s behavior is the fact that the presence of recycles also turns the control of highly interconnected systems into a formidable task. In particular, and in contrast to standard control problems for individual process units, answering the question for a suitable loop-pairing as raised by Foss is by no means trivial in the plantwide context.

¹Similarly, in 1996 Skogestad concludes that *“The issue of control structure design is very important in applications, but it has received relatively little attention in the control community during the last 40 years.”* [76]

²Adopting this view, the motivation behind the revived interest in plantwide control problems is clearly rather driven by a ‘market pull’ than a ‘technology push’.

Given this challenge, and additionally inspired by the afore-mentioned Tennessee Eastman problem, research in plantwide dynamics and control has recently resulted in a plethora of investigations related to the topic. They range from recommendations concerning the control of the Tennessee Eastman process [9, 52, 65, 66], to rather general investigations of recycle effects [13, 45, 56, 60, 95] and the development of complete plantwide control design procedures [48, 74, 86, 97].

A thorough classification and evaluation of all approaches is beyond the scope of this thesis, and the reader is referred to some of the outstanding reviews devoted to the topic [39, 41, 78]. Briefly summing up the main developments so far, the basic distinction between the two most important classes of approaches is probably best captured in the labels ‘process-oriented’ vs. ‘optimization based’. While process-oriented approaches boil down to the attempt of utilizing classical process engineering knowledge in order to develop heuristics for setting up a basic regulatory control structure for stable plant operation (see, e.g., [48]), the optimization-based approaches typically try to minimize some cost function and thus rather focus on optimizing the plant’s economics. Skogestad’s *self-optimizing control*, e.g., is based on a “*systematic procedure for finding suitable controlled variables based on only steady-state information*” [75].

At present, none of the approaches can be regarded as **the** most promising approach and there is no consensus as to which approach will eventually turn out as being most successful. A significant drawback of any optimization-based approach is its dependence on the existence of suitable mathematical models the optimization procedure is applied to and the availability of suitable optimization methods to solve the resulting complex optimization problems. In contrast, process-oriented approaches rely to a great extent on the experience and insight of the practitioner in charge of setting up a plantwide control strategy. Besides these problems, maybe the largest obstacle on the way to efficient control structure designs for complete plants is the fact that still the **understanding of fundamental characteristics of integrated processes** has not yet reached a stage that may be accepted as a solid basis for any control structure design method. In particular, it is widely accepted that still a more thorough comprehension of the basic, typically nonlinear effects introduced by recycles on the overall plant dynamics is required.

And this is where **this thesis** sets in. Its aim is to contribute to a better insight into the possible patterns of behavior that can be attributed to the effects recycles have on the overall dynamics of an integrated chemical plant. In particular, focus is on features of recycle systems that are beyond the basics that are already well established like the snowball effect mentioned above.

The aspired better understanding may on one hand be obtained by considering **simple model systems** lending themselves for an **analytical treatment**, in our case suitably simplified reactor-separator systems. On the other hand, insight into the characteristics of large integrated plants may as well be enhanced by considering appropriate **industrial case studies** requiring **numerical investigations**, thus adding to the merely handful of case studies like the Tennessee Eastman process, the HDA process, or the classical FCC unit presented in the literature, so far [18, 17, 2].

Both aspects will be addressed within this thesis, and the particular case study extensively studied in what follows is the industrial production of acetic acid, one of the most important intermediates in the organic industries with capacities of several million tons a year [91].

1.2 Acetic acid production: An industrial case study

Apart from the production of acetic acid via biological means, there are nowadays basically three main commercial methods for chemically producing synthetic acetic acid: Ethylene- and acetylene-based processes employing the acetaldehyde oxidation route, the manufacture via hydrocarbon oxidation, and acetic acid synthesis making use of methanol carbonylation [1, 91].

Although a first production plant based on the latter route was already built and operated by BASF in the mid 1960s, it was not until the late 1960s, when Monsanto discovered a particularly effective rhodium- and iodide-based catalyst, that methanol carbonylation was established as the method of choice for producing acetic acid on an industrial scale. In contrast to the BASF process that is based on CoI_2 as catalyst and requires severe operating conditions of about 250 °C and 680 bar, the rhodium-based Monsanto process can be operated under comparatively mild conditions of approximately 180 °C and 30 bar. This implies that the Monsanto process, nowadays owned by BP Chemicals, has the lowest overall production costs on a newly constructed plant basis, and thus all new acetic acid production plants rely on that technology. Recently, efforts have been directed towards replacing the extremely expensive rhodium catalyst by cheaper alternatives like iridium acetate, thus trying to render methanol carbonylation even more economical [26].

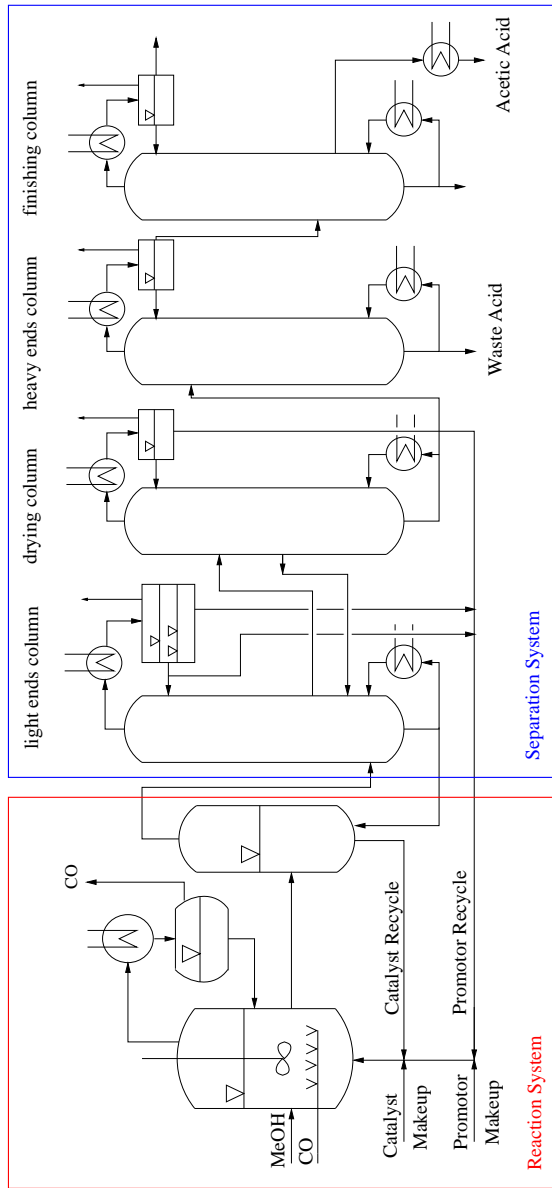


Figure 1.1: Simplified flowsheet of the acetic acid production plant relying on methanol carbonylation according to the Monsanto process.

Figure 1.1 shows a simplified flowsheet of the Monsanto process, consisting of the catalyst-containing *reaction system* and the *liquid separation system*. The exothermic, homogeneously catalysed, liquid-phase synthesis reaction



is carried out in a continuous stirred tank reactor at boiling point conditions. Thanks to the highly effective catalyst, a rhodium carbonyl complex (*Rh*) that is activated by means of the promotor methyl iodide (CH_3I , *MeI*), the selectivity of the reaction mechanism is about 99 % with respect to methanol (CH_3OH , *MeOH*), and 90 % with respect to carbon monoxide (*CO*). This has led leading experts to label the reaction mechanism “*one of the triumphs of modern organometallic chemistry*” [49]. Minor side reactions include the water gas shift reaction and the formation of methyl acetate. Details of the reaction mechanism and the reaction kinetics are given in Appendix A.1.

A special feature of the process is the subtraction of the heat of reaction by means of evaporative cooling. This means that parts of the reaction mixture are evaporated and subsequently recycled to the reactor after liquefaction in an overhead condenser. Under standard operating conditions, CO is supplied in slight excess, and the unconverted *CO* leaves the process through this partial condenser, along with traces of the other components.

In order to operate the process economically, it is crucial to avoid any loss of the expensive catalyst. To ensure the complete recovery of the catalyst, the liquid reaction mixture is fed to an adiabatically operated flash separator. The essentially nonvolatile catalyst is completely recycled to the reactor, along with large portions of the liquid mixture.

The catalyst-free vapor product stream leaving the reaction system enters the first distillation column of the liquid separation system. The main purpose of this column is the recovery of the light-boiling promotor *MeI* accomplished by means of a liquid-liquid phase split in a decanter atop the column. While *MeI* and a water-rich stream are recycled to the reactor, the main product stream is withdrawn from an intermediate tray and fed to a second column, where most of the remaining inert component water is separated and recycled to the reactor. Almost pure acetic acid is obtained as bottoms product of the second column, and the final two distillation columns merely help to separate the remaining traces of undesired by-products, in particular methyl acetate.

From the perspective of plantwide dynamics and control, the two final columns are of no interest, as there is no interaction with the upstream units via recycles. In contrast, owing to the wealth of nested recycles leading to a high degree of interconnection, the

reaction system together with the first two distillation columns is downright perfect for investigating problems of plantwide dynamics and eventually plantwide control. It will therefore serve as the basis of all forthcoming studies within this thesis.

1.3 Outline of the thesis

In order to achieve its purpose and contribute to a better understanding of the nonlinear phenomena that may be encountered in recycle systems, the thesis follows a clearly structured strategy:

In a type of **top-down dissection** process, the highly integrated production plant is first decomposed into smaller sub-units, i.e., a sort of **disintegration** is employed to break the recycle structure of the overall plant. The smallest subsystem resulting from this decomposition and to be considered within this thesis is the stand-alone synthesis reactor, which will be studied in detail in Chapter 3.

Once a sufficient understanding of the isolated reactor's behavior is attained, the process of **bottom-up reaggregation** of the overall plant is initiated by closing the recycle from the flash to the reactor to come up with the reaction system as depicted in Fig. 1.1. Already for this comparatively small reactor-separator system with just one recycle, a large number of control configurations are conceivable. The nonlinear phenomena exhibited by the reaction system when operated with the various different control structures are the topic of Chapter 4.

Again, once a sufficient understanding of the sub-unit's (here: the reaction system's) behavior is attained, the process of re-aggregation is continued to come up with the next higher level of system integration. Consequently, the behavior of the integrated system featuring a couple of nested recycles is studied in Chapter 5.

Throughout the thesis, special emphasis is on physical interpretations of the observed phenomena. In this regard, the main advantage of the described step-wise approach is that recycle effects on each level of system integration can clearly be distinguished from effects attributable to the respective sub-system. Moreover, insight into possible patterns of behavior is further enhanced by combining numerical investigations with purely analytical studies of suitably simplified model systems whenever possible. As already mentioned at the end of Section 1.1, this helps on one hand to derive results of greater generality than it would be the case if only the complex multi-component case study had been considered.

On the other hand, the improved process understanding based on the results obtained for the simplified model systems eventually leads to the derivation of a new plantwide control structure for the Monsanto process in Chapter 6.

To start with, however, and before turning to the step-wise analysis of the acetic acid production plant and its subsystems as just outlined, the mathematical model of the production process is presented in detail in the following Chapter 2.

In this context it may be worth noting that this model is not only the basis for all investigations within this thesis. It is also used by production engineers of the company AZOT in Sewerodonetsk (Eastern Ukraine), which runs a plant licensed by BP with a capacity of about 150000 tons/a according to the Monsanto process. They rely on the dynamic plant model as the basis of a training simulator that has been developed in cooperation with the Technical University of Donetsk and that is used to assist in teaching operating personnel [21].

Chapter 2

Mathematical model of the acetic acid production plant

In this chapter, the mathematical models of the various processing units are presented, which are used within this thesis to describe the behavior of the industrial case study introduced in the previous chapter.

To this end, first the basic control structure of the overall plant model is presented, before the focus is switched to the models of the individual units.

Subsequently, a comparison of steady-state simulation results of the basecase model with measurements from the industrial plant is presented. General considerations regarding principle problems that are typically encountered when simulating plants with recycles conclude the chapter.

2.1 Basic plantwide control structure

As mentioned in the introduction, the impact of plantwide control structure selection on the dynamics of integrated chemical production plants is the main focus of the investigations within this thesis. It is therefore important to be aware of the fact that, in terms of modeling, the choice of a particular control structure is reflected by certain physical assumptions employed when modeling the individual process units. E.g., a typical assumption widely used when modeling chemical processing units is that of a constant molar holdup. This assumption is a suitable approximation for a processing unit with

perfect level control, supposed changes in the density of the mixture are negligible. Similarly, assuming isothermal or isobaric operation of a specific unit corresponds in practice to perfect temperature and pressure control, respectively.

Obviously, assuming perfect control is a simplification that is not perfectly realistic, but nevertheless has two major advantages: On one hand, it significantly reduces the modeling effort, as models relying on some type of perfect control assumption are by far easier to develop than models with the respective quantities variable. On the other hand, it helps to clearly identify and analyze the behavior of the individual units by excluding effects that may be due to controller dynamics or controller tuning.

As a consequence of the above, investigating different control structures requires a variety of models reflecting exactly these choices of particular control configurations. This basically leads to the necessity of developing whole families of flexible process unit models. Section 2.4 will briefly present a very comfortable way of efficiently creating such model libraries.

Here, the presentation will be restricted to what will be called the *basecase model* of the overall acetic acid production process. Obviously, this basecase model reflects **exactly one basic plantwide control structure**. Different model formulations of certain process units required for the implementation of different control structures will not be presented in detail, but will only be commented on briefly wherever necessary.

Figure 2.1 illustrates the basic overall plant control structure. It is characterized by the following main SISO control loops:

- The reactor and flash levels are controlled by manipulating the respective liquid effluent streams.
- The small recycle stream from the bottoms of the first column to the flash is flow-controlled.
- The bottoms level of the first column is controlled by manipulating the heat input to the reboiler.
- The level of the sidedraw tray of the first column is set by manipulating the sidedraw flow rate.
- The composition of the vapor stream entering the overhead condenser of the first column is assumed to be controlled by means of a makeup stream. This makeup is necessary to avoid depletion of the inerts water and methyl iodide in the overall

plant, as both leave the system in traces through the partial condenser atop the reactor, but are not supplied by any other external feed.

- Both liquid levels of the decanter are controlled by manipulating the respective effluent stream (see also Section 2.3.2), and the recycle of the light aqueous phase to the reactor is flow-controlled.
- The bottoms level of the second column is controlled via the bottoms flow rate, and the reboiler duty is fixed.
- Both the minor internal recycle from the second to the first column and the aqueous distillate recycle from the second column to the reactor are flow-controlled.

Moreover, the following control loops are not indicated in Fig. 2.1 for reasons of better clarity, but are nevertheless part of the basic control structure and reflected in the physical assumptions underlying the models of the individual units:

- The two reactant feed streams are assumed to be flow-controlled into the reactor.
- The liquid level in the partial condenser is controlled by the liquid recycle stream to the reactor.
- Throughout this thesis, pressures within all the individual units are assumed constant by means of appropriate (perfect) pressure control loops.

It should be noted that the reactor temperature may be controlled to some extent by pre-heating of the methanol feed stream. However, this additional control loop (indicated by the dashed lines in Fig. 2.1) only serves for fine tuning of the reactor operation. As the interest within this thesis is on the whole range of potential reactor and plant dynamics that include operating regions corresponding to values of the pre-heating far beyond its operating limits, the temperature control loop will be assumed not be closed within the forthcoming investigations, i.e. a fixed temperature of the methanol feed stream will be assumed.

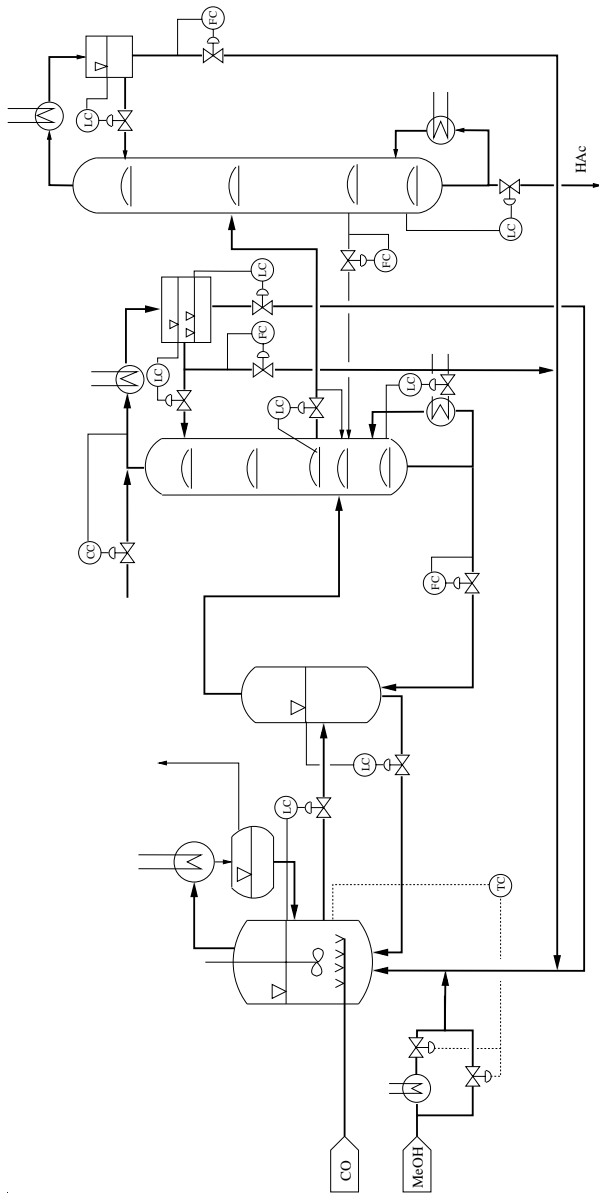


Figure 2.1: The basic plantwide control structure of the acetic acid production plant.

Based on these considerations concerning the plant's control structure, the models of the individual units will be presented in what follows. The main focus clearly will be on the reactor model as the core of any chemical production process and thus the most important unit of the overall system. The models of the various condensers, the flash, and the distillation columns will only briefly be commented on, as they are all basically standard models as described in any reasonable textbook on thermal separation operations (see, e.g., [72]). Only the less standard decanter model will be introduced in some more detail, while trivial models like mixers (simply described by algebraic, steady-state material balances and an energy balance) or perfect separators are completely omitted.

All the individual vapor-liquid two-phase systems are represented as equilibrium models in order to reduce computational loads for overall plant simulations that rule out the use of more detailed rate-based non-equilibrium models like the well-known two-film models. For the models employed to describe the required volumetric and calorimetric physical properties the reader is referred to Appendix A.2.

2.2 Models of the reaction system units

The reaction system consists of the reactor itself, an overhead partial condenser, and the flash separator. It is modeled as a five-component system ($NC = 5$) containing water, acetic acid, methyl iodide, and the two reactants methanol and carbon monoxide.

2.2.1 Hybrid reactor model

As mentioned in the introduction, the synthesis reactor under standard conditions is operated in the boiling two-phase regime. However, as this thesis aims at investigating the plant's dynamics over a wide range of operating conditions, a suitable reactor model should also account for the possibility of transitions to the purely liquid one-phase regime. Such transitions are triggered by discrete implicit events, in the given case the drop of the reactor temperature below the boiling point of the reaction mixture. Adopting a classification as introduced in [43], the reactor model therefore constitutes a *hybrid system* involving a coupling between continuous dynamics and state-dependent discrete events. More specifically, such systems are sometimes also denoted as *switched systems*.

Models for reactors subject to phase switches are hardly found in the literature. One example is presented in [96], where a simple switching model formulation for a CSTR

operated at the boiling point is proposed. In this model, the reactor temperature follows from a dynamic energy balance, and the pressure difference between vapor pressure and atmospheric pressure is the driving force for the evaporating stream as well as the indicator for switches between the two thermodynamic regimes. However, the model clearly is no classical equilibrium model as the temperature does not follow from the summation condition of the vapor phase mole fractions.

The hybrid reactor model employed within this thesis is based on an idea and uses similar assumptions as presented in [28] for a continuously operated, spatially distributed evaporator.

It is assumed that the dynamics of the vapor phase ($n''_R, y_{i,R}$) can be neglected, and that the liquid holdup is constant, such that

$$\frac{dn_R}{dt} = \frac{dn'_R}{dt} = 0 \quad . \quad (2.1)$$

Based on these assumptions, component material balances $\frac{dn_{i,R}}{dt} = n'_R \frac{dx_{i,R}}{dt}$ and the liquid phase summation condition,

$$n'_R \frac{dx_{i,R}}{dt} = Fx_{i,F} - L_R x_{i,R} - V_R y_{i,R} + \nu_i r_0 V'_R \quad , \quad i=1, \dots, NC-1 \quad , \quad (2.2)$$

$$0 = 1 - \left(\sum_{i=1}^{NC} x_{i,R} + x_{Rh} \right) \quad , \quad (2.3)$$

are used to compute the mole fractions of all components in the liquid mixture. Note that, for simplicity, all reactor feed streams in this formulation have been lumped to one stream F that comprises external reactant feeds as well as internal recycles from downstream units. Moreover, the amount of rhodium catalyst in the liquid phase x_{Rh} is regarded as a fixed parameter within this thesis.

The hybrid model formulation centers on the idea that the energetic state of the reaction mixture determines its aggregate state. On one hand, the molar enthalpy of the reactor h_R follows from the dynamic energy balance

$$n_R \frac{dh_R}{dt} = Fh_F - L_R h'_R(T_R) - V_R h''_R(T_R) \quad . \quad (2.4)$$

On the other hand, the enthalpy of a two-phase system is the sum of the enthalpies of the two phases, $n_R h_R = n'_R h'_R + n''_R h''_R$. Upon defining the vapor fraction ψ_R as the ratio of the vapor phase molar holdup to the overall molar holdup, $\psi_R := \frac{n''_R}{n'_R + n''_R}$, the overall molar enthalpy h_R is given by

$$h_R(T_R) = (1 - \psi_R) h'_R(T_R) + \psi_R h''_R(T_R) \quad . \quad (2.5)$$

Equation (2.5) therefore constitutes an implicit formulation for the computation of the vapor fraction ψ_R . To avoid negative values of ψ_R , a potentially fictitious vapor fraction ψ_R^* is additionally introduced, and equation (2.5) is modified to

$$h_R = (1 - \psi_R^*)h'_R(T_{R,S}) + \psi_R^*h''_R(T_{R,S}), \quad (2.6)$$

yielding $\psi_R^* \in (-\infty, +\infty)$. Obviously, negative values of ψ_R^* indicate that the reaction mixture is pure liquid, values of $\psi_R^* \in (0, 1)$ identify the reaction mixture as two-phase vapor-liquid, and values of $\psi_R^* > 1$ indicate that the reaction mixture is pure vapor. Fig. 2.2 illustrates the Petri net representation of this switching mechanism based on ψ_R^* .

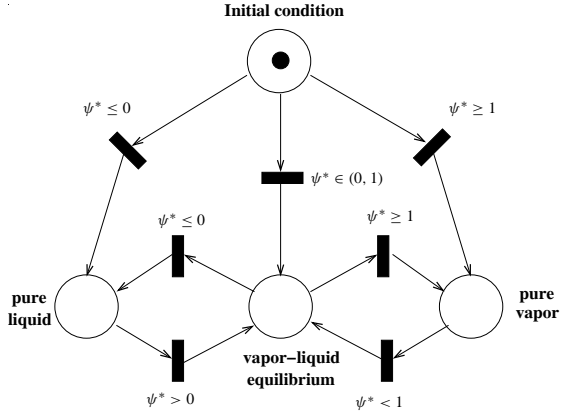


Figure 2.2: Petri net representation of possible phase transitions in the hybrid reactor model.

The *real, physically meaningful* vapor fraction $\psi_R \in [0, 1]$ is then given by

$$0 = \begin{cases} \psi_R & \text{if } \psi_R^* < 0 \\ \psi_R - \psi_R^* & \text{if } 0 \leq \psi_R^* \leq 1 \\ \psi_R - 1 & \text{if } \psi_R^* > 1 \end{cases} \quad (2.7)$$

It should be noted that the case of a purely gaseous, super-heated reaction mixture corresponding to $\psi_R^* > 1$ is merely included for the sake of completeness and is of no practical interest. Moreover, it is important to note that in Eq. (2.6) the enthalpies are evaluated at

the potentially fictitious boiling point temperature $T_{R,S}$.

The actual reactor temperature T_R corresponds to $T_{R,S}$ only in the two-phase regime,

$$0 = \begin{cases} h_R - h'_R(T_R) & \text{if } \psi_R^* < 0 \\ T_R - T_{R,S} & \text{if } 0 \leq \psi_R^* \leq 1 \\ h_R - h'_R(T_R) & \text{if } \psi_R^* > 1 \end{cases} . \quad (2.8)$$

In the one-phase regimes it follows implicitly from the respective enthalpy correlations.

The boiling point temperature $T_{R,S}$ itself is determined by means of the summation condition of the mole fractions in the vapor phase,

$$0 = 1 - \sum_{i=1}^{NC} y_{i,R} . \quad (2.9)$$

The vapor mole fractions in turn follow from vapor-liquid equilibrium calculations

$$0 = y_{i,R} p_R \varphi_i(T_{R,S}) - x_{i,R} \gamma_i(T_{R,S}) p_{i,S}(T_{R,S}) \varphi_{0,i,S}(T_{R,S}) \quad , \quad i=1,\dots,NC . \quad (2.10)$$

Note that these calculations are dispensable in the case of a purely liquid system where the $y_{i,R}$ are simply fictitious variables. For the calculation of saturation pressures $p_{i,S}$, activity coefficients γ_i , and fugacity coefficients $\varphi_i, \varphi_{0,i,S}$ see Appendix A.2.

For the calculation of the vapor and liquid streams leaving the reactor, V_R and L_R , respectively, it is additionally assumed that the ratio of the molar *flows* leaving the system is equal to the ratio of the corresponding molar *holdups*, i.e.,

$$\psi_R = \frac{V_R}{V_R + L_R} . \quad (2.11)$$

This assumption allows a numerically robust model formulation and is well-justified, as comparisons with an alternative, more standard model formulation have shown.

Then, the overall material balance, using (2.1), reads

$$\frac{dn_R}{dt} = 0 = F - L_R - V_R + \sum_{i=1}^{NC} \nu_i r_0 \mathcal{V}'_R , \quad (2.12)$$

or, using (2.11),

$$0 = L_R - (F + \sum_{i=1}^{NC} \nu_i r_0 \mathcal{V}'_R) (1 - \psi_R) \quad , \quad (2.13)$$

$$0 = V_R - (F + \sum_{i=1}^{NC} \nu_i r_0 \mathcal{V}'_R) \psi_R \quad . \quad (2.14)$$

Remarks:

- The model formulation as just outlined is used for modeling the plant's 'basecase control structure' with constant reactor level, i.e. $n'_R = \text{const.}$ Later on within this thesis, models with variable reactor level and the liquid reactor effluent stream being flow-controlled will be required. Without going into details here, in those cases the respective model modifications involve the substitution of the steady-state total material balance (2.13) by the dynamic total material balance

$$\frac{dn_R}{dt} = F - L_R - V_R + \sum_{i=1}^{NC} \nu_i r_0 \mathcal{V}'_R \quad , \quad (2.15)$$

in which the perfectly flow-controlled reactor effluent stream L_R is a parameter of the system. Moreover, the additional terms $x_{i,R} \frac{dn_R}{dt}$ and $h_R \frac{dn_R}{dt}$ have to be subtracted from the right hand sides of the component material balances (2.2) and the energy balance (2.4), respectively.

- At standard two-phase operating conditions, the steady-state simulation results obtained with this model excellently match measurements from the real production plant (see Section 2.5 for details).

However, it is implicitly assumed that CO is completely dissolved once the model is purely liquid phase, which is certainly not perfectly correct. Nevertheless, the error introduced by this assumption seems tolerable and not too severe, as the non-dissolved CO completely leaves the system in the overhead partial condenser and thus has no recycle effects on the plant dynamics. Moreover, if the given model is considered representative for a larger class of processes where one of the reactants is distinctly light-boiling, yet not supercritical, such that definitely no gaseous stream leaves the reactor in the one-phase regime, then the qualitative results obtained for the given system should be representative for this larger class of similar processes.

2.2.2 Condenser and flash models

The models of the partial condenser and the flash are basically identical vapor-liquid equilibrium models with the only difference being the thermodynamic state of the respective feed streams (saturated vapor in case of the condenser and liquid for the flash). Both models assume constant molar holdups and neglect vapor holdups, and both are governed by

a stationary total material balance (2.16), $NC - 1$ dynamic component material balances (2.17), and a quasi-steady-state energy balance (2.18),

$$0 = F_j - L_j - V_j \quad , \quad (2.16)$$

$$n_j \frac{dx_{i,j}}{dt} = F_j x_{F,j} - L_j x_{i,j} - V_j y_{i,j} \quad , \quad (2.17)$$

$$0 = F_j h_{F,j} - L_j h'_j - V_j h''_j + Q_j \quad , \quad (2.18)$$

with $j \in \{C, fl\}$ indicating the respective processing units. The liquid and vapor summation conditions along with NC vapor-liquid equilibrium relations as presented for the reactor complete the models.

Obviously, the external heat stream is negative for the condenser, $Q_C < 0$, and zero for the adiabatic flash, $Q_{fl} = 0$. The cooling of the partial condenser Q_C is achieved by means of a temperature-controller, such that the resulting condenser temperature matches plant measurements under standard operating conditions, $T_C = 322$ K. This helps to avoid large variations in the condenser temperature that would occur for a fixed cooling rate Q_C , as T_C is extremely sensitive with respect to the vapor flow rate entering the condenser.

An alternative, simplified condenser model employed in all continuation studies within this thesis assumes separation of a fixed percentage η of the CO before it enters the condenser ($\eta = 98,4\%$ under standard operating conditions), and total condensation of the remaining components. In that case, the energy balance (2.18) is unnecessary, and $V_C = 0$.

2.3 Models of the separation system units

In contrast to the reaction system, the separation system is modeled as a ternary system. Thanks to the high selectivity of the reaction mechanism, only traces of methanol enter the first distillation column, and the remaining CO is purged in the decanter. Thus, a restriction to the components water, acetic acid, and methyl iodide is justified.

The separation system basically consists of the two distillation columns and the decanter atop the first column. As fairly standard equilibrium stage models of the columns are employed within this thesis, the details of deriving the model equations are not given here. Instead, the equations are just summarized without too many further comments.

2.3.1 The distillation columns

Figure 2.3 shows the sketch of the most general internal tray of a staged distillation column, featuring both liquid and vapor feeds and sidraws. Based on the standard as-

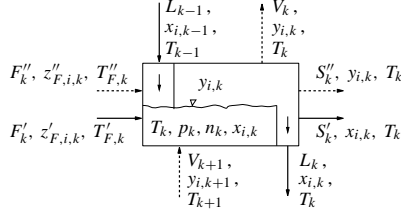


Figure 2.3: Internal tray k of a distillation column.

sumptions employed for equilibrium stage models of distillation columns like constant pressure, constant molar holdups with negligible vapor holdup, and applicability of the quasi-steady-state assumption for the energy balance (see, e.g. [72, 87]), the model describing one internal tray is given by a total material balance (2.19), $NC - 1$ component material balances (2.20), and an energy balance (2.21):

$$0 = L_{k-1} + V_{k+1} - L_k - V_k + F'_k + F''_k - S'_k - S''_k \quad , \quad (2.19)$$

$$\begin{aligned} n_k \frac{dx_{i,k}}{dt} &= L_{k-1}x_{i,k-1} + V_{k+1}y_{i,k+1} - L_kx_{i,k} - V_ky_{i,k} \\ &\quad + F'_kz'_{i,k} + F''_kz''_{i,k} - S'_kx_{i,k} - S''_ky_{i,k} \quad , \end{aligned} \quad (2.20)$$

$$\begin{aligned} 0 &= L_{k-1}h'_{k-1} + V_{k+1}h''_{k+1} - L_kh'_k - V_kh''_k \\ &\quad + F'_kh'_{F,k} + F''_kh''_{F,k} - S'_kh'_k - S''_kh''_k \quad . \end{aligned} \quad (2.21)$$

Additionally, as in any equilibrium model, the two summation conditions and the vapor-liquid equilibrium relations complete the tray model. Obviously, for a standard internal tray without feeds and sidraws, the streams connecting the tray to the column's environment are zero, $F'_k = F''_k = S'_k = S''_k = 0$. Moreover, the condenser represents stage 1, and the reboiler is stage N .

Usually, the sidraw streams are parameters that determine how much liquid and/or vapor is subtracted from the respective tray. One exception is the sidraw tray of column 1, where the sidraw stream $S'_{9,C1}$ is used to control the tray's holdup (see Fig. 2.1). In the model, this very specific situation is approximated by the assumption of constant molar

overflow from this tray, i.e., $L_{9,C1} = \text{const.}$, and the tray's total material balance yields the sidedraw stream required to keep the holdup constant.

2.3.2 The Decanter

The decanter of the given production process is operated continuously, the phase split itself is supposed to occur instantaneously, and it is assumed that the control structure depicted in Figure 2.4 is applied, i.e., the heavy organic phase is level-controlled and also the overall decanter level is fixed.

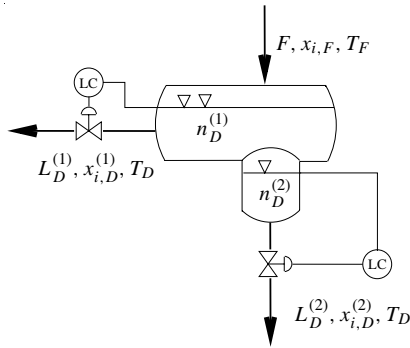


Figure 2.4: The decanter operated with a control structure fixing both liquid levels.

In a liquid three-component system with a miscibility gap, the liquid-liquid equilibrium between the two phases with compositions $x_{i,D}^{(1)}$ and $x_{i,D}^{(2)}$ is given by

$$0 = \gamma_i^{(1)} x_{i,D}^{(1)} - \gamma_i^{(2)} x_{i,D}^{(2)} \quad , \quad i = 1, \dots, 3 \quad . \quad (2.22)$$

Moreover, it holds that the overall holdup n_D as well as the overall individual component holdups $n_D x_{i,D}$ are the sum of the respective holdups of the two phases, i.e.,

$$n_D = n_D^{(1)} + n_D^{(2)} \quad , \quad (2.23)$$

$$n_D x_{i,D} = n_D^{(1)} x_{i,D}^{(1)} + n_D^{(2)} x_{i,D}^{(2)} \quad , \quad (2.24)$$

where $x_{i,D}$ is the overall mole fraction of component i in the decanter. This yields

$$\frac{n_D^{(1)}}{n_D^{(2)}} = \frac{x_{i,D}^{(2)} - x_{i,D}}{x_{i,D} - x_{i,D}^{(1)}} \quad , \quad (2.25)$$

commonly known as the lever rule in a system with liquid-liquid equilibrium. Upon defining

$$\beta := \frac{n_D^{(1)}}{n_D} \quad , \quad (2.26)$$

which implies

$$n_D^{(2)} = (1 - \beta)n_D \quad , \quad (2.27)$$

this yields

$$0 = x_{i,D} - \left(\beta x_{i,D}^{(1)} + (1 - \beta)x_{i,D}^{(2)} \right) \quad , \quad i = 1, \dots, 3 \quad . \quad (2.28)$$

Along with the summation condition

$$0 = \sum_{i=1}^{NC} \left(x_{i,D}^{(2)} - x_{i,D}^{(1)} \right) \quad , \quad (2.29)$$

Eqns. (2.22) and (2.28) completely determine the liquid-liquid equilibrium (i.e., $\beta, x_D^{(1)}, x_D^{(2)}$) for a given overall composition $x_D = (x_{1,D}, x_{2,D}, x_{3,D})$.

This overall composition is in general determined by the dynamic component material balances

$$n_D \frac{dx_{i,D}}{dt} = Fx_{i,F} - L_D^{(1)}x_{i,D}^{(1)} - L_D^{(2)}x_{i,D}^{(2)} \quad , \quad i = 1, 2 \quad , \quad (2.30)$$

and the overall summation condition

$$0 = 1 - \sum_{i=1}^{NC} x_{i,D} \quad . \quad (2.31)$$

In addition, the streams from the two phases ($L_D^{(1)}$ and $L_D^{(2)}$) follow from the specific control system used to operate the decanter. Assuming that the overall holdup is perfectly controlled ($n_D = \text{const.}$) as shown in Fig. 2.4, the algebraic total material balance

$$0 = F - L_D^{(1)} - L_D^{(2)} \quad (2.32)$$

determines one of the two effluent streams. Moreover, additionally controlling the holdup of the organic phase also fixes the holdup of the light phase (see Eq. (2.23)), and thus, the given control structure corresponds to fixing β . As a consequence, the system has only one dynamic variable (e.g. $x_{1,D}$, see Fig. 2.5). Thus, the other composition follows from the LLE (Eqns. (2.22), (2.28), and (2.29)), and one dynamic component material balance has to be replaced by its quasi-stationary version, e.g.

$$0 = Fx_{2,F} - L_D^{(1)}x_{2,D}^{(1)} - L_D^{(2)}x_{2,D}^{(2)} \quad , \quad (2.33)$$

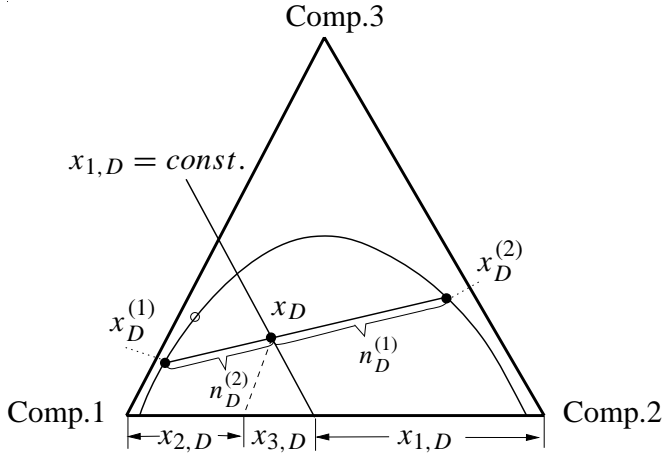


Figure 2.5: Graphical representation of the liquid-liquid equilibrium and the lever rule. For fixed holdups $n_D^{(1)}$ and $n_D^{(2)}$, corresponding to perfect level control as given in Fig. 2.4, the overall composition x_D is determined by the intersection of the straight line representing the dynamic variable $x_{1,D}$ with the one tie line which is compatible with β . For the decanter of the acetic acid production process, component 1 corresponds to water, component 2 to methyl iodide, and component 3 to acetic acid.

which determines the second effluent stream from the decanter.

Summarizing, the variables $x_D, x_D^{(1)}, x_D^{(2)}, L_D^{(1)}$ and $L_D^{(2)}$ describing the decanter from Fig. 2.4 with perfectly controlled $n_D^{(1)}$ and $n_D^{(2)}$ (and therefore fixed β) follow from Eqns. (2.22), (2.28), (2.29), one dynamic component material balance (2.30), one algebraic component material balance (2.33), and Eqns. (2.31) and (2.32). An energy balance is not required as it is assumed that the condensation of the distillate stream from the column is performed in the condenser and the subcooled liquid leaves the decanter at the same unaltered temperature $T_D = T_F$, i.e., the minor energy effects stemming from the demixing due to the liquid phase split are neglected.

2.4 Remarks on model implementation and simulation tools

All the mathematical models required for numerical simulations of the entire production plant have been implemented within the simulation environment DIVA [29, 40, 51, 54]. To this end, the sets of equations have been symbolically implemented in the declarative, Lisp-like Code-Generator language for DIVA. The Code-Generator subsequently generates the FORTRAN subroutines required by DIVA [38, 62].

Further studies have shown that an implementation of the models in the object-oriented process modeling tool **ProMoT** is particularly advantageous [50, 88, 89]. General features of object-oriented methods like data encapsulation or the concept of inheritance (see also [6]) are especially well-suited for modeling large-scale processes like the acetic acid production plant as they offer a great amount of flexibility for creating flowsheet alternatives – a prerequisite not only for efficient plant design, but also for the task of control structure selection. The main concepts in this respect are the bottom-up development of an object-oriented knowledge base for the simplified implementation of submodels on the level of process units, the efficient aggregation of process unit models on the flowsheet level, and the flexibility to effectively perform top-down refinements for problem-specific applications. The latter feature is particularly useful for modifying process unit models according to a modification of the plant’s control structure (see also [61] for the use of ProMoT to efficiently create a model family of reactor separator networks).

The numerical routines contained in the simulation environment DIVA are not restricted to a variety of efficient integration algorithms for large DAE systems, but do also include algorithms for optimization and parameter estimation, and, – most extensively employed within this thesis – for the continuation of steady state solutions [36, 51]. In addition, the continuation routines in DIVA also contain algorithms for stability analysis and for the detection of singularities, i.e., for the detection of both static and dynamic bifurcations.

2.5 Steady-state simulation results

Thanks to the cooperation with the company AZOT actually running a production plant based on the Monsanto process (cf. Section 1.2), measurements of various variables

under standard operating conditions are available and can be used for a comparison with steady-state simulation results obtained with the plant model described above. For the simulation results listed in Table 2.1, the reactor model has been completely isolated from its environment, i.e., in addition to the external feeds (the reactants), also the recycles from other plant units take on the role as ‘internal reactor feeds’, with their values fixed to the values under standard operating conditions.

Given the complexity of the multi-component, two-phase reacting system, the agreement of the simulation results with the plant measurements is excellent. Most notably, in spite of the huge influence the dissolved CO has on the reactor’s boiling point temperature, and in view of the difficulty to accurately predict gas solubilities (cf. Appendix A.2.1), the calculated reactor temperature is remarkably close to the actual one. Bearing in mind that side reactions and the components involved in them have been neglected, a better agreement seems hardly imaginable.

Table 2.2 summarizes the steady-state simulation results for the isolated reactor, the reaction system, and the entire plant, and compares them to actual plant measurements. In contrast to Table 2.1, the methanol feed temperature in all the simulations has been adjusted such that throughout the calculated reactor temperature matches the actual reactor temperature. The following observations stand out:

- Comparing the results from Tables 2.1 and 2.2, it is obvious that the influence of the feed temperature $T_{F,MeOH}$ on the reactor temperature ($\partial T_R / \partial T_{F,MeOH}$) is rather small, as a feed temperature increase of about 74 K is required to raise the reactor temperature by merely 6,6 K. This also rules out $T_{F,MeOH}$ as an efficient manipulated variable to control the reactor temperature over the wide range of operating conditions that will be investigated in the remainder of this thesis. It is also worth noting that the increase in T_R comes along with only a tiny decrease in $x_{CO,R}$,

variable	measurement	sim.
$T_R [K]$	458.0	451.4
$L_R [kmol/s]$	1.0534	1.066
$x_{H_2O,R}$	0.4224	0.4188
$x_{MeOH,R}$	$6.2 \cdot 10^{-4}$	$5.3 \cdot 10^{-6}$
$x_{HAc,R}$	0.543	0.537
$x_{MeI,R}$	0.0323	0.0322
$x_{CO,R}$	0.002	0.01
$V_R [kmol/s]$	0.0376	0.0082
$y_{HAc,R}$	0.129	0.117
$y_{CO,R}$	0.348	0.629

Table 2.1: Steady state simulation results of the isolated reactor with $T_{F,MeOH} = 346.15K$.

variable	measured data	reactor	reaction system	complete plant
$T_{F,MeOH} [K]$	346.15	420.18	444.46	413.50
Reactor:				
$L_R [kmol/s]$	1.0534	1.0645	1.114	1.0756
$x_{H_2O,R}$	0.4224	0.4193	0.364	0.298
$x_{MeOH,R}$	$6.2 \cdot 10^{-4}$	$3.5 \cdot 10^{-6}$	$3.6 \cdot 10^{-6}$	$4.0 \cdot 10^{-6}$
$x_{HAc,R}$	0.543	0.537	0.588	0.651
$x_{MeI,R}$	0.0323	0.0322	0.037	0.0391
$x_{CO,R}$	0.0017	0.0093	0.0094	0.0096
$T_R [K]$	458.0	458.0	458.0	458.0
$V_R [kmol/s]$	0.0376	0.0076	0.0068	0.0078
$y_{HAc,R}$	0.129	0.117	0.128	0.139
$y_{CO,R}$	0.348	0.629	0.635	0.648
Flash:				
$V_{Fl} [kmol/s]$	0.2932	-	0.306	0.3042
$y_{H_2O,Fl}$	0.447	-	0.434	0.367
$y_{HAc,Fl}$	0.4366	-	0.4176	0.479
$y_{MeI,Fl}$	0.1091	-	0.108	0.113
$T_{Fl} [K]$	389.0	-	391.2	392.7
Column 2:				
$L_{B,C2} [kmol/s]$	0.0926	-	-	0.0916
$x_{HAc,B,C2}$	0.9995	-	-	1.0
$T_{B,C2} [K]$	426.25	-	-	430.06

Table 2.2: Comparison of measured data from the real plant with simulation results for the isolated reactor, the reaction system, and the overall plant.

which in turn means that the influence of $x_{CO,R}$ on T_R under boiling conditions is tremendous.

- In spite of the fact that not only the reactor model but all the models of the plant's individual process units in stand-alone operation show excellent agreement with actual plant data (not presented here in detail), it holds as a general trend that the more recycles are closed, the worse the agreement between measured and calculated data.

The following section will address this remarkable feature of the overall plant model with its large number of recycle streams.

2.6 Principle problems in simulating integrated processes

Performing *plantwide simulations* is by no means trivial. This assessment is supported by the fact that one of the leading experts in the field of *plantwide control* has just recently seen the necessity to publish a book that is meant to serve as an introduction to plantwide simulations using commercial software packages [47]. However, two important aspects of plantwide simulation have not been covered by Luyben and are outlined in what follows.

Almost all studies dealing with integrated processes are devoted to investigations of plant behavior and its dependence on the operating parameters, or analyze a plant's response to external disturbances. This is most natural, as these are the problems a plant operator encounters in practice. However, simulation studies performing off-line investigations rely on mathematical models, and as no model will ever match reality to perfection, the potential effects of model inaccuracies – not to say model errors – on simulation is an important topic in its own right. Obviously, a simple rule of thumb would suggest that *'the larger the inaccuracy, the larger the simulation error compared to real data.'* This rather simplistic viewpoint seems to be justified when comparatively simple systems are to be considered. However, potential effects of model inaccuracies in more complicated systems, and in particular in recycle systems, are less evident and need further elucidation.

To this end, simple reactor-separator systems as depicted in Fig. 2.6 are considered in this section, with the first-order reaction $A \rightarrow B$ carried out in an isothermal CSTR with constant molar holdup. The reaction mixture is fed to a flash separator with constant heating and constant holdup. The underlying mathematical models are described in Section 4.1. However, no mathematical details are required for the purely illustrative studies presented here.

2.6.1 Sensitivity with respect to model inaccuracies

Focus is first on the effect of model inaccuracies in case of a standard series connection without recycle between reactor and downstream flash separator (System S1, Fig. 2.6(a)),

as compared to the case with liquid recycle from the flash to the reactor (System S2, Fig. 2.6(b)). To investigate the influence of model inaccuracies, it is assumed that the

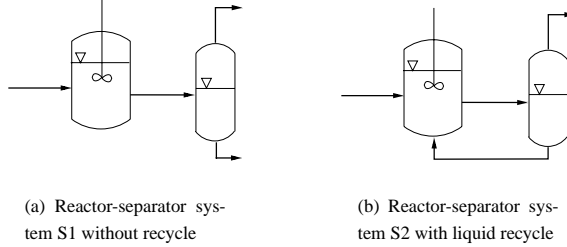


Figure 2.6: Model systems for studying sensitivities with respect to model inaccuracies.

description of the vapor-liquid equilibrium in the flash is subject to a multiplicative (i.e. purely quantitative) model error e_i , such that the VLE is given as

$$y_i = K_i e_i x_i \quad , \quad i \in \{A, B\} \quad . \quad (2.34)$$

Here it is assumed that the equilibrium constant K_i accurately describes the real system, and $e_i = 1$ indicates that the model perfectly matches reality, i.e. that there is no model inaccuracy. Note that the errors e_i may, e.g., be interpreted as errors in the calculation of the components' activity coefficients. In what follows, it is assumed that $e_A = 1$, and that the only model inaccuracy is $e_B = e$.

Figure 2.7 shows the steady-state values of the liquid mole fraction $x_{A,fl}$ of the light-boiling component A in the flash, depending on the value of the quantitative model error e . The parameters chosen for this example are given in Appendix A.2.2, and the reference state x_{ref} has been chosen such that $x_{A,fl} = 0, 1$ for $e = 1$ in both systems. Obviously, the effect of the model inaccuracy e on $x_{A,fl}$ is far more drastic for the system S2 with recycle (solid line in Fig. 2.7) as compared to the system S1 without recycle (dashed line in Fig. 2.7).

Using the general concept of parametric sensitivities as outlined e.g. in [85], and defining the normalized sensitivity of a state x with respect to the model error e as

$$S(x, e) := \frac{e}{x} \cdot \frac{\partial x}{\partial e} \quad , \quad (2.35)$$

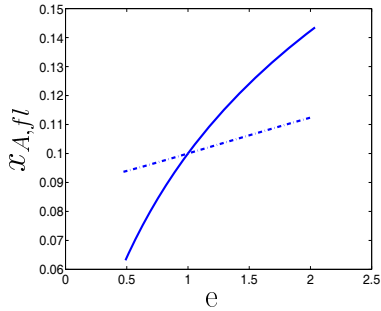


Figure 2.7: Influence of model inaccuracies.

it turns out that locally around the chosen reference state

$$S_{S1}(x_{A,fl}, e)|_{x_{ref}} = \frac{e}{x_{A,fl}} \cdot \frac{\partial x_{A,fl}}{\partial e}|_{x_{ref}} = 0.1 \quad \text{and} \quad S_{S2}(x_{A,fl}, e)|_{x_{ref}} = 0.6 \quad , \quad (2.36)$$

i.e., the mole fraction $x_{A,fl}$ in the system with recycle is six times as sensitive to variations in e as compared to the system without recycle.

Although it is clear that no general law can ever be deduced from an example (see, e.g., [71]), the presented simulation result nevertheless helps to induce the heuristic stating that *strong parametric sensitivity with respect to model inaccuracies* is a common feature in most recycle systems.

This characteristic is also supported by intuition: Obviously, the model inaccuracy in the flash leads – via the recycle – to a deviation in the feed conditions of the upstream reactor. Thus, there is not only a downstream propagation of simulation errors caused by model inaccuracies, but typically an amplification of errors within the recycle paths. Of course, there is in principle the possibility that model errors cancel out, but such a situation would have to be termed a ‘lucky coincidence’ and is rather an exception to the rule in recycle systems. Moreover, it has to be noted that with each additional inaccuracy and each additional recycle the overall error typically grows significantly. This is due to the fact that – in contrast to systems without recycles – one model error usually affects many internal streams, in particular if there are nested recycles.

This also helps to explain why in systems with many recycles a situation may occur, where for each individual stand-alone process unit a comparison of simulation results with plant data shows only small deviations, and yet the simulation results for the complete model with all recycles closed are hardly satisfying.

Besides this *integration of model errors in recycle systems*, that may result in unsatisfying simulation results, potential problems related to model inaccuracies in recycle systems that are even more drastic are exposed in the following section.

2.6.2 Effects of model inaccuracies on the existence of steady-state operating points in recycle systems

Consider again the simple recycle system depicted in Fig. 2.6(b), and assume again that the flash is constantly heated. Moreover, assume that the holdup in the reactor is constant, which may be achieved by either (i) manipulating the reactor effluent stream while keeping the feed stream fixed (to be denoted as control structure “CS1”), or by (ii) manipulating the feed stream while keeping the reactor effluent stream fixed (denoted as control structure “CS2”).

Now consider a plant with the flowsheet as presented in Fig. 2.6(b). The goal of modeling is to set up and implement a simulation model, that should subsequently be used for further investigations of the plant’s behavior. Obviously, the first goal in this respect is to correctly reproduce the plant’s actual operating steady state. Furthermore, it is assumed that besides the flowsheet, all operating parameters under which the plant is actually running are known. However, it is supposed that the description of the vapor-liquid equilibrium of component B in the flash according to

$$y_{B,fl} = K_B e_B x_{B,fl} \quad , \quad (2.37)$$

with $K_B = \frac{p_B^s}{p_{fl}} \gamma_B$ is potentially subject to a model error e_B . In what follows, it is assumed that this model error occurs in the calculation of the activity coefficient γ_B .

Figure 2.8 displays the dependence of the steady states of the two model systems on the model parameter γ_B . The parameters have again been chosen as given in Appendix A.2.2. Then, the following problems may be encountered when trying to simulate this system:

- (a) Suppose the actual (though unsuitable) plant control structure is CS2 and this control structure is also implemented in the model. Moreover, assume the correct value of γ_B is $\gamma_B = \gamma_B^{(2)}$ (see point A in Fig. 2.8 (a)), but the model calculates $\gamma_B = \gamma_B^{(1)}$. In this case, the model has no steady-state solution, i.e., *although the correct control structure has been selected, the quantitative model inaccuracy renders the model system ‘unsolvable’*.

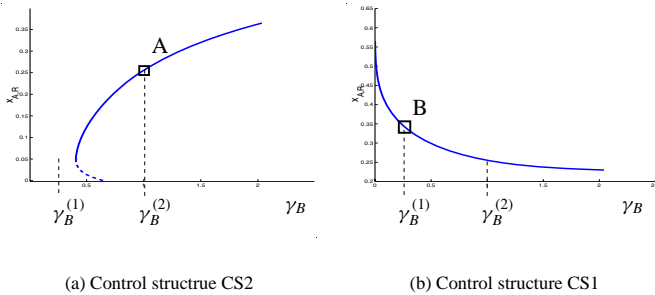


Figure 2.8: Steady-state values of $x_{A,R}$ depending on γ_B , for the two different control structures CS1 and CS2.

- (b) Suppose at the real plant the (suitable) control structure CS1 is implemented and works properly. Moreover, suppose the correct value of the activity coefficient is $\gamma_B = \gamma_B^{(1)}$, such that point B in Fig. 2.8 (b) represents the system's actual operating point. Assume that the model even correctly calculates this value of $\gamma_B = \gamma_B^{(1)}$. In this case, one will not be able to even calculate a steady-state solution for a model employing the wrong control structure CS2, as for the given operating conditions, CS2 does not exhibit a steady state. In other words, a model with a structural model error *may not even yield any solution and may thus be 'unsolvable' in spite of correct physical property calculations, simply because a wrong control structure selection is taken as a basis of the model.*

Note that this example also shows that an unsuitable control structure might even erroneously be deemed acceptable due to an error in the calculation of the physical properties. Assume again that the unsuitable control structure CS2 is implemented, and a correct calculation of the activity coefficient $\gamma_B = \gamma_B^{(1)}$ would actually reveal the control structure's inaptness for plant operation. However, a model employing control structure CS2 and subject to a wrong calculation of γ , yielding $\gamma_B = \gamma_B^{(2)}$, would come up with the acceptable, yet wrong steady state A (see Fig. 2.8 (a)), and this could lead to the rushed conclusion that the model along with the control structure it employs is acceptable.

These considerations reveal a fundamental problem in discerning the cause for a potential 'unsolvability' of the model of an integrated process, as it may be due to either model inaccuracies or a bad choice of the system's control structure. In particular for large sys-

tems, with a large number of possible control configurations and many physical property calculations, it may be very hard to figure out the actual cause in case one is unable to find a steady-state solution. In fact, one may spend a large amount of time trying to improve the model accuracy in terms of physical property calculations, while a change of control structure would have been sufficient.

Note that similar problems may also occur in the design stage for a new process, where a particular flowsheet might be ruled out simply because a bad control structure has been chosen.

It is important to keep in mind that the problems presented in this section are related to *modeling inaccuracies and offline simulations* only, and are not encountered when operating a real plant. Nevertheless it is important to be aware of them whenever one faces the task of *simulating* large integrated systems.

In the remainder of this thesis it will always be presumed that physical property calculations are sufficiently accurate to rule out problems as described above, in particular the one related to model inaccuracies as described under item (a). Instead, focus will be on the behavior of recycle systems for different control configurations, and the influence of *operating parameters* will be in the centre of interest, rather than the influence of *physical property parameters* and inaccuracies in describing them.

Chapter 3

Nonlinear Analysis I: Isolated reactor

The nonlinear behavior of chemical reactors has been in the centre of interest for a long time. Particularly the steady-state multiplicity features of both isothermal and non-isothermal *pure liquid phase CSTRs* have been thoroughly studied (see, e.g., [63] for a detailed overview). In contrast, relatively little attention has been paid to the characteristics of autorefrigerated or evaporatively cooled *two-phase reactors* [46].

As the industrial case study considered throughout this thesis employs a reactor operated at the boiling point, the focus of the forthcoming investigations will concentrate on the behavior of such two-phase reactors that are cooled by subtracting latent heat via evaporation of parts of the liquid reaction mixture. In particular, by considering a suitably simple binary model system, the *physical mechanism leading to steady-state multiplicities in two-phase reactors operated at the boiling point* will be identified. This new explanation relates the occurrence of multiple steady states to an interplay between reaction kinetics and the vapor-liquid equilibrium, and helps to explain the numerical simulation results obtained for the more complex multi-component industrial reactor, as presented in the last part of this chapter.

To start with, however, and in order to enable a better classification and an easier assessment of this recently revealed mechanism [90], the next section will briefly recall some of the classical results on multiple steady states in isothermal and non-isothermal CSTRs.

3.1 Classical results: Multiple steady states in isothermal and non-isothermal pure liquid-phase CSTRs

Arguably the best known and most intensely studied mechanism that may lead to the existence of multiple steady states in continuous stirred tank reactors is due to thermokinetic effects in a CSTR sustaining an irreversible first order exothermic reaction $A \rightarrow P$. To understand the origin of multiplicities in such a system, consider the setup depicted in Fig. 3.1 (a). The most important assumptions in the derivation of the classical results include a constant reaction volume \mathcal{V} , perfect mixing of the reaction mixture and thermodynamically ideal behavior of the mixture. This system can be described by the component material balance for reactant A ,

$$\frac{dc}{dt} = \frac{q}{\mathcal{V}}(c_F - c) - k_0 e^{-\frac{E}{RT_R}} c \quad , \quad (3.1)$$

where c denotes the concentration of A , and the energy balance

$$\frac{dT_R}{dt} = \frac{q}{\mathcal{V}}(T_F - T_R) + \frac{k_w A_W}{\rho c_p \mathcal{V}}(T_c - T_R) + \frac{(-\Delta h_R^*)}{\rho c_p} k_0 e^{-\frac{E}{RT_R}} c \quad . \quad (3.2)$$

Extensive parametric studies of the steady-state and dynamic behavior of this system have been conducted, see e.g. [3, 82, 83], to name a few. In particular the application of catastrophe and singularity theory has turned out to be an invaluable tool both for predicting the maximal number of steady-state solutions, as well as for a complete classification of parameter regions with qualitatively different behavior for this and various other reacting systems (see, e.g., [7, 44]).

However, the most intuitive explanation of multiplicity can be attributed to the early work of van Heerden [84], and allows a graphical interpretation of the underlying mechanism. Solving the steady-state version of Eq. (3.1) for the concentration c_S , and inserting this into the steady-state version of Eq. (3.2), one obtains

$$\underbrace{\left(\frac{q}{\mathcal{V}} + \frac{k_w A_W}{\rho c_p \mathcal{V}} \right) T_{R,S} - \frac{q}{\mathcal{V}} T_F - \frac{k_w A_W}{\rho c_p \mathcal{V}} T_c}_{Q_R} = \underbrace{\frac{(-\Delta h_R^*)}{\rho c_p} \frac{k_0 e^{-\frac{E}{RT_{R,S}}} c_F}{1 + k_0 \frac{q}{\mathcal{V}} e^{-\frac{E}{RT_{R,S}}}}}_{Q_G} \quad .$$

Clearly, the steady-state temperatures $T_{R,S}$ of the given system follow from the intersections of the linear heat removal line Q_R and the nonlinear heat generation curve Q_G , see Fig. 3.1 (b). Depending on the various parameter values, up to three steady states are possible, one at low conversion and low temperature, one at intermediate conversion

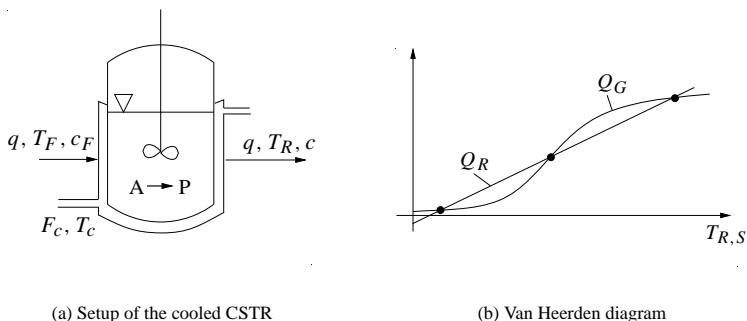


Figure 3.1: Setup of the cooled CSTR sustaining an exothermic first order reaction (a), and Van Heerden diagram offering an interpretation of the steady states of the non-isothermal reactor as the intersections of the heat removal line Q_R and the heat generation curve Q_G (b).

and intermediate temperature, and one at high conversion and high reactor temperature. A straightforward stability analysis reveals that the intermediate steady state is a saddle point, whereas the other two steady states are statically stable equilibria ([53], see also Appendix B.1 for a definition of the notion of *static stability*). The instability of the intermediate steady state is due to the fact that here the slope of the heat removal curve is smaller than the slope of the heat generation curve,

$$\frac{dQ_R}{dT_{R,S}} < \frac{dQ_G}{dT_{R,S}} \quad (3.3)$$

Therefore, any increase in reactor temperature will be further amplified, as the accompanying increase in heat released by the exothermic reaction is larger than the increase in heat removed by both cooling and heat subtraction with the effluent stream. In other words, there is a *positive feedback mechanism* which destabilizes the steady state at intermediate conversion, i.e., the **thermokinetic effects** induced by the nonlinearity of the reaction kinetics may lead to an exothermic self-acceleration of the reaction.

Note that this result can be generalized insofar as typically the combination of some type of nonlinearity *and* some positive feedback mechanism is required for steady-state multiplicity and the associated instability of one of the steady states. It should also be noted that the mere existence of a nonlinearity without positive feedback is usually not sufficient for instability. This becomes clear when considering an endothermic irreversible

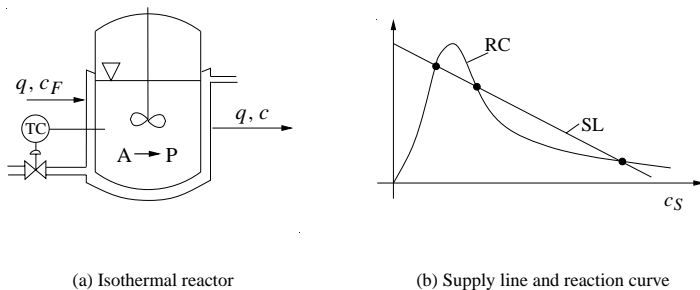


Figure 3.2: (a) Setup of the isothermal (e.g. temperature-controlled) CSTR sustaining a reaction with self-inhibition, and (b) a diagram offering an interpretation of the steady states of the reactor as the intersections of a material supply line SL and a consumption curve due to reaction RC .

reaction, where in spite of the nonlinear temperature dependence of the reaction rate no multiplicity can occur due to the lack of positive feedback.

Multiple steady states are also encountered in isothermal reaction systems as the one depicted in Fig. 3.2(a). Again, a nonlinearity is required for multiplicity. As an example, consider a reaction mechanism with self-inhibition as found for instance in enzyme catalyzed reactions in biochemical systems with substrate inhibition [57], where the reaction rate is a rational fraction in the reactant concentration c ,

$$r_0 = k_0 \frac{c^m}{1 + k_1 c^n}, \quad n > m. \quad (3.4)$$

If the order of the denominator n exceeds the order of the numerator m , then the reaction rate increases with the amount of reactants at low reactant concentrations, but decreases beyond a certain amount of reactants in the system. At steady state, the component material balance for reactant A that governs the system behavior in such an isothermal reactor may be rearranged to give

$$\underbrace{\frac{q}{V}(c_F - c_S)}_{SL} = \underbrace{k_0 \frac{c_S^m}{1 + c_S^n}}_{RC}. \quad (3.5)$$

Here, the steady states are the intersections of the linear material supply line SL and the nonlinear reaction curve RC representing the consumption of reactant A . Again, the

positive feedback mechanism leading to the destabilization of the steady state at intermediate conversion is evident: Any increase of reactant concentration c_S will be further amplified, as due to the comparatively small reaction rate less reactant is consumed and removed with the effluent than supplied with the feed. The corresponding slope condition indicating static instability in this case reads

$$\frac{dRC}{dc_S} < \frac{dSL}{dc_S} \quad (3.6)$$

Note that besides this **self-inhibition**, also nonlinearities in the reaction rate introduced by **autocatalysis** may cause the occurrence of multiple steady states in isothermal CSTRs, as described in detail in [23, 24].

Equipped with these fundamental insights into potential sources of multiplicity in simple reacting systems, focus is now directed towards the nonlinear behavior of an evaporatively cooled reactor as employed in the industrial case study.

3.2 General evaporatively cooled reactor

Insight into the potential sources of multiplicity in one-phase reacting systems as presented in the previous section was facilitated to a great extent by considering a suitably simple model that nevertheless still captures the main features of many real system. Indeed, it is always most instructive to illustrate a physical phenomenon by means of the simplest model featuring the key characteristics that put forth the mechanism that is to be illustrated¹.

Turning to the case of an evaporatively cooled reactor, such a simple, yet suitable model involves a binary mixture in a CSTR that is operated at the boiling point. Fig. 3.3 illustrates this principle setup. It is assumed that the irreversible equimolar first order reaction $A \rightarrow B$ is carried out in a perfectly mixed liquid phase. The liquid phase is supposed to be in thermodynamic equilibrium with the vapor phase and the vapor stream leaving the reactor. This vapor phase is assumed to be instantaneously and

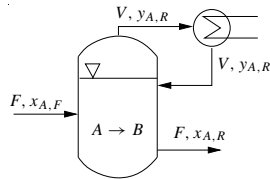


Figure 3.3: Setup of the evaporatively cooled reactor with condenser.

¹In the words of Albert Einstein: “Everything should be made as simple as possible, but not simpler.”

totally condensed and recycled to the reactor.

This implies that the dynamics of the overhead condenser are neglected, which seems reasonable as long as the condenser holdup is small compared to the reactor holdup. Based on these assumptions, the vapor flow rate V through the condenser does not affect the component material balance of the reactor, and thus there is no need to consider an energy balance in order to determine V . Assuming a constant molar holdup n_R in the reactor, the given system is governed by the dynamic material balance for component A ,

$$n_R \frac{dx_{A,R}}{dt} = F(x_{A,F} - x_{A,R}) - n_R k_0 e^{-\frac{E}{RT_R}} x_{A,R} \quad , \quad (3.7)$$

where $x_{A,F}$ is the feed concentration of reactant A . The temperature dependence of the reaction rate is modeled with an Arrhenius type of expression.

Furthermore, it is assumed that the vapor pressures can be described by the Clausius-Clapeyron equation. This implies that the molar volume of the liquid phase is neglected in comparison with the molar volume of the vapor phase, and that the vapor phase is regarded as an ideal gas, corresponding to the assumption of moderate pressure in the reactor (see, e.g., [12]). Then, the vapor pressure $p_{i,S}$ of component i in the reactor is given as

$$p_{i,S} = p_0 e^{\frac{\Delta h_{V,i}}{R} \left(\frac{1}{T_{SN,i}} - \frac{1}{T_R} \right)} \quad , \quad (3.8)$$

where $\Delta h_{V,i}$ is the enthalpy of vaporization of component i and $T_{SN,i}$ is the component's normal boiling point temperature at standard pressure p_0 . Moreover, supposing that the mass transfer rate between the liquid and the vapor is fast compared to all other dynamics in the system, and neglecting non-idealities in the behavior of the two phases, thermodynamic equilibrium between an ideal vapor and an ideal liquid phase can be assumed. This vapor-liquid equilibrium is given by

$$y_{i,R} = \frac{p_{i,S}(T_R)}{p} x_{i,R} \quad , \quad (3.9)$$

with the vapor pressure $p_{i,S}$ following from the Clausius-Clapeyron equation as shown above. The boiling point condition

$$0 = 1 - \sum_{i=1}^2 y_{i,R} \quad (3.10)$$

determines the bubble point of the mixture. Note that by assuming thermal equilibrium, the boiling point temperature is an algebraic variable in this system, i.e., it is algebraically

coupled to the composition of the system by the boiling point condition (3.10), and hence follows dynamic changes in the mole fractions without delay. From (3.8), (3.9), and (3.10), it follows that

$$1 = x_{A,R} \frac{p_0}{p} e^{\frac{\Delta h_{V,A}}{R} \left(\frac{1}{T_{SN,A}} - \frac{1}{T_R} \right)} + (1 - x_{A,R}) \frac{p_0}{p} e^{\frac{\Delta h_{V,B}}{R} \left(\frac{1}{T_{SN,B}} - \frac{1}{T_R} \right)}. \quad (3.11)$$

For simplicity of the forthcoming investigations, it may be assumed that

$$\Delta h_{V,A} = \Delta h_{V,B} = \Delta h_V, \quad (3.12)$$

which is a reasonable assumption in many cases. In the given context, it helps to eliminate the explicit dependence of the material balance (3.7) on the reactor temperature. To this end, using (3.12), Eq. (3.11) can be solved for

$$e^{-\frac{\Delta h_V}{RT_R}} = \frac{p}{p_0 \left(x_{A,R} e^{\frac{\Delta h_V}{RT_{SN,A}}} + (1 - x_{A,R}) e^{\frac{\Delta h_V}{RT_{SN,B}}} \right)}. \quad (3.13)$$

Then, with $e^{-\frac{E}{RT_R}} = \left(e^{-\frac{\Delta h_V}{RT_R}} \right)^{\frac{E}{\Delta h_V}}$, one obtains

$$e^{-\frac{E}{RT_R}} = \left(\frac{p}{p_0} \right)^{\frac{E}{\Delta h_V}} \cdot \frac{1}{\left(x_{A,R} e^{\frac{\Delta h_V}{RT_{SN,A}}} + (1 - x_{A,R}) e^{\frac{\Delta h_V}{RT_{SN,B}}} \right)^{\frac{E}{\Delta h_V}}}. \quad (3.14)$$

Upon defining

$$\alpha := \frac{E}{\Delta h_V}, \quad (3.15)$$

$$\beta := -1 + e^{\frac{\Delta h_V}{R} \left(\frac{1}{T_{SN,A}} - \frac{1}{T_{SN,B}} \right)}, \quad (3.16)$$

$$Da := \frac{n_R k_0}{F} \left(\frac{p}{p_0} \right)^\alpha e^{-\frac{E}{RT_{SN,B}}}, \quad (3.17)$$

and with

$$\left(x_{A,R} e^{\frac{\Delta h_V}{RT_{SN,A}}} + (1 - x_{A,R}) e^{\frac{\Delta h_V}{RT_{SN,B}}} \right) = e^{\frac{\Delta h_V}{RT_{SN,B}}} \left(1 + x_{A,R} e^{\frac{\Delta h_V}{R} \left(\frac{1}{T_{SN,A}} - \frac{1}{T_{SN,B}} \right)} - x_{A,R} \right),$$

Eq. (3.14) can be further condensed to

$$e^{-\frac{E}{RT_R}} = \frac{Da F}{n_R k_0} \cdot \frac{1}{(1 + \beta x_{A,R})^\alpha}. \quad (3.18)$$

Based on these derivations, the material balance eq. (3.7) boils down to

$$\frac{n_R}{F} \frac{dx_{A,R}}{dt} = (x_{A,F} - x_{A,R}) - Da \frac{x_{A,R}}{(1 + \beta x_{A,R})^\alpha} \quad (3.19)$$

Note that in this equation, by definitions (3.15) and (3.16), it holds that $\alpha > 0$, whereas $\beta > -1$. Moreover, it follows from the definition of β that positive values of β correspond to component A being more volatile, while negative values of β correspond to A being the heavy-boiling component.

From here on, the steady-state material balance

$$0 = (x_{A,F} - x_{A,R}) - Da \frac{x_{A,R}}{(1 + \beta x_{A,R})^\alpha} = f(x_{A,R}; Da, \alpha, \beta, x_{A,F}) \quad (3.20)$$

serves as the basis for all further investigations. Owing to the successful elimination of the reactor temperature, Eq. (3.20) is a scalar nonlinear algebraic equation in the variable $x_{A,R}$, depending on the four distinguished parameters $Da, \alpha, \beta, x_{A,F}$. It therefore naturally lends itself to an in-depth analysis based on singularity theory. However, the analysis presented in what follows is rather based on the application of graphical methods as introduced in the previous section. As already mentioned, such graphical illustrations help to considerably facilitate the interpretation of physical phenomena.

It should be noted that throughout, interest is confined to the physically meaningful region $0 \leq x_{A,R} \leq x_{A,F}$, with $x_{A,F} \in [0, 1]$. This is due to the fact that for the system considered, it holds that at steady state the mole fraction of reactant A can never exceed its feed condition, as A is merely consumed in the irreversible reaction.

The steady states of system (3.19), i.e. the solutions of eq. (3.20), are the intersections of the reaction curve

$$RC := \frac{Da x_{A,R}}{(1 + \beta x_{A,R})^\alpha} \quad (3.21)$$

and the supply line

$$SL := x_{A,F} - x_{A,R} \quad (3.22)$$

A *necessary* condition for the existence of more than one intersection is a change in sign of the first derivative of RC , corresponding to the existence of an extremum in RC , see Fig. 3.4. This condition is fulfilled for

$$\alpha > 1 \quad (3.23)$$

Note that this implies

$$\lim_{x_{A,R} \rightarrow \infty} RC = 0 \quad (3.24)$$

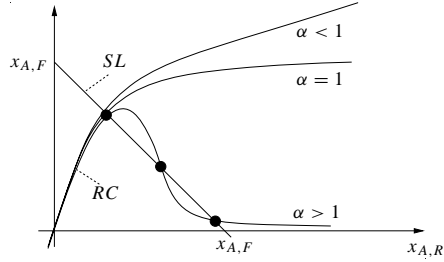


Figure 3.4: Supply line SL and reaction curve RC for an evaporatively cooled reactor. For $\alpha > 1$, up to three steady states are feasible.

However, this condition is not yet *sufficient* for the existence of multiple steady states. In order to guarantee the occurrence of multiple intersections, there must in addition exist parameter combinations for which RC is tangent to SL , i.e., the reaction curve RC must have a slope of -1,

$$\frac{dRC}{dx_{A,R}} = \frac{Da[\beta x_{A,R}(1-\alpha) + 1]}{(1 + \beta x_{A,R})^{\alpha+1}} \stackrel{!}{=} -1 \quad , \quad (3.25)$$

and simultaneously fulfill the steady-state material balance (3.20). If these conditions are complied with, then there exist arbitrarily small perturbations of the parameters that yield three intersections and hence three steady-state solutions. For fixed $x_{A,F}$, the set of values $\beta(\alpha)$, i.e., the curve in the $(\alpha-\beta)$ -parameter plane corresponding to these conditions, is the limit point set separating the region with three solutions from the region with only one solution. Inserting (3.20) into (3.25) equates to

$$0 = \alpha\beta x_{A,R}^2 + \beta x_{A,F}(1-\alpha)x_{A,R} + x_{A,F} \quad . \quad (3.26)$$

This equation has two solutions $x_{A,R}^{(1,2)}$ that correspond to the turning points in the bifurcation diagram $x_{A,R}(Da)$,

$$x_{A,R}^{(1,2)} = \frac{(\alpha-1)\beta x_{A,F} \pm \sqrt{\beta^2 x_{A,F}^2 (1-\alpha)^2 - 4\alpha\beta x_{A,F}}}{2\alpha\beta} \quad . \quad (3.27)$$

They are feasible if and only if they are real-valued, corresponding to a positive discriminant

$$\beta x_{A,F} (\beta x_{A,F} (1-\alpha)^2 - 4\alpha) > 0 \quad , \quad (3.28)$$

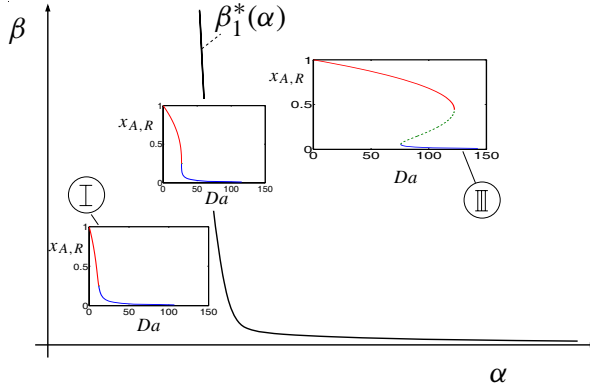


Figure 3.5: $(\alpha - \beta)$ - parameter chart including bifurcation diagrams $x_{A,R}(Da)$ in the different regions. The hysteresis variety $\beta_1^*(\alpha)$ separates region III, where the bifurcation diagram $x_{A,R}(Da)$ exhibits up to three steady states, from region I with only one steady state. Stable branches are represented by solid lines, unstable branches are designated by dashed lines. All bifurcation diagrams have been obtained for fixed $x_{A,F} = 1$ and $\alpha = 2$.

and if they fulfill $0 \leq x_{A,R}^{(1,2)} \leq x_{A,F}$. Thus, for the case of $\beta > 0$,

$$\beta_1^* := \frac{4\alpha}{x_{A,F}(1-\alpha)^2} \quad (3.29)$$

defines the hysteresis variety of (3.20)², i.e., the given system exhibits three steady-state solutions for $\beta > \beta_1^*(\alpha)$. In addition, it is easily shown that if $\alpha > 1$, indeed both limit points $x_{A,R}^{(1,2)}$ are positive and smaller than $x_{A,F}$.

Thus, a binary system with a first order reaction in a two-phase CSTR at the boiling point can exhibit up to three steady states over a certain range of the parameter Da in a clearly defined region of the $(\alpha - \beta)$ - parameter space, see Fig. 3.5. That is, if β is sufficiently large, and for reactions that are neither too slow nor too fast, two stable steady states – one at high and one at low conversion – do coexist with one unstable steady state at

²The same result can be derived more formally, relying on the framework provided by singularity theory. For the given case, it is easily shown that the general conditions defining a hysteresis variety, $f = f_x = f_{xx} = 0, f_{xxx} \neq 0, f_{Da} \neq 0$ (with x standing for $x_{A,R}$, and assuming Da to be the bifurcation parameter) exactly yield relation (3.29). For a general introduction to hysteresis varieties and singularity theory, see also [22].

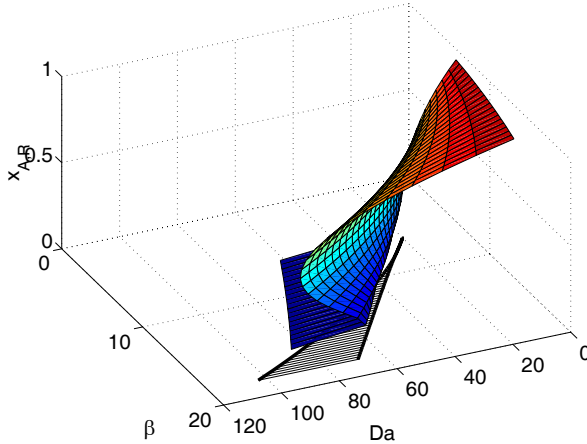


Figure 3.6: Three-dimensional plot of the fold for fixed $x_{A,F} = 1$ and $\alpha = 2$, including the branching set in the $(\beta - Da)$ - parameter plane. There are three steady-state solutions $x_{A,R}$ for parameter values in the hatched region of the $(\beta - Da)$ - plane.

intermediate conversion, as indicated by region III in Fig. 3.5. In contrast, for $\beta < \beta_1^*$, region I in Fig. 3.5, one stable steady state exists for all Da . A three-dimensional diagram of the corresponding cusp for fixed values of α and $x_{A,F}$ is shown in Fig. 3.6.

Again, stability or, respectively, instability of these steady states follows from the slope condition as outlined in Section 3.1, eq. (3.6). From Fig. 3.4 it is obvious that any disturbance of the intermediate steady state leading to an increase in $x_{A,R}$ is further amplified, because more reactant is supplied than consumed by the reaction, thus driving the system to the low conversion steady state. Accordingly, the two steady states at low and high conversion are stable by virtue of the same static stability argument relying on the slope condition.

This rather mathematical explanation of the system's stability and multiplicity features as presented so far is intimately linked to the **physical origin** of the steady-state multiplicity in the evaporatively cooled reactor. Again, a positive feedback mechanism can be identified, which destabilizes a branch of steady states and drives the system to one of the other two branches of stable equilibria.

The underlying physical mechanism is governed by the temperature-dependence of the

reaction rate. In the case of $\beta > 0$, i.e., with A being more volatile than B , an *increase in reactant concentration* $x_{A,R}$ results in a decrease in the boiling point temperature $T_R(x_{A,R})$, and thus also *causes a drop in the reaction rate*³. This will lead to a decrease in conversion and therefore a further increase in $x_{A,R}$. Thus, the **positive feedback effect** corresponds to a special type of **self-inhibition** of the reaction mechanism.

This self-inhibitory nature of the kinetics becomes even more obvious when compared to the classical isothermal self-inhibition observed in biochemical systems with substrate inhibition as introduced in Section 3.1, eq. (3.4). It has been shown that self-inhibition of the reaction mechanism occurs if the polynomial degree of the denominator is larger than the polynomial degree of the reaction rate's numerator. This corresponds to the necessary condition $\alpha > 1$ for the evaporatively cooled reactor studied in this section. Hence, by virtue of a conclusion by analogy, it is possible to infer that the origin of steady-state multiplicities in the given system clearly is attributable to the self-inhibitory character of the underlying physical mechanism.

Still, the exact nature of the origin of multiplicity requires some further clarification. As shown, self-inhibition by itself is a necessary, but by no means sufficient condition. In fact, the self-inhibition caused by the impeding effect of reactant A on the boiling point temperature has to be large enough, as mathematically given by eq. (3.29). This becomes even more evident when considering the case of $-1 < \beta < 0$, i.e. a scenario with the product being more volatile than the reactant. It is straightforward to show that this assumption implies

$$\frac{dRC}{dx_{A,R}} = \frac{Da[\beta x_{A,R}(1 - \alpha) + 1]}{(1 + \beta x_{A,R})^{\alpha+1}} > 0 \quad \forall \alpha > 0, x_{A,R} \in [0, 1] \quad . \quad (3.30)$$

Thus, in that case, there is always exactly one intersection with the supply line, corresponding to a unique, stable steady state.

In contrast, as shown above and to emphasize this fact once more, if the reactant is the light-boiling component ($\beta > 0$), the system may exhibit up to three steady states. For this to be the case, a second necessary condition has to be complied with, i.e., the difference in boiling point temperatures between light-boiling reactant A and heavy-boiling product B has to be sufficiently large, exceeding a certain value represented by $\beta_1^*(\alpha)$. Only then, the positive feedback effect due to **phase-equilibrium-driven self inhibition** is large enough to cause instabilities and steady-state multiplicities.

³Note that the supposed increase in $x_{A,R}$ also directly increases the reaction rate according to the mass action law kinetics, and has to be overruled by the decreasing effect due to the decreasing boiling point temperature, such that there is a net decrease of the reaction rate.

So far, the investigations have been confined to the case of a first order reaction. It is, however, no problem to extend the analysis to reactions of arbitrary order, as shown in [90]. Without going into details of the derivations, the key results along with the main conclusions are briefly summarized in what follows:

- The necessary condition of a sufficiently large self-inhibition causing steady-state multiplicity can be generalized to *reactions of arbitrary order* $n \geq 0$. It holds that $\alpha > n$ is a prerequisite for the existence of multiple steady states, i.e., the order of self-inhibition – typically the order of the denominator in a rational rate expression, here α – has to exceed the order of the actual concentration dependency. In particular, this implies that there are no limitations in terms of the ratio of the activation energy to the enthalpy of vaporization for *zeroth order reactions* to exhibit steady-state multiplicity, as by definition $\alpha > 0$ is guaranteed. This clearly demonstrates that, apart from the standard temperature dependence of the reaction rate as expressed by the Arrhenius law, no special type of kinetics whatsoever is required for the existence of multiple steady states.

Moreover, it can be shown that a binary system in an evaporatively cooled reactor as studied throughout this section can exhibit at most two steady states if the reaction is of order zero, and up to three steady states for reaction orders $n \geq 1$.

- In any case, a necessary condition for multiplicity is that reactant A has to be far more volatile than product B . This implies that the inhibitory mechanism clearly is attributable to temperature effects on the reaction rate and therefore **different from the origin of multiplicities due to self-inhibition or autocatalysis in isothermal systems** as presented in Section 3.1.

The actual difference in boiling point temperatures required for potential multiplicities varies with the order of the reaction kinetics and depends on further physical parameters, in particular on the activation energy of the reaction.

Moreover, for reactions where reactant A is heavy-boiling ($\beta < 0$), or where reactant and product are equally volatile ($\beta = 0$), the mechanism as derived in this section cannot come into effect for any order of the reaction rate law. And, as just explained, it cannot even lead to instabilities in closely boiling mixtures either.

- On the other hand, it is worth noting that this mechanism may even come into effect for endothermic reactions. This underlines the fact, that the nature of the mechanism that has been presented is **different from the thermokinetic origin of multiplicities in exothermic systems**. Endothermic reactions are rather unlikely

for evaporatively cooled reactors, as such reactors are typically used to provide efficient cooling for strongly exothermic reactions. However, endothermic reactions in boiling liquid do occur in reactive distillation (see, e.g., [79]).

- The explanatory power of the physical interpretation derived above is by no means restricted to applications involving evaporatively cooled reactors. In fact, also multiplicities in other reactive systems operated at the boiling point like reactive distillation columns (see [80] for a detailed discussion of reactive distillation processes), for which so far rather tentative explanations have prevailed, can now be explained by means of this mechanism of **phase-equilibrium-driven self-inhibition**. One striking example is the ethylene glycol synthesis in a reactive distillation column as first proposed by Parker [58] and studied in detail in [14]. Also in this system, one of the reactants fed to a reactive tray has a boiling point temperature markedly below the boiling point of all other components. In this context it has to be pointed out that a reactive tray can be regarded as just another form of a two-phase reactor operated at the boiling point. The observed steady-state multiplicity in this reactive column can therefore be traced back to the self-inhibitory mechanism whose derivation the present chapter has been devoted to.
- The results presented in this section have recently been confirmed and extended to the ternary case by the group of Malone and coworkers [68]. Their more formal analysis is based on a slightly different setup, i.e., a reactive flash without recycle and with a constant ratio V/F adjusted via the flash heating rate. The conclusions in terms of explaining the physical cause for multiplicities in liquid systems operated at the boiling point, however, is identical to the results derived above. Malone et al. have also shown that under certain conditions a binary reactive flash where the reactant is the heavy component, may also exhibit up to three steady states. In this case, of course, the physical mechanism yielding multiplicity is different from the self-inhibition as described in this section. Instead, the origin of multiplicities in this case can be traced back to the coupling of the material and energy balances along with the vapor-liquid equilibrium, and foremost requires large heats of reaction [67]. Hence, the origin of multiplicities in this case is of thermokinetic nature. This most clearly underlines the difference to the self-inhibitory mechanism proposed in this section, which is completely independent of any heat effects described by an energy balance.

So far, the results derived have been based on a suitably simple model, involving a binary, thermodynamically ideal mixture, a standard kinetic rate expression, assuming total reflux of the condensed vapor, and neglecting vapor phase dynamics. However, the identified physical mechanism does not hinge on these simplifications and the possibilities they bring along in terms of formally proving certain results as done above. Instead, the explanatory character of the deduced physical interpretation is of greater generality and carries through to more complex systems. This will be shown by an application of the theoretical results to the industrial reactor case study in the following section.

3.3 Industrial case study of an evaporatively cooled reactor

The basis of the investigations in this section is the detailed model of the evaporatively cooled reactor serving for the production of acetic acid as introduced in Chapter 2.

It is assumed that the reactor level is constant due to perfect control via manipulation of the reactor effluent stream as in the basecase control structure introduced in Section 2.1. For simplicity, it is furthermore assumed that a constant ratio of CO is separated in the overhead condenser, while all other components are completely recycled. This is very similar to the real plant, where actually about 98% of the vapor leaving the overhead partial condenser is CO (corresponding to about 95% of the CO in the reactor vapor stream), with only traces of the other components present. Given these assumptions, the condenser can be treated as a total condenser for the remaining stream, which therefore still contains some CO .

For simulating this isolated reactor-condenser system, all feed streams are fixed to the values they take on at standard operation in the complete plant. More specifically, this means that all internal recycle streams from downstream units to the reactor that are variable in the plantwide context, i.e. the recycles from the flash as well as the recycles from the two columns, are here treated as fixed feed streams.

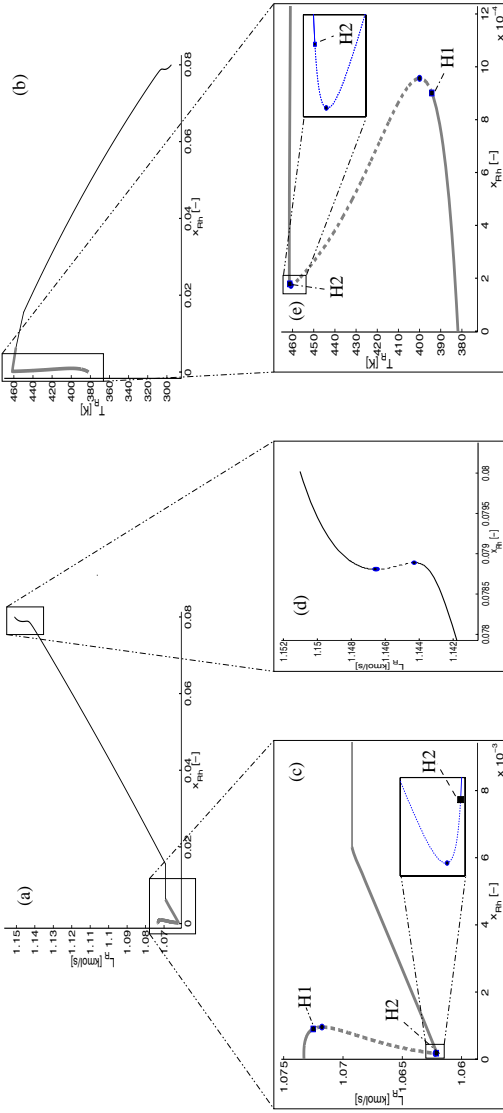


Figure 3.7: Multiplicity features of the reactor-condenser system of the acetic acid plant. Subfigures (a) and (b) show the two hysterises in the two-phase regime (thin lines) and in the one-phase regime (thick lines), (a) for the reactor effluent stream L_R , and (b) the reactor temperature T_R , respectively. Subfigures (c) - (e) are zooms of the multiplicity regions and additionally contain stability information. Solid lines denote stable branches, dashed lines correspond to unstable branches, squares designate Hopf bifurcation points, and dots mark real bifurcation points.

Figure 3.7 shows the results of a continuation in the amount of rhodium catalyst x_{Rh} , which is a parameter in the reactor model. According to the rate equation (A.2), the reaction rate is proportional to the amount of catalyst. Hence, varying x_{Rh} corresponds to varying the system's Damkohler number, which renders x_{Rh} a suitable continuation parameter. It should be noted that in general it is best to choose those operating parameters as continuation parameters which can also in practice be directly manipulated, like the various streams within a system. However, for the given system with its multiple reactor feeds, manipulation of one feed stream would alter the stoichiometry of the feed conditions, and would thus introduce undesired further effects. Therefore, in all cases where the reactor effluent stream is used to maintain the reactor level at setpoint and therefore is not eligible as continuation parameter, the choice of x_{Rh} as continuation parameter is most appropriate.

As can be seen from Figure 3.7, the reactor-condenser system of the industrial case study exhibits two distinct regions with three steady states. The first of these hystereses occurs for low values of x_{Rh} in the two-phase regime, as indicated by the thick lines. The physical mechanism causing these multiplicities is exactly the one derived in the previous section. In the acetic acid reactor, it is the dissolved CO that takes over the part of the light boiling component, i.e., the more CO is dissolved in the reaction mixture, the lower the boiling point temperature of the mixture, and vice versa. Thus, also in this system the self-inhibition of the reaction mechanism induced by the interplay of the vapor-liquid equilibrium with the temperature-dependent reaction kinetics comes into effect and causes the occurrence of up to three steady states. As can be seen from the zooms of the boiling regime in Figs. 3.7 (c) and (e), the two steady states corresponding to low and high conversion are stable, whereas the intermediate conversion steady state is unstable. This perfectly matches the theoretical considerations of the previous chapter.

Two aspects are particularly noteworthy:

- The stable steady states corresponding to low conversion are marked by low boiling point reactor temperatures and comparatively large reactor effluent flowrates. Vice versa, the stable steady states corresponding to high conversion are characterized by high reactor temperatures and smaller molar reactor effluent flowrates. This obviously stems from the fact that e.g. at low conversion, the small reaction rate has two main effects: (i) Only few of the 'light' component CO is consumed, which results in the low boiling point temperature. (ii) Simultaneously, the non-equimolarity of the reaction (recall that for every mole of acetic acid produced, two

moles of reactants are consumed) in combination with the reduced consumption of reactants causes the comparatively high molar effluent stream required for constant liquid reactor level.

Obviously, at high conversion the circumstances and explanations are just reciprocal.

- The theoretical results derived in the previous section for an *ideal binary system with complete condenser recycle* can be seamlessly carried forward to the *non-ideal multi-component system with only partial condenser recycle* as studied in the current section. This underscores the fact that the deduced self-inhibition mechanism is not an artifact due to simplifying assumptions.

The second hysteresis occurs for unrealistically high values of x_{Rh} in the one-phase, pure liquid regime (thin lines in Fig. 3.7, in particular zoom (d)). Nevertheless, knowledge of this second region with multiple steady states will prove extremely helpful for understanding the nonlinear behavior of the complete reaction system with the flash recycle closed in Chapter 4.

As far as the physical origin of the second hysteresis is concerned, an easy simulation experiment supports the assertion that it must be due to thermokinetic effects. Rendering the single phase reactor isothermal by applying temperature control, the hysteresis for large x_{Rh} disappears. This clearly indicates that the steady-state multiplicity for large Damkoehler numbers must be caused by temperature effects as present in the classical cases of thermokinetically controlled reactions. In fact, it cannot be caused by equilibrium-driven self-inhibition, as it occurs in the pure liquid regime.

Some additional remarks concerning the Hopf bifurcation points in the two-phase regime of Fig. 3.7 conclude this section. Both Hopf points (denoted by squares) are located very close to the two turning points (denoted by dots) of the two-phase hysteresis, and mark the points where the low- and high-conversion steady states, respectively, lose stability. In order to determine the nature of the limit cycles originating from the two Hopf bifurcation points, the dynamic responses of the system following impulse-like disturbances of the unstable steady states just beyond the Hopf points have been simulated.

Figure 3.8 (a) shows the transient to a permanent oscillation corresponding to a stable limit cycle that emanates from the high conversion Hopf point H2. However, the range of x_{Rh} -values for which this limit cycle is stable is extremely small, and continuations of the limit cycle confirm that it loses stability for values of x_{Rh} just marginally below the Hopf point H2.

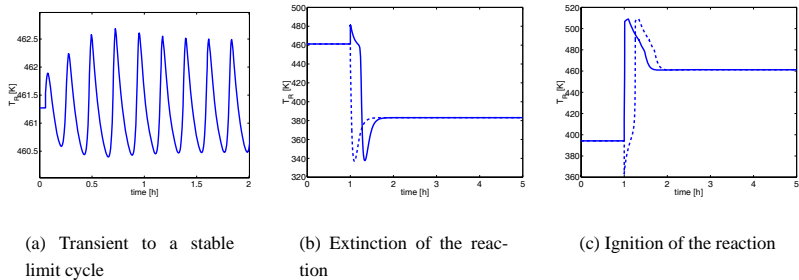


Figure 3.8: Transients of the reactor-condenser system after impulse-like disturbances of different unstable steady states as depicted in Fig. 3.7: (a) for values of x_{Rh} immediately below the Hopf point H2 in the tiny range of x_{Rh} -values for which a stable limit cycle exists, (b) for values of x_{Rh} just below the region with stable limit cycles where the disturbance of the unstable steady state causes an extinction of the reaction, and (c) for values of x_{Rh} just beyond the subcritical Hopf Point H1, where the disturbance of the unstable steady state leads to the ignition of the reaction.

This is in agreement with the dynamic simulation results depicted in Fig. 3.8 (b), that display the transients to the low-conversion stable steady state after impulse-like disturbances of the system's unstable steady states for values of x_{Rh} still very close to H2. Here, the dashed line corresponds to the transient after a -1% disturbance of $x_{H_2O,R}$ (resulting in a direct jump to the stable low-conversion steady state), while the solid line marks the transient after a +1% disturbance of $x_{H_2O,R}$ (entailing an inverse response before dropping off to the low-conversion steady state).

In contrast, no stable limit cycle can be found for values of x_{Rh} just beyond the low-conversion Hopf point H1. Instead, the transients following positive and negative impulse-like disturbances of the unstable steady state beyond H1 as depicted in Fig. 3.8 (c) both lead to the high-conversion branch of stable steady states. As the existence of a stable limit cycle on the side of the stable steady states of the low-conversion branch for values of x_{Rh} below H1 is topologically infeasible, and as there is obviously no stable limit cycle on the unstable branch 'right' to H1 (otherwise, this stable limit cycle would have attracted transients originating from a disturbed unsteady state), it can be concluded that the Hopf point H1 is subcritical.

Thus, there is only a tiny region of x_{Rh} -values for which the reactor-condenser system

may exhibit permanent oscillatory behavior with small amplitudes. This range of parameter values is so small that it is of no practical interest. Therefore, it will not be studied in more detail within this thesis.

As far as the physical origin of the Hopf points is concerned, it is worth noting that their occurrence seems to be related to the fact that parts of the reactant CO leave the system through the overhead condenser. Further simulation studies have revealed that the Hopf points disappear once total condensation and complete recycling of the reactor vapor stream are assumed.

However, as already mentioned, this phenomenon is of little practical relevance in the context of the acetic acid production process and will therefore not be further pursued within this thesis, but may as well be the topic of future research.

Instead, a short summary will briefly resume the main results derived in this chapter, before attention is shifted to the behavior of the complete reaction system with the flash recycle to the reactor closed in Chapter 4.

3.4 Summary

This section has revealed phase-equilibrium-driven self-inhibition as the mechanism which may cause steady-state multiplicities in two-phase reactive systems operated at the boiling point. More specifically, for the derived mechanism to become effective and result in the occurrence of multiple steady states, one of the reactants has to be far more volatile than the other components and the ratio of the reaction's activation energy to the system's mean enthalpy of vaporization has to exceed the order of the reaction rate in terms of concentration dependency.

This result is of high practical importance as its application fields encompass many types of systems operated at the boiling point like evaporatively cooled reactors or reactive distillation columns.

Chapter 4

Nonlinear Analysis II: Reactor-separator systems with one recycle

While the previous chapter was concerned with the investigation of the nonlinear behavior of stand-alone evaporatively cooled reactors, focus in the present chapter is directed towards the dynamics of reactor-separator systems with exactly one recycle.

Such systems are the fundamental building blocks of larger integrated systems, and therefore insight into the possible patterns of behavior these systems may exhibit is quintessential for understanding highly integrated systems in general. Up to now, research on plantwide control has been occupied to an overwhelming extent with the search for suitable control structures for simple reactor-separator systems. Although an extension to larger plants is clearly not straightforward, starting with a reasonable simplified system is a good strategy to gain some fundamental insight into the behavior of recycle systems.

Several studies have tried to extract key features of recycle systems by means of **linear systems theory**. The most notable contributions reveal that material and energy recycling typically moves the poles of the plant towards, and possibly across the imaginary axis, leading to increased time constants, increased low-frequency disturbance sensitivity, and possibly even instability of the integrated plant [56]. Moreover, it has been shown that not only parallel paths in integrated systems change or add zeros [56], but that also recycling may introduce non-minimum phase behavior in integrated plants [31, 32].

So far, the common key result of all studies explicitly addressing the **nonlinear characteristics of recycle processes** is the difference of the integrated system's behavior when

compared to the behavior of the stand-alone units. To be more precise, it has been shown how recycles may induce instability, steady-state multiplicities, and oscillatory behavior in reactor-separator systems although the isolated individual units exhibit unique and stable steady states [10, 37, 60, 70, 95]. Most of the cited investigations do also stress the influence of specific control strategies on the characteristics of recycle systems. Moreover, it has been shown in a recent study how delay effects may destabilize the steady state of a reactor separator system which is stable if the delay is negligible [8].

In the present chapter, focus is on a systematic study of the nonlinear behavior of reactor-separator systems for a number of practically interesting control configurations.

In order to convey a first idea of the possible nonlinear phenomena caused by recycles, Section 4.1 serves as an introduction to the systematic analysis of reactor-separator systems, thus **setting the stage for all further investigations into recycle systems** within this thesis. Different combinations of possible control structures are introduced, and for a simple binary model system made up of an isothermal liquid phase reactor and a flash separator with liquid recycle, analytical results are obtained. These results help to get across a flavor of the **surprisingly complex behavior** that may be encountered even in very simple recycle systems and that can be attributed to the impact of the recycle on the system behavior. Subsequently, in Section 4.2, a binary reactor-separator system is considered where the reactor is evaporatively cooled. This corresponds to the industrial case study and leads to the numerical investigations of the basic reactor-separator system of the multicomponent acetic acid production process in Section 4.3.

4.1 Isothermal, binary liquid-phase reactor with flash separator and liquid recycle

Consider the reactor-separator system depicted in Fig. 4.1. It is assumed that the irreversible first order reaction $A \rightarrow B$ is carried out in a perfectly mixed, isothermal, isobaric liquid phase CSTR. The ideal binary reaction mixture leaving the reactor is fed to an isobaric flash separator, and the liquid recycle stream to the reactor is assumed to serve as the manipulated variable to keep the flash holdup constant.

The behavior of this system for various combinations of flow and flash control strategies has been studied extensively by Zeyer et al. [95] for the case of A being the heavy boiling component (see Table 4.1 for a summary of their results). **In this section**, these

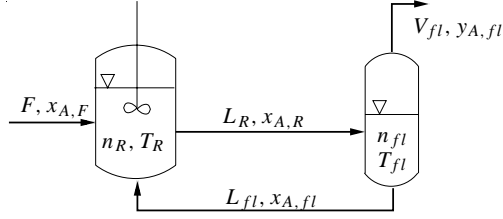


Figure 4.1: Setup of the reactor separator model system.

studies are extended to the case where **A is the light boiling component**, as is the case in the industrial example investigated throughout this thesis, where the liquid flash recycle guarantees the recovery of the nonvolatile Rhodium catalyst. In contrast to [95], the aim of this section is not so much an in-depth study including detailed numerical investigations of several possible bifurcation phenomena. Instead, focus is on qualitative analytical results providing insight into the issues of stability and feasibility of different control structures. Wherever possible, an interpretation of results based on graphical tools employing supply lines and consumption curves is given.

Relying on the assumptions as given above, the reactor separator system is in general described by the following set of equations (see [95] for details of deriving the model equations):

Total material balance of the reactor:

$$\frac{dn_R}{dt} = F + L_{fl} - L_R \quad . \quad (4.1)$$

Component material balance of the reactor:

$$\frac{d(n_R x_{A,R})}{dt} = F x_{A,F} + L_{fl} x_{A,fl} - L_R x_{A,R} - n_R k x_{A,R} \quad . \quad (4.2)$$

Total material balance of the flash:

$$0 = L_R - V_{fl} - L_{fl} \quad . \quad (4.3)$$

Component material balance of the flash:

$$n_{fl} \frac{dx_{A,fl}}{dt} = L_R x_{A,R} - L_{fl} x_{A,fl} - V_{fl} y_{A,fl} \quad . \quad (4.4)$$

Quasi-stationary energy balance of the flash:

$$0 = L_R c_P (T_R - T_{fl}) - V_{fl} \Delta h_{V,fl} + Q_{fl} \quad . \quad (4.5)$$

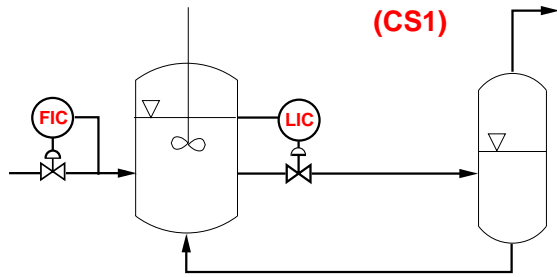
Moreover, the liquid mole fractions of component B follow from the summation conditions for the liquid phases in the reactor and the flash. The vapor mole fractions y_{fl} are obtained from vapor-liquid equilibrium relations $y_{fl} = y_{fl}(x_{fl}, T_{fl})$, and as thermodynamic equilibrium between the vapor and the liquid phase in the flash is assumed, the flash temperature follows from the vapor summation condition in the flash.

The combinations of flow and flash control structures introduced by Zeyer et al. also provide the basis for the investigations within this and following sections. The three different flow control strategies are depicted in Fig. 4.2: (a) Control structure CS1 relies on the reactor effluent stream L_R as manipulated variable to control the reactor holdup or liquid reactor level, respectively, while the feed flow rate F is fixed; (b) control structure CS2 uses the feed flow to control the reactor holdup while the reactor effluent stream L_R is fixed; and (c) control structure CS3 is characterized by flow control of both F and L_R , which means that in this case the reactor holdup is variable.

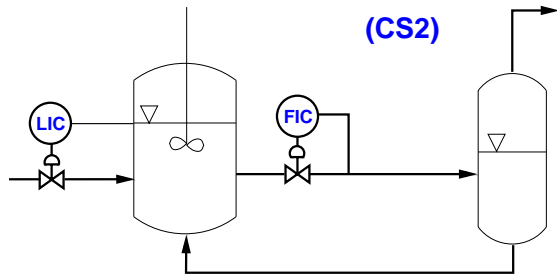
For simplicity, ideal controllers will be assumed. In particular, this is reflected in the assumption $n_R = const.$ for the level control of the reactor.

In what follows, the behavior of the given binary reactor-separator system with liquid recycle will be investigated for possible combinations of these three flow control strategies just introduced with three different flash control strategies.

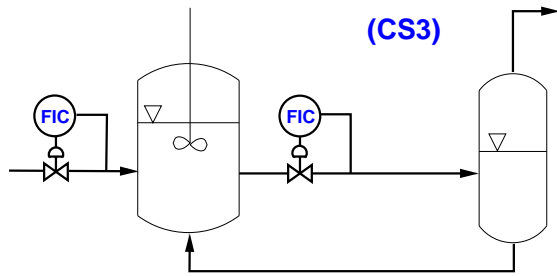
Depending on the chosen overall control structure, the system of equations (4.1)-(4.5) can be further simplified. To keep the presentation compact, details of these simplifications that reflect the impact of the specific control structures are omitted in what follows, and are only hinted at instead. Again, details can be found in [95].



(a) F fixed



(b) L_R fixed



(c) F and L_R fixed

Figure 4.2: Possible level and flow control structures considered within this thesis.

4.1.1 (p,T)-flash

Fig. 4.3 illustrates the flash control structure applied to keep both the molar holdup or liquid level, respectively, in the flash drum and the flash temperature constant. The liquid flash effluent stream L_{fl} is adjusted to guarantee level control, while the flash heating rate is the manipulated variable to control the flash temperature T_{fl} .

Given that an isobaric binary system is considered, it follows from the Gibbs phase rule that for constant T_{fl} the equilibrium compositions $x_{A,fl}, y_{A,fl}$ are fixed, and the energy balance (4.5) of the flash is not required. Moreover, for the flash to be operable in the case of A being the light boiling component, the feasibility condition

$$x_{A,fl} \leq x_{A,R} \leq y_{A,fl} \quad (4.6)$$

has to be complied with.

I) Control structure CS1 with (p,T)-flash

As shown in [95], for a combination of flow control structure CS1 with an isobaric isothermal flash, the internal streams may be obtained from the flash material balances, $V_{fl} = F$ follows from the overall material balance, and the system (4.1)-(4.5) can be reduced to a scalar, linear differential equation in $x_{A,R}$,

$$n_R \frac{dx_{A,R}}{dt} = F(x_{A,F} - y_{A,fl}) - n_R k x_{A,R} \quad (4.7)$$

The steady-state version of (4.7) can be written as

$$\underbrace{F(x_{A,F} - y_{A,fl})}_{SL} = \underbrace{n_R k x_{A,R}}_{RC} \quad (4.8)$$

where SL denotes the supply line and RC the reaction curve of the system. It holds that

$$\frac{dSL}{dx_{A,R}} = 0 < n_R k = \frac{dRC}{dx_{A,R}} \quad (4.9)$$

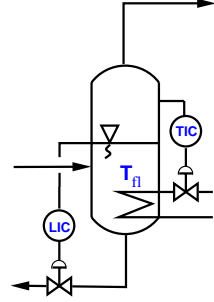


Figure 4.3: (p,T)-flash

i.e., the well-known slope condition indicates the stability of the system's unique steady state. Fig. 4.4 shows that any disturbance to the system leading to an increase in $x_{A,R}$ increases the consumption of $x_{A,R}$ according to the reaction term, while the supply of A remains unaltered. Thus, the disturbance is counteracted, and the steady state is statically stable, independent of the boiling sequence. As the system is governed by a scalar, linear differential equation, this also implies dynamic stability of the unique steady state (see also Appendix B.1).

Note that for this simple system the steady state solution $x_{A,R}$ can easily be calculated explicitly and is given as

$$x_{A,R} = \frac{F(x_{A,F} - y_{A,fl})}{n_R k} \quad (4.10)$$

Recalling the feasibility conditions (4.6) for A light boiling, also the feasible bounds of operation in terms of the operating parameter F can be calculated explicitly, yielding

$$F \in [F_{min}, F_{max}] \quad , \quad (4.11)$$

where

$$F_{min} = \frac{n_R k x_{A,fl}}{x_{A,F} - y_{A,fl}} \quad , \quad F_{max} = \frac{n_R k y_{A,fl}}{x_{A,F} - y_{A,fl}} \quad (4.12)$$

For A light boiling and $F < F_{min}$, corresponding to large reactor residence times and therefore high conversion, there will be only a small amount of the volatile reactant in the flash, and at the given fixed flash temperature no vapor will leave the flash. Consequently, the internal streams will accumulate and tend to infinity. In contrast, for $F > F_{max}$, a negative liquid flash stream would be required to keep $n_{fl} = const$, which corresponds to an actual accumulation of the molar holdup in the flash.

This is exactly the reverse situation when compared to the case where A is heavy boiling [95].

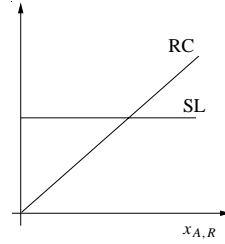


Figure 4.4: Supply line SL and reaction curve RC for CS1, independent of the boiling sequence.

II) Control structure CS2 with (p,T)-flash

Similarly to the previous subsection, it is easily shown that in this case the governing scalar, linear differential equation is given by

$$n_R \frac{dx_{A,R}}{dt} = L_R \frac{x_{A,R} - x_{A,fl}}{y_{A,fl} - x_{A,fl}} (x_{A,F} - y_{A,fl}) - n_R k x_{A,R} \quad , \quad (4.13)$$

with eigenvalue

$$\lambda_{CS2} = \frac{L_R x_{A,F} - y_{A,fl}}{n_R y_{A,fl} - x_{A,fl}} - k \quad . \quad (4.14)$$

Here, the sign of the eigenvalue is not immediately obvious. However, the steady-state version of (4.13) can be written as

$$L_R \underbrace{\frac{x_{A,R} - x_{A,fl}}{y_{A,fl} - x_{A,fl}} (x_{A,F} - y_{A,fl})}_{SL} = \underbrace{n_R k x_{A,R}}_{RC} \quad , \quad (4.15)$$

where again SL denotes the supply line and RC the reaction curve of the system. It holds that

$$\frac{dSL}{dx_{A,R}} = L_R \frac{x_{A,F} - y_{A,fl}}{y_{A,fl} - x_{A,fl}} > n_R k = \frac{dRC}{dx_{A,R}} \quad . \quad (4.16)$$

This is because from (4.13) it follows that at steady state

$$L_R \frac{x_{A,F} - y_{A,fl}}{y_{A,fl} - x_{A,fl}} = n_R k \underbrace{\frac{x_{A,R}}{x_{A,R} - x_{A,fl}}}_{>1} > n_R k \quad . \quad (4.17)$$

Therefore, according to the slope-condition, the system's unique steady state is statically unstable if A is light boiling, and with the same argument it can be shown that the system is stable for A heavy boiling (see also Figs. 4.5(a) and (b)). Note that (4.16) implies $\lambda_{CS2} > 0$, which also proves the instability of the given system.

The physical interpretation of this instability is straightforward: Suppose the system is subject to a disturbance leading to an increase in $x_{A,R}$. In the case of A being the light boiling component, with the feed to the flash fixed as well as T_{fl} , $x_{A,fl}$, $y_{A,fl}$, this leads to an immediate decrease in the recycle stream L_{fl} back to the reactor at the same unaltered composition due to the lever rule, as can be seen in Fig. 4.5 (c). To keep $n_R = const$ with this control configuration, F would then have to be increased. I.e., although the increase in $x_{A,R}$ leads to a higher reaction rate ($r = kx_{A,R}$) with more A being consumed, more fresh A is supplied than consumed, as can be seen from eq. (4.16). Dynamically, the recycle stream goes to zero, while A accumulates in the reactor, up to the point that the

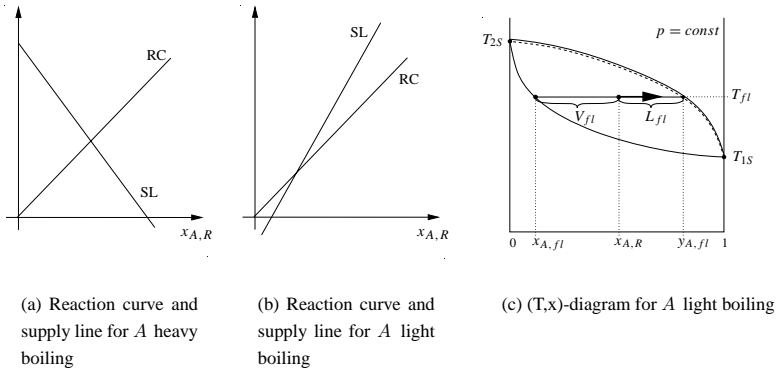


Figure 4.5: Supply lines and reaction curves for a static stability analysis of control structure CS2 and (p,T)-flash, depending on the boiling sequence ((a) and (b)), and (T,x)-diagram for A light boiling, including the impact of an increase in $x_{A,R}$ according to the lever rule (c).

feasibility boundary is crossed.

For the case of a disturbance leading to a decrease in $x_{A,R}$ just the opposite effect occurs, i.e. A decreases further and the recycle stream increases until the vapor stream from the flash reaches zero.

As this system is unstable, further investigations in feasibility are dispensable. It should therefore just be remarked that for the given control structure a lower feasibility bound $L_{R,min}$ for the existence of the unstable solution can be established, while there is no corresponding upper bound on L_R .

III) Control structure CS3 with (p,T)-flash

In the case of both F and L_R being flow-controlled, the reactor holdup is a dynamic variable. With the two flash streams following from the flash material balances, the governing

system of equations then reads

$$n_R \frac{dx_{A,R}}{dt} = F(x_{A,F} - x_{A,R}) + L_R \frac{(x_{A,R} - y_{A,fl})(x_{A,fl} - x_{A,R})}{x_{A,fl} - y_{A,fl}} - n_R k x_{A,R} \quad (4.18)$$

$$\frac{dn_R}{dt} = F - L_R \frac{x_{A,fl} - x_{A,R}}{x_{A,fl} - y_{A,fl}} \quad (4.19)$$

This system has a unique steady state, as (4.19) can uniquely be solved for $x_{A,R}$, while (4.18) can uniquely be solved for n_R . Moreover, as explained in [95], this steady state is feasible for all admissible parameters $F < L_R$ that allow for a steady state.

The Jacobian of this second order system is given as

$$J = \begin{pmatrix} \frac{L_R y_{A,fl} - x_{A,R}}{n_R x_{A,fl} - y_{A,fl}} - k & -\frac{k x_{A,R}}{n_R} \\ \frac{L_R}{x_{A,fl} - y_{A,fl}} & 0 \end{pmatrix} \quad (4.20)$$

Obviously, for A light boiling (i.e., $x_{A,fl} \leq x_{A,R} \leq y_{A,fl}$), it holds that

$$\det(J) = \frac{L_R k x_{A,R}}{n_R (x_{A,fl} - y_{A,fl})} < 0 \quad (4.21)$$

$$\text{tr}(J) = \frac{L_R}{n_R} \cdot \frac{y_{A,fl} - x_{A,R}}{x_{A,fl} - y_{A,fl}} - k < 0 \quad (4.22)$$

Thus, this configuration is always unstable, whereas for A heavy boiling it is always stable.

Dynamically, an increase in $x_{A,R}$ reduces the recycle stream (cf. Fig. 4.5(c)) and thus leads to a *vanishing reactor holdup*, accompanied by a further increase in $x_{A,R}$. Analogously, a decrease in $x_{A,R}$ increases the recycle stream and thus leads to an *accumulating reactor holdup*.

Again, static instability can be interpreted in terms of a supply line and a reaction curve: At steady state, solving (4.19) for L_R and inserting in (4.18) leads, after rearranging, to

$$0 = \underbrace{\frac{L_R x_{A,F} - y_{A,fl}}{n_R x_{A,fl} - y_{A,fl}} x_{A,fl} + \frac{L_R y_{A,fl} - x_{A,F}}{n_R x_{A,fl} - y_{A,fl}} x_{A,R}}_{SL} - \underbrace{k x_{A,R}}_{RC} \quad (4.23)$$

As $SL(x_{A,R} = 0) = \frac{L_R x_{A,F} - y_{A,fl}}{n_R x_{A,fl} - y_{A,fl}} x_{A,fl} < 0$, for feasibility of an intersection between the two straight lines SL and RC, corresponding to a unique steady state, it must hold that

$$\frac{dSL}{dx_{A,R}} > \frac{dRC}{dx_{A,R}} \quad (4.24)$$

This clearly indicates the static and therefore also dynamic instability of the given control structure (cf. Appendix B.1).

Note that feasibility of the intersection requires $RC(x_{A,R} = y_{A,fl}) < SL(x_{A,R} = y_{A,fl})$. This equates to the requirement $L_R > n_R k \frac{y_{A,fl}}{x_{A,F} - y_{A,fl}}$, which is always fulfilled for all admissible $L_R > F^1$.

4.1.2 Q_{fl} fixed

Fig. 4.6 illustrates a flash control structure with constant flash heating rate Q_{fl} . Again, the liquid flash effluent stream L_{fl} is adjusted to guarantee flash level control.

As T_{fl} is no longer constant for the constantly heated flash, also $x_{A,fl}$ and $y_{A,fl}$ are no longer fixed parameters in this system, and the energy balance of the flash (4.5) and the general dependencies $y_{A,fl}(x_{A,fl})$, $T_{fl}(x_{A,fl})$, $\Delta h_{V,fl}(y_{A,fl}(x_{A,fl}))$ have to be taken into account. Note that due to these implicit dependencies, a simple treatment in terms of graphical arguments as in the preceding section is no longer possible.

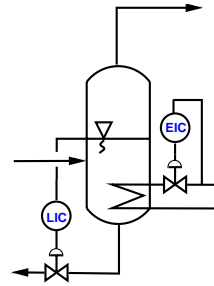


Figure 4.6: Flash with Q_{fl} fixed.

D) Control structure CS1 with Q_{fl} fixed

With $L_{fl} = L_R - V_{fl}$ and $V_{fl} = F$, the two flash streams can be eliminated from (4.1)-(4.5), and one obtains the second order system

$$n_R \frac{dx_{A,R}}{dt} = Fx_{A,F} + (L_R - F)x_{A,fl} - L_R x_{A,R} - n_R k x_{A,R} \quad , \quad (4.25)$$

$$n_{fl} \frac{dx_{A,fl}}{dt} = L_R x_{A,R} - (L_R - F)x_{A,fl} - F y_{A,fl} \quad , \quad (4.26)$$

with

$$L_R(x_{A,fl}) = \frac{F \Delta h_{V,fl} - Q_{fl}}{c_P(T_R - T_{fl})} \quad (4.27)$$

¹At steady state, solving (4.19) for F shows that $L_R > F$ corresponds to $x_{A,R} < y_{A,fl}$, and insertion into (4.18) yields the above requirement.

from the flash energy balance. Here, the Jacobian of the system is given by

$$J = \begin{pmatrix} -\frac{L_R}{n_R} - k & \frac{1}{n_R} \left(L_R + (x_{A,fl} - x_{A,R}) \frac{dL_R}{dx_{A,fl}} \right) \\ \frac{L_R}{n_{fl}} & \frac{1}{n_{fl}} \left(-L_R - F \frac{dy_{A,fl}}{dx_{A,fl}} - (x_{A,fl} - x_{A,R}) \frac{dL_R}{dx_{A,fl}} \right) \end{pmatrix}. \quad (4.28)$$

As

$$\frac{dL_R}{dx_{A,fl}} = \frac{1}{c_P(T_R - T_{fl})} \left(F(\Delta h_{V,A} - \Delta h_{V,B}) \frac{dy_{A,fl}}{dx_{A,fl}} + L_R c_P \frac{dT_{fl}}{dx_{A,fl}} \right), \quad (4.29)$$

where $\frac{dy_{A,fl}}{dx_{A,fl}} > 0$, and $\frac{dT_{fl}}{dx_{A,fl}} < 0$ for A light boiling, it holds that $\frac{dL_R}{dx_{A,fl}} < 0$ for

$$\Delta h_{V,A} < \Delta h_{V,B} \quad \text{and} \quad T_R > T_{fl}. \quad (4.30)$$

In this case, it also holds that $tr(J) < 0$ and $det(J) > 0$. In all other cases, no statement about the sign of $\frac{dL_R}{dx_{A,fl}}$ and as a consequence the sign of $tr(J)$ and $det(J)$ is possible. Note that under the given conditions (4.30), for $L_R > F$ it is required from (4.27) that

$$F > \frac{Q_{fl}}{\Delta h_{V,fl} - c_p(T_R - T_{fl})} = F_{min},$$

i.e., there is a lower feasibility bound on F . Moreover, it can be shown that the stable steady state obtained for $F > F_{min}$ is unique (see Appendix B.2).

Thus, the given control structure is guaranteed to exhibit a unique, stable steady state for $\Delta h_{V,A} < \Delta h_{V,B}$ and $T_R > T_{fl}$, while for all other combinations, instabilities and multiplicities are possible.

II) Control structure CS2 with Q_{fl} fixed

With $F = V_{fl}$ and $L_{fl} = L_R - V_{fl}$, this system with fixed L_R is described by

$$n_R \frac{dx_{A,R}}{dt} = V_{fl} x_{A,F} + (L_R - V_{fl}) x_{A,fl} - L_R x_{A,R} - n_R k x_{A,R}, \quad (4.31)$$

$$n_{fl} \frac{dx_{A,fl}}{dt} = L_R x_{A,R} - (L_R - V_{fl}) x_{A,fl} - V_{fl} y_{A,fl}, \quad (4.32)$$

where V_{fl} follows from the flash energy balance

$$V_{fl}(x_{A,fl}) = \frac{L_R c_P (T_R - T_{fl}) + Q_{fl}}{\Delta h_{V,fl}}. \quad (4.33)$$

The Jacobian of this system is given by

$$J = \begin{pmatrix} -\frac{L_R}{n_R} - k & \frac{1}{n_R} \left(L_R - V_{fl} + (x_{A,F} - x_{A,fl}) \frac{dV_{fl}}{dx_{A,fl}} \right) \\ \frac{L_R}{n_{fl}} & \frac{1}{n_{fl}} \left(-(L_R - V_{fl}) - V_{fl} \frac{dy_{A,fl}}{dx_{A,fl}} + (x_{A,fl} - y_{A,fl}) \frac{dV_{fl}}{dx_{A,fl}} \right) \end{pmatrix}, \quad (4.34)$$

with

$$\frac{dV_{fl}}{dx_{A,fl}} = -\frac{1}{\Delta h_{V,fl}} \left(V_{fl}(\Delta h_{V,A} - \Delta h_{V,B}) \frac{dy_{A,fl}}{dx_{A,fl}} + L_{RCP} \frac{dT_{fl}}{dx_{A,fl}} \right) \quad (4.35)$$

For $\Delta h_{V,A} < \Delta h_{V,B}$, it is straightforward to prove that $\frac{dV_{fl}}{dx_{A,fl}} > 0$ and $tr(J) < 0$. However, independent of the values of $\Delta h_{V,A}$ and $\Delta h_{V,B}$, no statement concerning the sign of $det(J)$ is possible, and thus it has to be concluded that for the given control structure, stability cannot be guaranteed for any combination of parameter values.

Indeed, the numerical simulation results depicted in Fig. 4.7 indicate that for both $\Delta h_{V,A} > \Delta h_{V,B}$, and $\Delta h_{V,A} < \Delta h_{V,B}$ the system may exhibit multiple steady states.

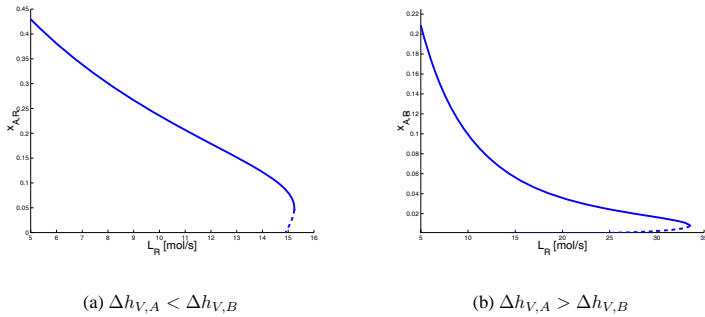


Figure 4.7: Bifurcation diagrams $x_{A,R}(L_R)$ for control structure CS2 and Q_{fl} fixed, parameter values as given in Appendix A.2.2.

Remark: The element J_{22} of the Jacobian in (4.34) determines the stability of the isolated, constantly heated flash with fixed feed $(L_R, x_{A,R})$. In Appendix B.3 it is shown that $J_{22} < 0$ holds independent of the boiling sequence, i.e., the stand-alone, constantly heated flash is always stable, which implies that multiplicities as illustrated in Fig. 4.7 are induced by the recycle.

III) Control structure CS3 with Q_{fl} fixed

The combination of a constantly heated flash and control structure CS3 with fixed F , fixed L_R , and variable holdup leads to the third order system

$$\frac{dn_R}{dt} = F - V_{fl} \quad , \quad (4.36)$$

$$n_R \frac{dx_{A,R}}{dt} = F(x_{A,F} - x_{A,R}) + (L_R - V_{fl})(x_{A,fl} - x_{A,R}) - n_R k x_{A,R} \quad , \quad (4.37)$$

$$n_{fl} \frac{dx_{A,fl}}{dt} = L_R x_{A,R} - (L_R - V_{fl})x_{A,fl} - V_{fl} y_{A,fl} \quad . \quad (4.38)$$

with V_{fl} according to (4.33) and $L_{fl} = L_R - V_{fl}$. The characteristic polynomial of the linearization of this third order system based on the Jacobian J of (4.36)-(4.38) is a third order polynomial

$$q(s) = a_3 s^3 + a_2 s^2 + a_1 s + a_0 \quad . \quad (4.39)$$

As shown in [95], the necessary and sufficient conditions for stability of a general, linear third order system as given in Appendix B.1 then correspond for the given system to the necessary and sufficient conditions

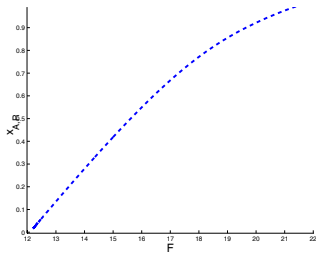
$$tr(J) < 0, \quad det(J) < 0, \quad det(J) - tr(J)(J_{11}J_{33} - J_{13}J_{31}) < 0 \quad (4.40)$$

for stability of (4.36)-(4.38). In the particular case of A being the light boiling component, it holds that

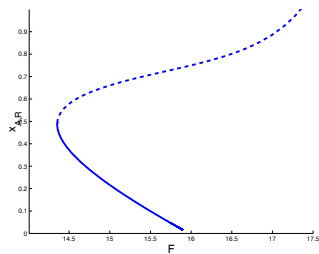
$$\begin{aligned} det(J) &= \frac{L_R k x_{A,R}}{n_R n_{fl}} \frac{dV_{fl}}{dx_{A,fl}} \\ &= -\frac{L_R k x_{A,R}}{n_R n_{fl} \Delta h_{V,fl}} \left(V_{fl} (\Delta h_{V,A} - \Delta h_{V,B}) \frac{dy_{A,fl}}{dx_{A,fl}} + L_R c_P \frac{dT_{fl}}{dx_{A,fl}} \right) \end{aligned} \quad (4.41)$$

is strictly positive for $\Delta h_{V,A} < \Delta h_{V,B}$. That is, in this case, the system definitely has no stable steady state and may exhibit no real bifurcations leading to steady-state multiplicities. For $\Delta h_{V,A} > \Delta h_{V,B}$, no statement regarding the sign of $det(J)$ is possible. This means that no conditions for stability in terms of the parameters can be derived. This is in contrast to the case of A being the heavy boiling component, for which stability is guaranteed for $\Delta h_{V,A} > \Delta h_{V,B}$.

The analytical results are backed by numerical studies. Fig. 4.8(a) displays the unique unstable steady state for $\Delta h_{V,A} < \Delta h_{V,B}$, and Fig. 4.8(b) shows that for $\Delta h_{V,A} > \Delta h_{V,B}$ the system exhibits a limit point and steady-state multiplicity.



(a) $\Delta h_{V,A} < \Delta h_{V,B}$



(b) $\Delta h_{V,A} > \Delta h_{V,B}$

Figure 4.8: Numerical simulation results for control structure CS3 and constantly heated flash, with feed flow rate F as continuation parameter, parameter values as given in Appendix A.2.2.

4.1.3 V_{fl} fixed

Another conceivable flash control strategy is depicted in Fig. 4.9. As always, the liquid effluent stream is the manipulated variable to achieve level control. Moreover, it is now assumed that the flash vapor stream V_{fl} can be directly adjusted by manipulating the flash heating rate.

Note that, at steady state and due to the equimolar reaction, the overall material balance of the plant requires the vapor effluent stream to equal the reactor feed stream F , i.e., $V_{fl} = F$. This implies that these two streams cannot be adjusted independently, and therefore, control structures CS1 and CS3, which both employ a strategy fixing F , are not compatible with a flash control strategy that fixes V_{fl} . Thus, only control structure CS2 will be considered in what follows.

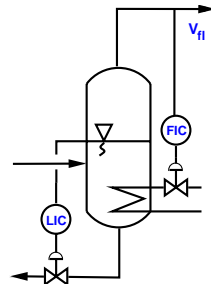


Figure 4.9: Flash with V_{fl} fixed.

Control structure CS2 with V_{fl} fixed

For fixed L_R and V_{fl} , the differential equations describing the system are

$$n_R \frac{dx_{A,R}}{dt} = V_{fl}x_{A,F} + (L_R - V_{fl})x_{A,fl} - L_Rx_{A,R} - n_Rkx_{A,R} \quad , \quad (4.42)$$

$$n_{fl} \frac{dx_{A,fl}}{dt} = L_Rx_{A,R} - (L_R - V_{fl})x_{A,fl} - V_{fl}y_{A,fl} \quad . \quad (4.43)$$

At steady state, eq. (4.42) can uniquely be solved for $x_{A,R}$, and upon substitution into (4.43), $y_{A,fl}(x_{A,fl})$ is obtained as

$$y_{A,fl} = \frac{1}{V_{fl}} \frac{L_R V_{fl} x_{A,F} - (L_R - V_{fl}) n_R k x_{A,fl}}{L_R + n_R k} \quad . \quad (4.44)$$

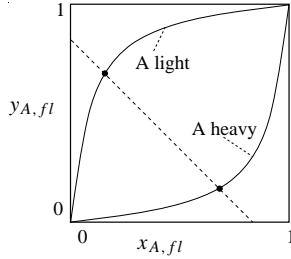


Figure 4.10: McCabe-Thiele diagram including the solution $y_{A,fl}(x_{A,fl})$ from (4.44).

Fig. 4.10 displays this solution $y_{A,fl}(x_{A,fl})$ as the straight dashed line with negative slope in the McCabe-Thiele diagram. The figure also contains the Baly curves representing the vapor-liquid equilibrium compositions in a binary system [77]. As can be seen, for thermodynamically stable systems, the solution of the overall system that corresponds to the intersection between the equilibrium curves and the material balance line given by eq. (4.44) is unique, independent of the boiling sequence and even for mixtures with homogeneous azeotropes.

Moreover, evaluating the trace and the determinant of the system's Jacobian, it is straightforward to show that in both cases the unique solution is stable. Finally, it should be noted that these solutions are feasible, as $x_{A,fl} < x_{A,R} < y_{A,fl}$ for all admissible values $L_R > V_{fl}$.

4.1.4 Summary and interpretation of the results for the ideal binary systems

Table 4.1 summarizes the results derived in the preceding sections and also includes the results for the case of *A* heavy boiling from [95].

Assessing the key findings of the above investigations, the following conclusions are most remarkable and should be borne in mind whenever one has to deal with recycle systems:

- Even though the individual units on their own are stable (see Appendix B.1), **the coupled reactor-separator system with recycle may exhibit instabilities, multiple steady states, and oscillatory behavior.** The origin of these phenomena can therefore clearly be attributed to the impact the recycle has on the overall behavior of the integrated system. This in turn can be explained as a consequence of the positive feedback character of material recycles, as it is well-known that positive feedback in general has a destabilizing effect.
- **A suitable choice for the system's overall control structure is of paramount importance.** Although throughout the presented investigations perfect control, i.e. the most efficient control conceivable in terms of performing setpoint control, has been assumed, many of the possible control structures have turned out to be unsuitable for operation of the simple reactor-separator system. Note that real controllers will have to deal with additional problems, in particular as many recycle systems are non-minimum-phase and show wrong-way behavior.
- **The choice of a suitable control structure depends to a great extent on the physical properties of the components involved.** For example, what may be a good control structure for a system where the reactant is the heavy-boiling component, may be unacceptable for a system with a reverse boiling sequence (see Table 4.1, (p,T)-flash and control structures CS2 and CS3).
- Independent of the boiling sequence, **the flash control strategy with fixed flash heating rate seems most problematic**, as it allows for the largest variety of nonlinear phenomena. This can intuitively be explained with the argument, that this control structure does not fix any of the flash variables, in contrast to the other two flash control strategies. This leaves more degrees of freedom for the flash dynamics, and therefore, the large variability in exhibiting various nonlinear phenomena seems hardly surprising.

- It is remarkable that for the given system design with liquid recycle, the case where (i) reactant A is the light-boiling component seems to be much more difficult to be satisfactorily operated than the system where (ii) A is heavy. Intuitively, this may be attributed to the fact that in case (i), the system design superimposes a non-natural structure that is contrary to the system's inherent physical properties. Typically, to recover a light-boiling component, it intuitively seems much more natural to recycle the vapor stream from the flash, just as is done in case of a liquid recycle of the heavy reactant. Therefore, one could conclude that whenever possible, **a system design should be in line with the physical characteristics of the system's components.**

However, there may be cases where it is necessary for economic reasons to violate this principle guideline. The process of acetic acid production introduced in previous chapters is a classical example, where the primary recycle does not obey this rule of thumb, but is nevertheless required to recover the expensive catalyst. Thus, this example illustrates the fundamental dilemma that in many production processes economic goals and operability issues are in conflict.

Endowed with these fundamental insights into potential patterns of behavior and associated control problems for systems with recycles, focus is next switched to a reactor-separator network in which the reactor is no longer assumed to be isothermal but evaporatively cooled, like in the industrial case study.

<u>Flow control strategy</u>	<u>Flash control strategy</u>					
	(p,T)-Flash		Q_{fl} fixed		V_{fl} fixed	
	A light	A heavy	A light	A heavy	A light	A heavy
F fixed (CS1)	unique, stable, infeasible for small & large F	unique, stable, infeasible, infeasible for small & large F	(i) $T_{fl} < T_R$ and $\Delta h_{V,A} < \Delta h_{V,B}$: unique, stable, infeasible for small F , (ii) Else: instabilities possible	(i) $T_{fl} < T_R$ and $\Delta h_{V,A} > \Delta h_{V,B}$: unique, stable, infeasible for small F . (ii) Else: multiplicities & limit cycles possible	not possible	
L_R fixed (CS2)	unique, unstable, infeasible for small L_R	unique, stable, infeasible for small L_R	Instabilities and multiplicities possible for all parameter combinations	unique, stable, infeasible for small L_R	unique, stable, always feasible for $L_R > V_{fl}$	unique, stable, always feasible for $L_R > V_{fl}$
F and L_R fixed (CS3)	unique, unstable, always feasible	unique, stable, always feasible	(i) $\Delta h_{V,A} > \Delta h_{V,B}$: unique and unstable, (ii) Else: Instability and multiplicities possible	(i) $\Delta h_{V,A} > \Delta h_{V,B}$: unique, stable, infeasible for small and large F_0 . (ii) Else: multiplicities possible	not possible	

Table 4.1: Behavior of the simple reactor-separator system for various combinations of flow and flash control strategies. Depending on the boiling sequence, different control configurations seem more or less favorable. Combinations that are most attractive are highlighted. Results for A heavy boiling are from [95].

4.2 Binary system with an evaporatively cooled reactor, flash separator and liquid recycle

So far, it has been shown that the presence of material and energy recycles can destabilize integrated systems and entail the occurrence of multiple steady states, although the stand-alone process units individually exhibit unique and stable steady states (Section 4.1). Moreover, potential steady-state multiplicities along with a physical interpretation of their origin have been revealed for stand-alone evaporatively cooled reactors (Chapter 3).

Now, the question that naturally arises is concerned with the combined effect of the above phenomena, i.e., what kind of nonlinear behavior may be induced by the interconnection of an evaporatively cooled reactor and a flash separator with a recycle stream from the flash to the reactor?

To answer this question, the next section focusses on the derivation of analytical results for a system configuration where the evaporatively cooled reactor is connected to an isobarically and isothermally operated flash.

The case of a flash control strategy fixing V_{fl} will just be commented on very briefly, while the adiabatic flash operation will be investigated in detail by means of numerical analysis of the industrial case study in Section 4.3.

4.2.1 Evaporatively cooled reactor and (p,T)-flash

Assuming again, as in Chapter 3, that the vapor leaving the evaporatively cooled reactor is completely and instantaneously recycled to the reactor, the mathematical model describing the given reactor separator system is governed by exactly the same set of equations (4.1)–(4.5) as the corresponding system with an isothermal liquid-phase reactor from Section 4.1. In addition, relations describing the vapor-liquid equilibrium between the two thermodynamic phases in the reactor are required. Moreover, the reactor energy balance may be used to determine the vapor flow rate from the reactor. And, most significantly, the reaction rate is now a nonlinear function of both reactant mole fraction and reactor temperature, $r_0 = r_0(x_{A,R}, T_R(x_{A,R}))$.

As explained in Section 3.2, under standard operating conditions the reactor temperature is the boiling temperature and therefore depends on the composition of the reaction mixture. It is due to this dependence, that the analysis turns out to be far more involved than in the preceding section. In order to keep it tractable, the assumptions and derivations

introduced in the analysis of the stand-alone evaporatively cooled reactor from Chapter 3 are carried over and applied to the present case. Thus, there is no need to reiterate the derivation of the model equations here. In addition, it is important to recall that assuming constant pressure and isothermal operation, the composition of a binary flash is fixed, such that the flash is a purely algebraic system. Thus, the dynamics and stability of the given system are completely determined by the scalar reactor material balance for component A .

D) Control structure CS1 and (p,T)-flash

The component material balance for the reactor-separator system with fixed feed, constant holdups and isobaric-isothermal flash operation is

$$\frac{dx_{A,R}}{dt} = \frac{F}{n_R}(x_{A,F} - y_{A,fl}) - k(T_R(x_{A,R}))x_{A,R} := f_{CS1} \quad (4.45)$$

(compare eq. (4.7)). It follows that the eigenvalue of this system is given by

$$\begin{aligned} \lambda_{CS1} &= \frac{df_{CS1}}{dx_{A,R}} = - \left(k(T_R(x_{A,R})) + \frac{\partial k}{\partial T_R} \frac{dT_R}{dx_{A,R}} x_{A,R} \right) \\ &= -k_0 e^{-\frac{E}{RT_R}} \left(1 + \frac{E}{RT_R^2} \frac{dT_R}{dx_{A,R}} x_{A,R} \right) . \end{aligned} \quad (4.46)$$

Obviously, stability hinges on $\frac{dT_R}{dx_{A,R}}$. If A is the heavy boiling component, then $\frac{dT_R}{dx_{A,R}} > 0$. This yields $\lambda_{CS1} < 0$, and therefore this configuration will always be stable. On the other hand, if A is the light boiling component as in the industrial case study, then $\frac{dT_R}{dx_{A,R}} < 0$, i.e. λ_{CS1} may be positive and there is potential instability in this case.

To study in-depth the situation where A is more volatile, it is most helpful to resort to the type of analysis presented in detail in Section 3. Relying on the same simplifying assumptions as employed in the derivation of the simplified component material balance of the evaporatively cooled reactor in Section 3.2, and making use of the definitions (3.15)-(3.17), and in particular of relation (3.18), the simplified component material balance for the combined system of the evaporatively cooled reactor and the (p,T)-flash is given by

$$\frac{n_R}{F} \frac{dx_{A,R}}{dt} = (x_{A,F} - y_{A,fl}) - \frac{Dax_{A,R}}{(1 + \beta x_{A,R})^\alpha} . \quad (4.47)$$

The steady states of this system are given as the intersections of the supply line SL

$$SL = (x_{A,F} - y_{A,fl}) \quad (4.48)$$

and the consumption curve RC

$$RC = \frac{Da x_{A,R}}{(1 + \beta x_{A,R})^\alpha} \quad , \quad (4.49)$$

as depicted in Fig. 4.11. Obviously, and in line with the findings for the stand-alone evaporatively cooled reactor, also the system with an additional (p,T)-flash and recycle may exhibit multiple steady states only if the reaction curve has an extremum. This coincides with the requirement that the self-inhibition of the reaction mechanism represented by the parameter α is larger than the order of the reaction rate's concentration dependency. Given $\alpha > 1$ in case of a first order reaction, up to two steady states are feasible if the

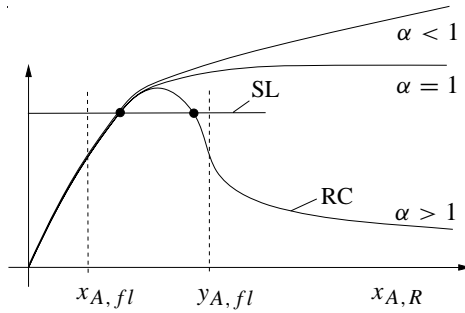


Figure 4.11: Supply line SL and reaction curve RC for the reactor-separator system involving an evaporatively cooled reactor and a (p,T)-flash with liquid recycle. Up to two steady states are possible if the necessary condition $\alpha > 1$ is fulfilled.

following conditions are complied with:

1. The derivative of the consumption curve with respect to $x_{A,R}$

$$\frac{dRC}{dx_{A,R}} = \frac{Da[\beta x_{A,R}(1 - \alpha) + 1]}{(1 + \beta x_{A,R})^{\alpha+1}} \quad , \quad (4.50)$$

has to be equal to zero for some $x_{A,R}^*$ in the feasible range $[x_{A,fl}, y_{A,fl}]$, otherwise at least one steady state is outside this feasible range. The extremum in RC occurs for

$$x_{A,R}^* = \frac{1}{\beta(\alpha - 1)} \quad . \quad (4.51)$$

Note that $RC > 0 \forall x_{A,R} > 0$, $\frac{dRC}{dx_{A,R}} > 0 \forall x_{A,R} < x_{A,R}^*$, $\frac{dRC}{dx_{A,R}} < 0 \forall x_{A,R} > x_{A,R}^*$. This guarantees that there is only the single extremum $x_{A,R}^*$. For $\beta > 0$, it holds that $x_{A,R}^* > x_{A,fl}$ if

$$\beta < \frac{1}{(\alpha - 1)x_{A,fl}} := \beta_1^* \quad , \quad (4.52)$$

and $x_{A,R}^* < y_{A,fl}$ if

$$\beta > \frac{1}{(\alpha - 1)y_{A,fl}} := \beta_2^* \quad . \quad (4.53)$$

That is, for $\beta_2^* < \beta < \beta_1^*$, the extremum in RC is within the feasible range.

2. This extremum has to be above the supply line, i.e.,

$$RC(x_{A,R}^*) > SL \quad , \quad (4.54)$$

where

$$RC(x_{A,R}^*) = \frac{Da(\alpha - 1)^{\alpha-1}}{\beta\alpha^\alpha} \quad .$$

Thus, for (4.54) to hold, i.e., to allow for an intersection of RC and SL corresponding to a steady state in the case $\alpha > 1$, it is necessary that

$$Da > (x_{A,F} - y_{A,fl}) \frac{\beta\alpha^\alpha}{(\alpha - 1)^{\alpha-1}} =: Da_1^* \quad . \quad (4.55)$$

For $Da = Da_1^*$, the reaction curve is tangent to the supply line and there is exactly one steady state.

3. In case the above conditions are fulfilled, it remains to be checked whether indeed both intersections are in the feasible range. For the low conversion steady state to be feasible (i.e., for an intersection of RC and SL for values $x_{A,R} \leq y_{A,fl}$), it must hold that

$$RC(x_{A,R} = y_{A,fl}) = \frac{D\alpha y_{A,fl}}{(1 + \beta y_{A,fl})^\alpha} < x_{A,F} - y_{A,fl} = SL \quad . \quad (4.56)$$

This equates to

$$Da < \frac{(1 + \beta y_{A,fl})^\alpha (x_{A,F} - y_{A,fl})}{y_{A,fl}} =: Da_3^* \quad . \quad (4.57)$$

The corresponding condition for the high conversion steady state to be feasible is $RC(x_{A,R} = x_{A,fl}) < SL$, i.e.

$$Da < (1 + \beta x_{A,fl})^\alpha \frac{x_{A,F} - y_{A,fl}}{x_{A,fl}} =: Da_2^* \quad . \quad (4.58)$$

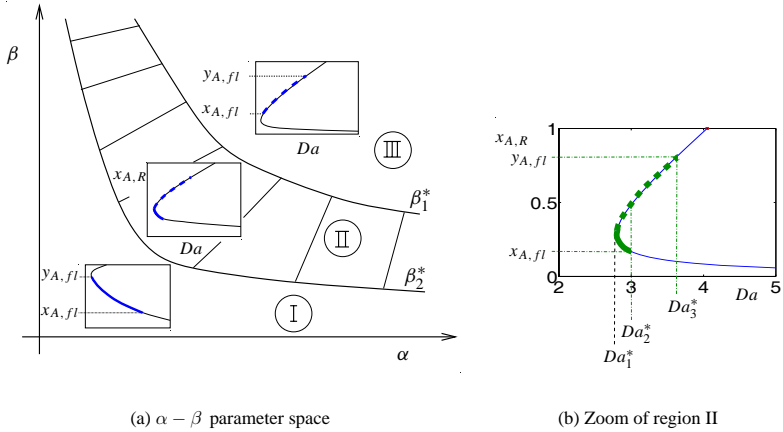


Figure 4.12: Bifurcation diagrams for the binary reactor-separator system involving an evaporatively cooled reactor and a (p,T)-flash for control structure CS1 in the different regions of the $\alpha - \beta$ parameter space.

Fig. 4.12 summarizes the steady-state features of the given system for different regions of the parameter space:

- For $\beta < \beta_2^*$, region I, only a single, stable high-conversion steady state is feasible for Damkoehler values $Da_2^* < Da < Da_3^*$.
- For $\beta_2^* < \beta < \beta_1^*$, region II, steady-state multiplicity may be encountered in a certain range of Damkoehler values:
 1. For $Da < Da_1^*$, no steady state is feasible (RC is located below SL in Fig. 4.11 for all $x_{A,R}$).
 2. For $Da_1^* < Da < Da_2^*$, two steady states are feasible. The high conversion steady state is stable, the low conversion steady state is unstable according to the slope condition.
 3. For $Da_2^* < Da < Da_3^*$, only the unstable low-conversion steady state is feasible.
 4. For $Da > Da_3^*$, there are no feasible steady states (both intersections of RC and SL in Fig. 4.11 are outside the feasible range).

- For $\beta > \beta_1^*$, region III, only an unstable low-conversion steady state is feasible for Damkoehler values $Da_2^* < Da < Da_3^*$.

For a **physical interpretation of these formal results**, it is interesting to compare the nonlinear characteristics of the given system with the two systems that may be regarded as limits of this system: In Section 4.1, it has been shown that an isothermally operated reactor connected to a (p,T)-flash with liquid recycle does not exhibit steady-state multiplicities, i.e., the positive feedback effect introduced by the material recycle is not strong enough to destabilize the system. On the other hand, the non-isothermal, evaporatively cooled reactor in stand-alone mode may feature up to three steady states (cf. Section 3.2). Thus, it is plausible to infer that the multiplicities encountered for the present system are to be attributed to the self-inhibitory mechanism of the temperature-dependent reaction rate. However, in contrast to the stand-alone reactor, the present specific control configuration fixes both the concentration of the recycle stream and the overall conversion of the integrated system. Thereby, the combined supply and subtraction of reactant within the reactor becomes independent of the actual one-pass conversion of the reactor (the supply line SL is no longer a function of reactant mole fraction $x_{A,R}$, but a constant). This reduces the variability of the nonlinear characteristics of the system. More specifically, the low-conversion steady-state of the stand-alone reactor becomes infeasible, as the liquid flash recycle contains a certain amount of heavy product, which results in a higher product concentration in the reactor and leads to an increase of the reactor boiling point temperature. This in turn increases the temperature-dependent reaction rate and guarantees a certain minimum conversion, such that the low-conversion (wash-out) steady state of the stand-alone reactor is infeasible in the given recycle system.

In other words: The constraints imposed by the separator on the behavior of the integrated system render one of the isolated reactor's solution branches infeasible.

II) Control structure CS2 and (p,T)-flash

In analogy to eq. (4.13) from the previous section, the governing scalar differential equation in this case is

$$\frac{dx_{A,R}}{dt} = \frac{L_R(x_{A,F} - y_{A,fl})}{n_R(y_{A,fl} - x_{A,fl})} (x_{A,R} - x_{A,fl}) - k(T_R(x_{A,R}))x_{A,R} \quad (4.59)$$

Relying on the same assumptions and derivations as above, and upon redefining the Damkoehler number Da as

$$Da := \frac{n_R k_0}{L_R} \left(\frac{p}{p_0} \right)^\alpha e^{-\frac{E}{RT_{SN,B}}} \quad (4.60)$$

equation (4.59) can be rewritten as

$$\frac{n_R}{L_R} \frac{dx_{A,R}}{dt} = \underbrace{\frac{(x_{A,F} - y_{A,fl})}{(y_{A,fl} - x_{A,fl})}}_{SL} (x_{A,R} - x_{A,fl}) - \underbrace{Da \frac{x_{A,R}}{(1 + \beta x_{A,R})^\alpha}}_{RC}. \quad (4.61)$$

For **A light boiling**, the supply line SL has a positive slope and is negative for $x_{A,R} = 0$ (see Fig. 4.13). Moreover, from

$$\frac{d^2 RC}{dx_{A,R}^2} = \frac{Da\alpha\beta[\beta x_{A,R}(\alpha - 1) - 2]}{(1 + \beta x_{A,R})^{\alpha+2}},$$

it follows that $d^2 RC/dx_{A,R}^2 < 0$ for $x_{A,R} < \frac{2}{\beta(\alpha-1)} = 2x_{A,R}^*$ and

$d^2 RC/dx_{A,R}^2 > 0$ for $x_{A,R} > 2x_{A,R}^*$.

This guarantees that there is at most one intersection between SL and RC , corresponding to a unique steady state.

This steady state is always unstable due to the slope condition and feasible for $RC(x_{A,R} = y_{A,fl}) < SL(x_{A,R} = y_{A,fl})$, i.e., for $Da < \frac{x_{A,F} - y_{A,fl}}{y_{A,fl}} (1 + \beta y_{A,fl})^\alpha$.

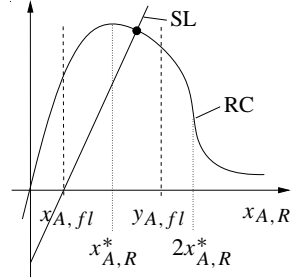


Figure 4.13: SL and RC for A light boiling.

For **A heavy boiling** ($\beta \in (-1, 0)$), the slope of the supply line is negative,

and $\frac{dRC}{dx_{A,R}} > 0 \forall x_{A,R} > x_{A,R}^*$, with $x_{A,R}^* < 0$ in this case (see Fig. 4.14).

Thus, there is a unique stable steady state, which is feasible if $RC(x_{A,R} = y_{A,fl}) < SL(x_{A,R} = y_{A,fl})$, corresponding to

$$Da < \frac{x_{A,F} - y_{A,fl}}{y_{A,fl}} (1 + \beta y_{A,fl})^\alpha.$$

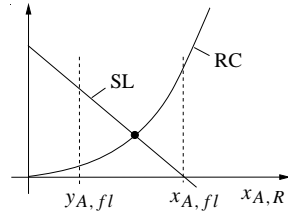


Figure 4.14: SL and RC for A heavy boiling.

III) Control structure CS3 and (p,T)-flash

For this system, the same set of equations (4.18) and (4.19) as in the case with the pure liquid reactor applies. Due to the temperature dependence of the reaction rate

$r_0 = k(T_R(x_{A,R}))x_{A,R}$, however, the element J_{11} of the Jacobian (4.20) of this non-isothermal system at steady state is now

$$\frac{\partial f_1}{\partial x_{A,R}} = \frac{L_R y_{A,fl} - x_{A,R}}{n_R x_{A,fl} - y_{A,fl}} - \left(\frac{\partial k}{\partial T_R} \frac{dT_R}{dx_{A,R}} x_{A,R} + k \right) .$$

This leads to

$$tr(J) = \frac{\partial f_1}{\partial x_{A,R}} , \quad (4.62)$$

$$det(J) = \frac{k x_{A,R}}{n_R} \frac{L_R}{x_{A,fl} - y_{A,fl}} . \quad (4.63)$$

If the reactant A is the light boiling component, no statement about the sign of $tr(J)$ is possible. However, $det(J) < 0$, and thus this configuration is always unstable and each steady state is a saddle point (see also Appendix B.1.2).

Note that for A heavy boiling, it holds that $det(J) > 0$ and $tr(J) < 0$ at steady state, indicating stability of the configuration. By means of the Lemma from Appendix B.2, the stable steady state is unique and it is straightforward to also prove its feasibility.

In terms of steady-state supply lines and reaction curves, control structures CS2 and CS3 are equivalent (cf. Figs. 4.13 and 4.14). As the system describing CS2 is scalar, the derived static stability considerations also imply dynamic stability and, respectively, instability. In contrast, for CS3 and A heavy boiling, the static stability inferred from Fig. 4.14 is only necessary for dynamic stability, which rigorously follows from consulting the system's eigenvalues.

Summary: Binary evaporatively cooled reactor and (p,T)-flash

In principle, for A light boiling, the self-inhibition of the reaction mechanism may cause multiplicities also in the system with liquid flash recycle. However, the system integration with the (p,T)-flash and liquid recycle superimposes an overall stoichiometry that alters the overall supply of reactant A to the reactor. As explained in detail above, employing control structure CS1 renders the supply independent of the conversion and reduces the number of possible steady states to two. Additionally fixing the internal flow rate L_R as in control structures CS2 and CS3, leads to a situation where a decreasing conversion increases the supply of reactant to the reactor. Thus, there clearly is a positive feedback effect that destabilizes any steady state and at the same time rules out any potential for multiplicities. Figure 4.15 summarizes the effects of the different control structures on

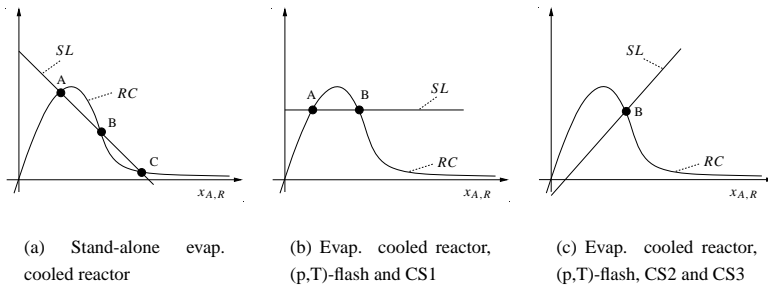


Figure 4.15: Steady-state multiplicity features of a binary system involving an evaporatively cooled reactor and a (p,T)-flash with liquid recycle, and with $\alpha > 1$ and reactant A the far more volatile component: (a) The stand-alone reactor exhibits three steady states A,B,C. Clearly, the higher the conversion (i.e., the smaller $x_{A,R}$), the larger the relative supply of reactant A as only small amounts of A are withdrawn from the reactor while the reactor feed is constant. (b) For control structure CS1 in the coupled system, the supply becomes independent of the conversion and this recycle effect rules out the low conversion steady state C. (c) For control structures CS2 and CS3, the recycle leads to a supply line that decreases with conversion and rules out both the low and high conversion steady states A and C, leaving over the unstable steady state at intermediate conversion, B.

the multiplicity features of the given recycle systems.

In contrast, for A heavy boiling, the stand-alone evaporatively cooled reactor always has a unique solution, and also the recycle in the integrated system featuring a (p,T)-flash and an isothermal reactor does not introduce steady-state multiplicities for any of the control structures. Thus, there is no positive feedback mechanism that may destabilize the combined system, such that in this case uniqueness and stability are guaranteed.

4.2.2 Flash control strategies with Q_{fl} fixed and V_{fl} fixed

As the temperature as well as the liquid and vapor compositions in the constantly heated flash are no longer constant but instead variable, *analytical* results for the reactor-separator system with an evaporatively cooled reactor and a flash with Q_{fl} fixed are hardly viable. Therefore, within this thesis, investigations of these systems will be restricted to a *numerical* analysis of the reactor-separator system of the industrial case study in Section

4.3. This practical example involves an adiabatic flash, i.e. a special case of a constantly heated flash with $Q_{fl} = 0$, that is often encountered in industrial plants.

As far as a flash control strategy relying on a fixed vapor flow rate is concerned, it holds that also here the balance equations (4.42) and (4.43) derived for the respective system with control structure CS2 in Section 4.1 are applicable. With the same arguments as there, also the recycle system with control structure CS2 and an evaporatively cooled reactor exhibits just one steady state. Without going into details of the straightforward derivations, it can easily be shown that here the necessary (yet not sufficient) condition both for $\det(J) < 0$ and $\text{tr}(J) > 0$ is

$$\frac{dT_R}{dx_{A,R}} < -\frac{RT_R^2}{E_a x_{A,R}}. \quad (4.64)$$

This condition can never be fulfilled for systems where A is the heavy boiling component. For typical binary systems where A is light boiling, it still is a very harsh condition that is very unlikely to be encountered in practice except for systems, where the effect of A on the system's boiling point temperature is huge.

Thus, it can be concluded that also in the case of a recycle system with an evaporatively cooled reactor, control structure CS2 in combination with a flash control strategy that fixes the flash vapor flowrate seems very attractive in terms of unique and stable operation, provided the feed flow rate is the manipulated variable used to control the reactor holdup. This theoretical result should be borne in mind, as it will be the basis for the derivation of a plantwide control structure for the industrial case study in Chapter 6.

4.2.3 Summary for recycle systems involving a two-phase reactor

The investigations of the integrated system involving an evaporatively cooled reactor and a flash with liquid recycle have revealed that the behavior of such a system is governed by a **combination of the effects** encountered for the stand-alone two-phase reactor and the simple isothermal recycle system.

In particular, if neither the recycle nor the inhibitory reaction mechanism in the two-phase reactor introduce instability and multiplicity of steady states, then also the coupled system features merely unique and stable steady states, as in all combinations where A is heavy boiling.

On the other hand, it has been shown how the introduction of the flash recycle alters the behavior of the evaporatively cooled reactor. For the case of a (p, T) -flash, the effect of

the recycle was the disappearance of either one or two of the isolated reactor's steady states. Just as well one could expect the introduction of further steady states in addition to the reactor's three stationary solutions due to the combination of effects from the two-phase reactor and the liquid recycle. A natural candidate for such a phenomenon is the system involving an evaporatively cooled reactor and a constantly heated flash, as such recycle systems display steady-state multiplicity even in case of isothermal one-phase reactor operation (see Section 4.1.4).

As already mentioned above, the analytical investigation of these systems is extremely difficult, and therefore numerical studies of the industrial production plant in the following section are presented instead.

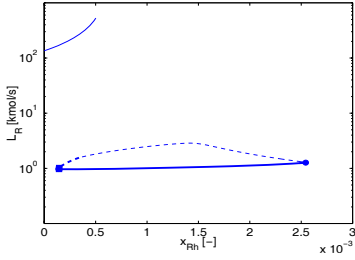
4.3 Industrial example

In this section, the reaction system of the acetic acid production plant is investigated in detail by means of numerical continuation studies. The flash is assumed to be operated adiabatically just like in the actual industrial process, and focus is on the impact of the three flow-control strategies CS1, CS2, and CS3 on the coupled system's behavior.

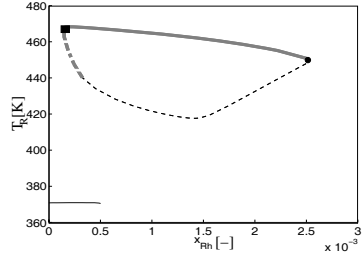
4.3.1 Control structure CS1

Figure 4.16 displays the results of numerical continuation studies for the industrial case study's reaction system operated with control structure CS1, i.e. the 'basecase control structure' as introduced in Section 2.1. As can be seen, there is an isola of steady-state solutions, with a stable two-phase branch for small values of the reactor effluent stream L_R , and an unstable branch for larger values of L_R , that is basically one-phase except for small values of the continuation parameter x_{Rh} . In addition, there exists a pure liquid-phase solution for very small values of x_{Rh} , featuring huge values of L_R (note the logarithmic ordinate in Fig. 4.16(a)). Obviously, this third solution is characterized by extremely large flow rates around the recycle loop, and is therefore not feasible in the real plant.

To better understand the origin of these steady-state characteristics of the coupled reactor-separator system and how they evolve from the isolated reactor's behavior captured in Fig. 3.7, it is most helpful to employ the additional model shown in Fig. 4.17.



(a) Reactor effluent stream L_R



(b) Reactor temperature T_R

Figure 4.16: Steady states of the industrial case study's reaction system operated with control structure CS1. Recall that thick lines indicate that the respective steady state is two-phase, while thin lines correspond to pure liquid phase steady states. Moreover, solid lines mark stable steady states, while dashed lines mark unstable steady states.

This virtual mixer allows to continuously close the recycle loop from the flash to the reactor by providing a mixture of the actual flash recycle $\{L_{fl}, x_{i,fl}, T_{fl}\}$ and a fixed feed $\{F_{fl,S}, x_{i,fl,S}, T_{fl,S}\}$, which corresponds to the flash quantities under standard operating conditions. The static virtual mixer is described by the following set of equations:

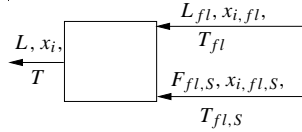


Figure 4.17: Virtual mixer.

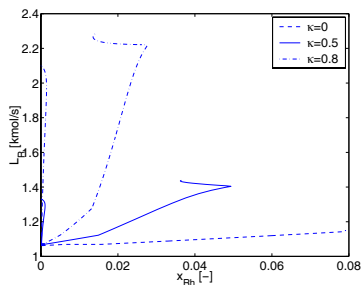
$$\begin{aligned}
 0 &= \kappa L_{fl} + (1 - \kappa) F_{fl,S} - L \quad , \\
 0 &= \kappa L_{fl} x_{i,fl} + (1 - \kappa) F_{fl,S} x_{i,fl,S} - L x_i \quad , \quad i = 1, \dots, NC - 1 \quad , \\
 0 &= 1 - \sum_{i=1}^{NC} x_i \quad , \\
 0 &= \kappa L_{fl} \sum_{i=1}^{NC} x_{i,fl} h_i(T_{fl}) + (1 - \kappa) F_{fl,S} \sum_{i=1}^{NC} x_{i,fl,S} h_i(T_{fl,S}) - L \sum_{i=1}^{NC} x_i h_i(T) \quad .
 \end{aligned}$$

Obviously, this mixer has no real-world counterpart and is a feature of the simulation

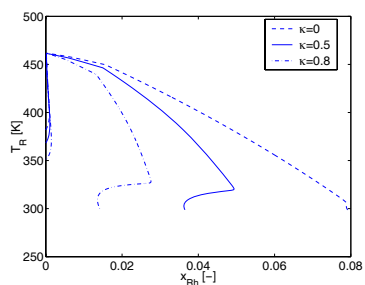
model only, but it nevertheless is of great explanatory use for understanding the evolution of the coupled system's characteristics from those of the stand-alone reactor. Clearly, $\kappa = 0$ corresponds to the case where the recycle is fully open and only fixed feed is supplied, while $\kappa = 1$ corresponds to the case where the recycle is completely closed. Based on this enhanced model of the reaction system, Figures 4.18 and 4.19 visualize the evolution of the isola in the coupled system from the steady-state characteristics of the stand-alone reactor.

Recalling the results from Section 3.3, Fig. 4.18 shows the two hysteresis curves of the isolated, evaporatively cooled reactor in the two-phase regime for very small values of x_{Rh} and in the one-phase regime for large values of x_{Rh} ($\kappa = 0$, dashed lines). Moreover, it can be seen how the one-phase hysteresis becomes more pronounced the further the flash recycle is closed. Once the recycle is almost closed ($\kappa \approx 0,915$), the two hystereses join to form the isola, and the isolated solution branch at higher reactor effluent rates and lower reactor temperatures (see Fig. 4.19) 'is born'.

It is noteworthy to observe by how much the final complete closing of the recycle increases the value L_R of the isolated solution branch. Although already in the simulation results for $\kappa = 0,9175$ and depicted in Fig. 4.19 the recycle is almost completely closed and thus only a very small external feed stream is provided, the substitution of this tiny external feed by the complete closing of the recycle results in an increase of L_R by a factor 40. This may be interpreted as a lucid example for the sensitivity of recycle systems to parameter variations as described in Section 2.6.1.

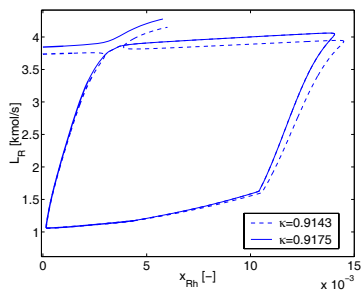


(a) Reactor effluent stream L_R

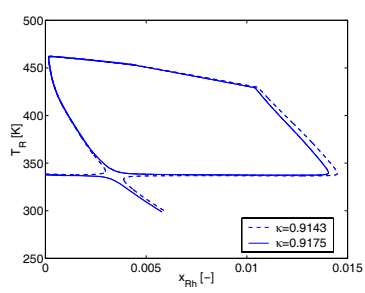


(b) Reactor temperature T_R

Figure 4.18: Evolution of the bifurcation diagrams for the reaction system operated with control structure CS1. While sequentially closing the flash recycle, the second hysteresis becomes increasingly pronounced.



(a) Reactor effluent stream L_R



(b) Reactor temperature T_R

Figure 4.19: Evolution of the bifurcation diagrams for the reaction system operated with control structure CS1 while sequentially closing the flash recycle: ‘Birth’ of the isola and the isolated solution branch.

4.3.2 Control structure CS2

In contrast to the basecase control structure studied in the previous section, where reactor level control is achieved by means of the reactor effluent stream, the external feed stream R_1 is used in control structure CS2 to keep the reactor level constant, see Fig. 4.20. In

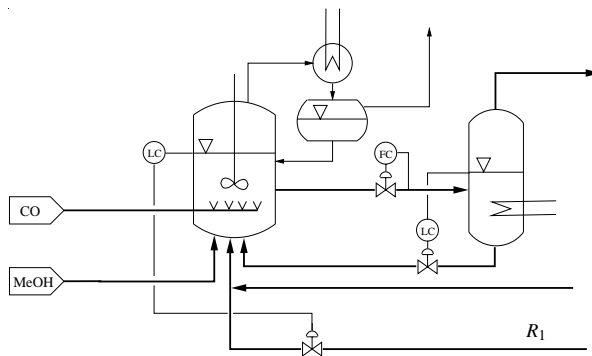


Figure 4.20: Control structure CS2 for the reaction system of the acetic acid production process. The recycle stream R_1 employed to control the reactor volume is an external feed to the isolated reaction system. In the overall plant operated with control structure CS2, the distillate stream from the second column is the manipulated variable for controlling the reactor volume, in contrast to the basecase control structure captured in Fig. 2.1, where this distillate stream is flow-controlled.

the overall plant, this recycle stream is the sum of the aqueous recycle from the decanter and the distillate stream from the second column, i.e., the modified plantwide control structure CS2 involves a modified operation of the second column, with the distillate stream no longer fixed, but serving as the manipulated variable to control the reactor level instead.

The results of a continuation in x_{Rh} for the reaction system operated with control structure CS2 are depicted in Fig. 4.21. Fig. 4.22 shows the evolution of the steady states from the respective stand-alone reactor's steady states by sequential closing of the recycle analogous to the previous section. In particular, it can be seen that just like for control structure CS1, an isola is about to develop from the two hystereses of the isolated reactor. However, before the two hystereses can join, the recycle stream R_1 used to control the

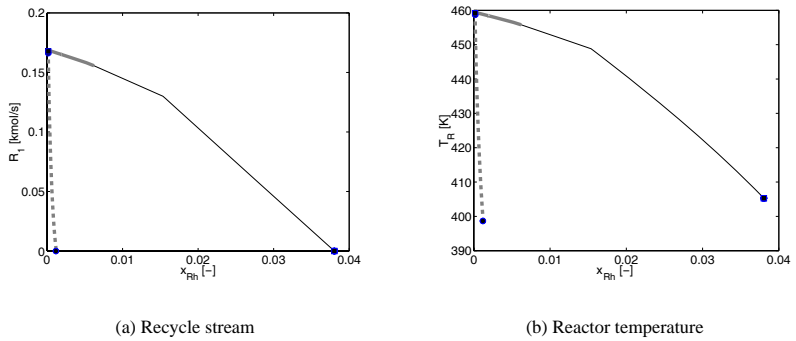


Figure 4.21: Steady states of the industrial case study's reaction system operated with control structure CS2 for a continuation in x_{Rh} .

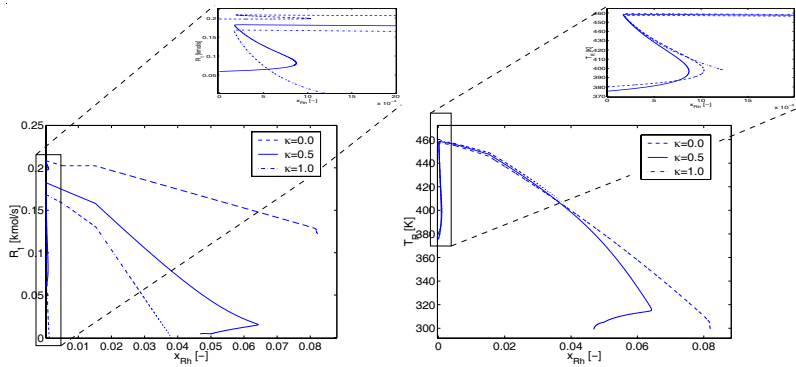


Figure 4.22: Evolution of the bifurcation diagrams for the reaction system operated with control structure CS2 while sequentially closing the flash recycle.

reactor level becomes zero, and the respective branches of steady states are cut off. This can best be seen from the zooms of the region with small values of x_{Rh} in Fig. 4.22.

Compared to control structure CS1, this second control structure is characterized by a much larger region with a unique stable steady state, and a comparatively small region with two steady states. Moreover, there is no isolated solution branch corresponding to the large recycle solution observed for CS1.

To complete the investigations of the system's steady-state characteristics, a model must be employed that allows for a variable reactor holdup in case the recycle stream can no longer keep the level constant, as this would require infeasible negative values $R_1 < 0$. Fig. 4.23 displays the results of a continuation study for such a system with potentially variable reactor volume and the reactor effluent stream as the continuation parameter. Note that choosing L_R as continuation parameter is particularly favorable, as it is a variable that can be directly manipulated for the given control structure (and in contrast to control structure CS1, where it is the manipulated variable to control the reaction volume).

To better understand the simulation results, first consider subfigure 4.23 (c), displaying the continuation results for the recycle stream R_1 . Obviously, the stationary solutions on

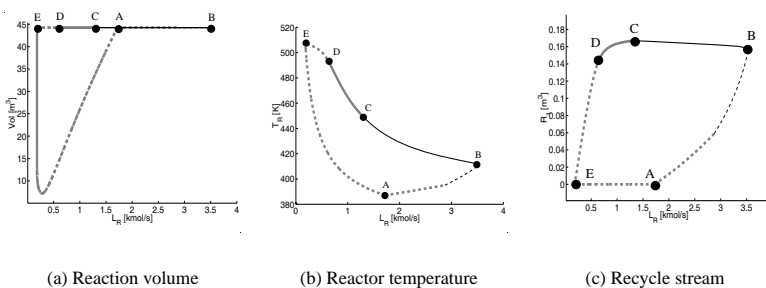


Figure 4.23: Steady states of the industrial case study's reaction system with control structure CS2 for variations in the reactor effluent stream L_R .

the curve from A to E via B, C and D are steady states for which a positive recycle stream $R_1 > 0$ is capable of controlling the reaction volume to setpoint, see subfigure 4.23 (a). Clearly, these steady states qualitatively correspond to the solutions for the continuation in x_{Rh} as depicted in Fig. 4.21. Just like there, for low Damkoehler numbers (i.e., small

values of x_{Rh} or, respectively, large values of L_R), an unstable low conversion branch of solutions with low temperatures (steady states between A and B in subfigure 4.23 (b)) coexists with a branch of stable solutions at higher conversion and higher temperatures ('left' to B). This latter branch of stable steady states is one-phase for large values of L_R and still comparatively moderate temperatures (B to C), it turns two-phase for smaller values of L_R and higher temperatures (C to D), and finally loses stability (beyond D). These unstable steady states are characterized by a constant decrease of the recycle flow rate in order to compensate the decrease in L_R , up to the point where R_1 vanishes (E). For even smaller values of L_R the reaction volume increases dramatically, as less material is withdrawn than supplied (not shown in Figs. 4.23 (a)-(c)).

In contrast, for increasing values of L_R with $R_1 = 0$, the reaction volume initially drops off sharply due to the increased withdrawal of material at high temperatures and high reaction rates. However, with further increasing L_R , the temperature and the reaction rate decrease, leading to an increase of the reaction volume due to lower conversion and increased flash recycle up to the volume's setpoint (achieved at steady state A). Here, the isola of steady-state solution closes, and beyond A, a positive $R_1 > 0$ can again compensate the increased material withdrawal via L_R .

Summarizing, also control structure CS2 exhibits an isola of steady state solutions, but in contrast to CS1, there exists no isolated solution branch with huge internal flowrates. Instead, fixing the reactor effluent stream excludes the potential for accumulation in internal streams, rendering control structure CS2 more attractive in terms of plant operation than control structure CS1. Only for operating parameters that make the operation of the 'original' control structure CS2 (i.e., with a fixed, controlled reactor volume) infeasible, accumulation or depletion of the reactor holdup may occur. This, however, may easily be avoided by employing only admissible reactor effluent streams.

The following subsection will investigate whether control structure CS3 yields an even more favorable system behavior.

4.3.3 Control structure CS3

Finally, as in the previous sections, also for the industrial case study the third flow-control structure with fixed feed, fixed effluent stream, and variable holdup as captured in Fig. 4.24 is investigated.

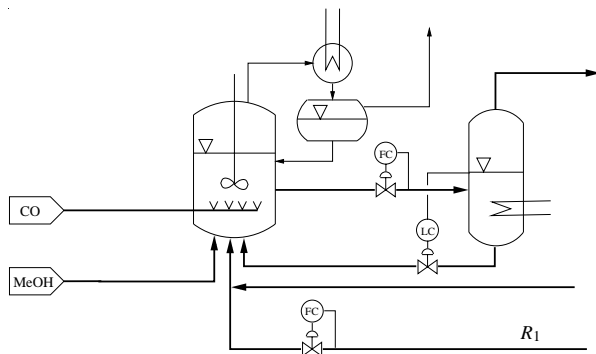


Figure 4.24: Control structure CS3 for the reaction system of the acetic acid production process. The reaction volume is not controlled and thus variable, and the recycle stream R_1 is flow-controlled as well as the external feeds to the reactor. In the overall plant operated with control structure CS3, the distillate stream from the second column is flow-controlled, just like in the basecase control structure captured in Fig. 2.1.

Fig. 4.25(a) displays the volume of the system's reaction mixture at steady state as a function of the reactor effluent stream L_R . As can be seen, the system may in principle be operated in a certain feasible range $L_R \in [L_{R,min}, L_{R,max}]$. For values of the operating parameter $L_R < L_{R,min}$, i.e., if not enough reaction mixture is withdrawn, accumulation in the reactor would require unrealistically large reactors. On the other hand, beyond the upper boundary $L_R > L_{R,max}$, too much reaction mixture would be withdrawn and the reactor would run empty. Moreover, within this feasible range, only a small range is acceptable for standard operation, as other values of L_R are either simply too large for standard operating conditions, or would require a really large reactor, which is also not desirable². Therefore, focus from here on is on the behavior of the given control structure within the feasible and acceptable range, as indicated in Fig. 4.25(b) and the zoomed part

²The volume of the reactor from the plant in Sewerodonetsk is about 45 m^3 .

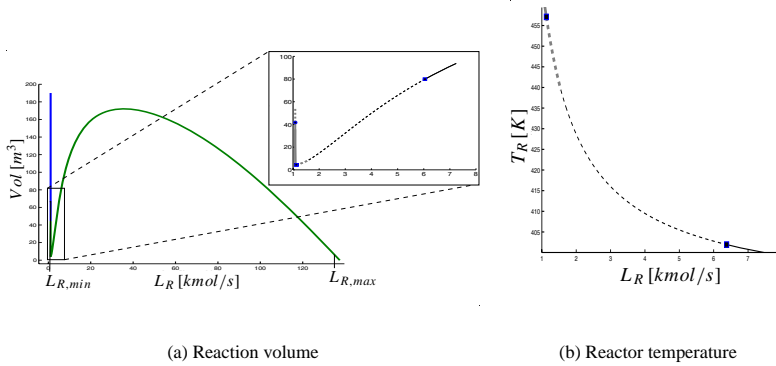


Figure 4.25: Reaction volume and reactor temperature of the acetic acid production plant's reaction system operated with control structure CS3, for variations in the reactor effluent stream L_R .

of Fig. 4.25(a). Within this range, the unique steady state loses its stability at two Hopf bifurcation points. The zoom in Fig. 4.25(a) and Fig. 4.25(b) capture the system's behavior in about the same range of the continuation parameter L_R . It can be inferred that beyond the supercritical Hopf point for small values of the reactor effluent stream L_R , the two-phase steady state is an unstable focus that coexists with a stable relaxation oscillation. Fig. 4.26 shows an example of these relaxation oscillations for $L_R = 3.0$ kmol/s. Note that although the unstable steady state for this value of L_R is purely one-phase, the oscillations briefly dip into the two-phase regime, and for small time intervals a vapor stream leaves the reactor. Beyond $L_R > 3.31$ kmol/s, also the relaxation oscillations become purely one-phase. An example is Fig. 4.27 for $L_R = 4.0$ kmol/s. A comparison of the two figures also indicates that the smaller L_R , the more pronounced the relaxation oscillations are.

To understand this phenomenon and the physical origin of the oscillations, a deeper inspection of the simulation results in Fig. 4.27 proves helpful.

Starting at t_1 , it can be observed that the temperature-dependent reaction rate has reached a minimum corresponding to the minimum in the reactor temperature. However, the low reaction rate has led to an accumulation of the reactants methanol (solid line in the corresponding subfigure) and CO (dashed lines) in the reactor. Once a certain threshold is reached, the large amount of reactants ignites the reaction and leads, together with the

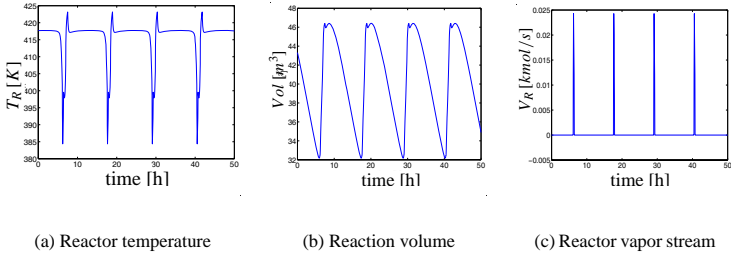


Figure 4.26: Relaxation oscillations of the industrial case study's reaction system operated with control structure CS3, for $L_R = 3.0$ kmol/s.

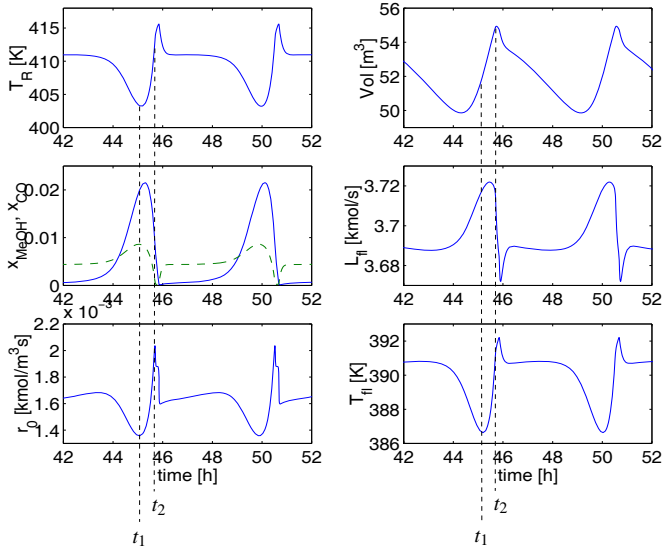


Figure 4.27: Relaxation oscillations for $L_R = 4.0$ kmol/s. From top to bottom, (i) first column: reactor temperature T_R , reactant mole fractions x_{MeOH} (solid) and x_{CO} (dashed), reaction rate r_0 , (ii) second column: reaction volume, flash effluent stream L_{fl} , and flash temperature T_{fl} .

rising temperature, to a reaction burst, that is driven by thermokinetic self-acceleration. Briefly after the peak in the reaction rate is reached at time instant t_2 , the reactor temperature reaches its maximum, while both reactants have almost completely been converted. Following the fast reaction dynamics is the comparatively slow process of reactant re-accumulation. As CO is supplied over-stoichiometrically, it initially accumulates faster than methanol, but then reaches a smaller maximum. This is because much more of the unconverted CO leaves the system via the flash vapor stream, while most of the unconverted methanol is kept within the system and recycles with the liquid flash stream to the reactor. Once enough reactants have accumulated, a new reaction burst is ignited and the cycle starts all over again.

The dynamics of the flash temperature follow those of the reactor temperature with a small time lag. As the flash temperature determines via the energy balance the flash vapor flowrate, and because of the assumption of a constant flash holdup, every increase in flash temperature is accompanied by a decrease in liquid flash recycle rate, and vice versa. Obviously, the reaction volume in the reactor is to a large extent influenced by the varying flash recycle rate and follows changes of the latter with a certain time lag (volume effects due to the non-equimolar reaction are by far less significant).

These considerations clearly indicate that the observed **relaxation oscillations are caused by an interplay between fast reaction dynamics and slow accumulation dynamics**. The latter are proportional to the operating parameter L_R and determine the rate of reactant accumulation. This also explains, why for small values of L_R , the period of the oscillations increases, while the reaction bursts become faster and more intense, resulting in larger amplitudes of the oscillations (compare Figs. 4.26 and 4.27).

On the other hand, for large L_R , the relative effect of the reaction bursts is smoothed out by the comparatively larger flow and accumulation effects, which are accompanied by smaller amplitudes and periods. This becomes most obvious for large values of L_R close to the second Hopf bifurcation point. Here, smooth oscillations corresponding to stable limit cycles prevail.

A deeper inspection of this transient from regions with relaxation oscillations to regions with smooth oscillations reveals the passing through a region with deterministic chaotic behavior. Table 4.2 shows the sequence of period doubling oscillations to chaos between the regions of smooth oscillations and relaxation oscillations. The corresponding simulation results

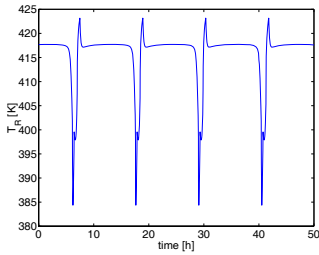
are displayed in Fig. 4.28 for the route from relaxation oscillations to chaos with ‘windows of periodic behavior’, and in Fig. 4.29 for the route from smooth oscillations via period-2-doubling to chaos. The figures contain time plots of the reactor temperature T_R and the corresponding trajectories in a three-dimensional phase space spanned by the water mole fraction, the reactor temperature, and the reaction volume.

Thus, and as neither of the individual units exhibits chaotic behavior, a **period-doubling route to chaos** has been found **in reactor separator systems that is induced by the recycle effects** on the overall system’s dynamics.

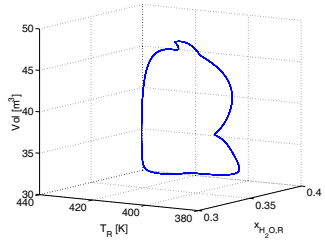
It should be noted that chaos is no new phenomenon in chemically reacting systems. However, in most of the published examples (see, e.g., [34, 94] and references therein), chaos can be traced back to be caused by the underlying reaction kinetics, while here the origin clearly is the positive feedback effect introduced by the flash recycle (see also [33] for chaotic dynamics in homogeneous tubular reactors with recycle from the reactor outlet to the reactor inlet, i.e., for chaotic behavior in a single-unit system with recycle as compared to the chaotic dynamics in a recycle system consisting of two operating units presented in this section).

$L_R \left[\frac{\text{kmol}}{\text{s}} \right]$	Dynamical state	Figure
3.0	relaxation osc.	4.26, 4.27, 4.28 (a), (b)
4.5	periodic window	4.28 (c), (d)
4.6	periodic window	4.28 (e), (f)
5.0	chaos	4.29 (a), (b)
5.3	period-4	4.29 (c), (d)
5.35	period-2	4.29 (e), (f)
5.8	smooth osc.	4.29 (g), (h)

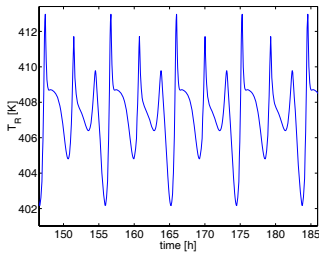
Table 4.2: Route to chaos for CS3.



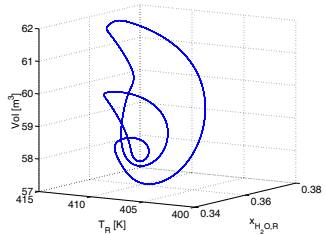
(a) Relaxation oscillations for $L_R = 3.0$ kmol/s



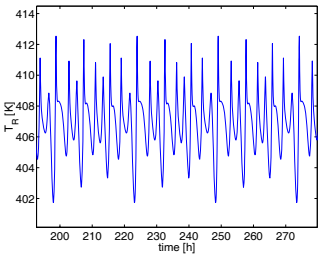
(b) Corresponding phase diagram



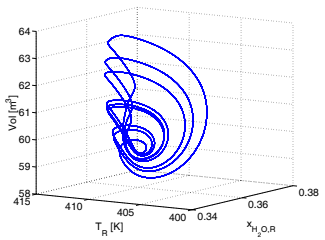
(c) Periodic oscillations for $L_R = 4.5$ kmol/s



(d) Corresponding phase diagram

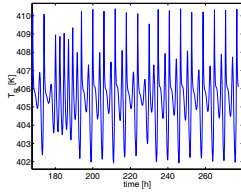


(e) Periodic oscillations for $L_R = 4.6$ kmol/s

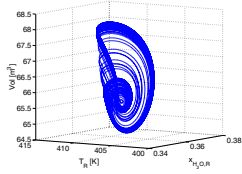


(f) Corresponding phase diagram

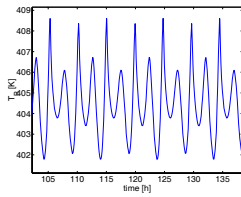
Figure 4.28: Periodic windows on the route from relaxation oscillations to chaos for the reaction system operated with control structure CS3.



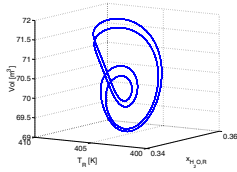
(a) Chaos, $L_R = 5.0 \frac{kmol}{s}$



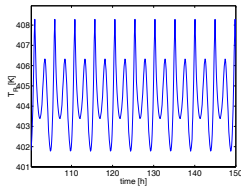
(b) Phase diagram



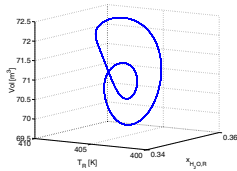
(c) P-4, $L_R = 5.3 \frac{kmol}{s}$



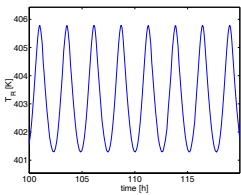
(d) Phase diagram



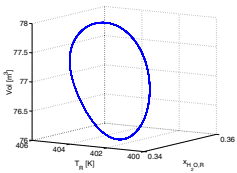
(e) P-2, $L_R = 5.35 \frac{kmol}{s}$



(f) Phase diagram



(g) P-1, $L_R = 5.8 \frac{kmol}{s}$



(h) Phase diagram

Figure 4.29: Period-doubling route from smooth oscillations to chaos for the reaction system operated with control structure CS3.

4.4 Summary: Nonlinear behavior of integrated systems with one recycle

The numerical investigations of the acetic acid production plant's reaction system have revealed an astonishing wealth of interesting nonlinear phenomena exhibited by this integrated system with exactly one recycle stream.

These phenomena include the existence of steady-state multiplicities in form of isolas with and without coexisting isolated solution branches, and even encompass the occurrence of chaotic behavior for the control structure leaving the reactor volume variable.

This variety in the integrated system's nonlinear characteristics is in line with the analytical results obtained for very simple reactor separator systems, as it could be shown that even for simple binary systems featuring one recycle stream, the positive feedback effect introduced by the material recycle may give rise to a large variability in the coupled system's behavior.

One especially interesting observation has shown how the coupled system's behavior may be interpreted as a combination of effects attributable to the individual systems' behavior on one hand, in particular due to the inhibitory reaction mechanism, and recycle effects on the other hand.

However, no more than three coexisting steady states have been found for the various control structures investigated within this chapter, although intuitively the combination of multiplicities induced by recycle and reaction mechanism effects could have spurred the expectation of more than only three coexisting steady states in the integrated system.

The following chapter will focus on the question whether additional recycles lead to even more complex patterns of behavior than already observed for the system with just one recycle.

Chapter 5

Nonlinear Analysis III: Production plant with nested recycles

The investigations in the preceding chapter have revealed the effects the introduction of a single recycle stream may have on the behavior of an integrated system. The purpose of the present chapter is to see whether additional, nested recycles with different time constants bring along additional effects.

The sheer size of even a simplified system with at least two recycles and thus typically at least three process units basically rules out the derivation of analytical results characterizing the integrated system's behavior. Therefore, like in Section 4.3, all investigations within this chapter are restricted to numerical studies of the industrial production plant with adiabatic flash operation.

The numerical analysis first focusses on the systems' steady-state characteristics by means of continuation studies. Dynamic simulation studies of the overall plant for the three control structures investigated throughout the thesis conclude the chapter.

5.1 Steady-state characteristics

5.1.1 System with recycles from first column closed

Figure 5.1 shows the steady states of the industrial case study operated with control structure CS1 and with the recycles from the first distillation column to the reaction system, in particular the reactor, closed. To be more precise, it is the recycles of the heavy organic

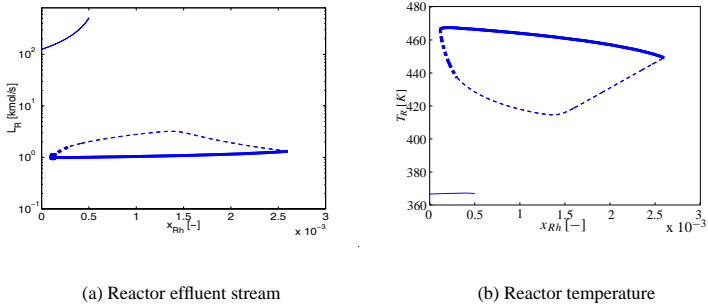


Figure 5.1: Steady states of the industrial case study operated with control structure CS1 and with the recycles from the first column to the reaction system closed.

phase and the aqueous phase from the decanter atop the first column that are assumed to be closed for the current studies.

As can be seen from comparisons with the corresponding simulation results for the isolated reaction system depicted in Fig. 4.16, closing those two recycles does not make much of a difference in terms of the integrated system's steady-state characteristics. Indeed, there are no qualitative differences, and even the quantitative differences are very small.

To see whether the final overall system integration by means of closing the recycle from the second column to the reactor alters this picture, the results of a continuation study of the complete plant are studied next.

5.1.2 Overall plant

The steady-state characteristics of the entire production plant are captured in Fig. 5.2. Again, just like in the case of closing the recycles from the first column, also closing the final recycle from the second column, which completes the system integration of the industrial production process, does not introduce any new features in terms of steady-state characteristics. Instead, differences to the steady-state results of the reaction system (Fig. 4.16) are hardly identifiable and purely quantitative in nature, which means that also the overall plant exhibits an isola of steady states and the isolated solution branch with high

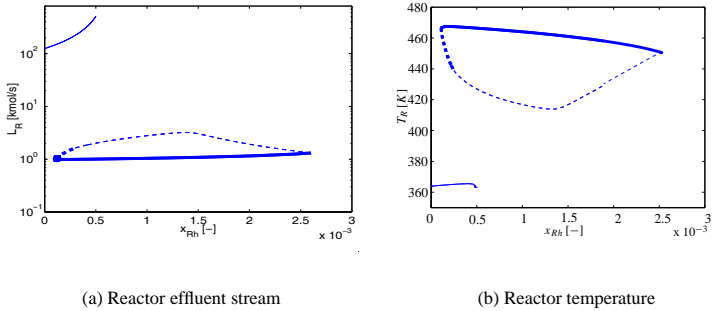


Figure 5.2: Steady states of the completely integrated industrial case study, i.e. with all recycles closed, and operated with control structure CS1.

internal flowrates.

5.1.3 Summary

The simulation results of this section have shown that no new features in terms of the integrated system's behavior are introduced by the additional recycles when compared to the characteristics of the isolated reaction system. The physical interpretation of this result is straightforward: As the flowrates within the reaction system are by far larger than all other flowrates in the entire plant, and in particular much larger than the downstream recycles, **it is the reaction system consisting of the reactor and the flash with liquid recycle from the flash to the reactor, which completely dominates the overall system's behavior.**

Two important remarks complement this analysis:

- To conclude that additional recycles do in general not involve the occurrence of additional patterns of behavior would certainly be rushed, not to say wrong. Instead, the 'dominance of the reaction system' has to be regarded as specific for the given system.
- The 'dominance of the reaction system' should also hold for the other control structures. The steady-state characteristics of the complete plant operated with control

structures CS2 and CS3 will therefore not be further studied within this thesis. Instead, concentration is next shifted to dynamic simulation studies of the overall plant in the following section.

5.2 Dynamic simulation studies

So far, the focus of all foregoing investigations has mainly been on the nonlinear steady-state characteristics of recycle systems. In contrast, this section aims at highlighting the dynamic features of the entire industrial production plant with adiabatic flash operation by means of dynamic simulation studies.

To this end, two particularly interesting scenarios are considered: (i) How do the three different flow-control structures cope with a specific **external disturbance**, and (ii) how suitable are the different control structures to perform **load changes**?

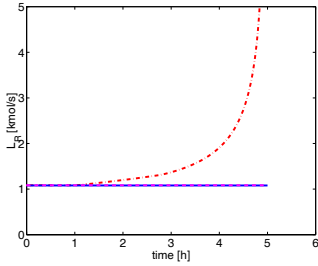
5.2.1 Feed disturbance

A typical disturbance in a chemical plant is a failure of some part of the utility system. Here, it is assumed that after one hour of standard operation, the feed pre-heating system suffers from some problem which leads to a **30 K step-decrease in feed temperature**.

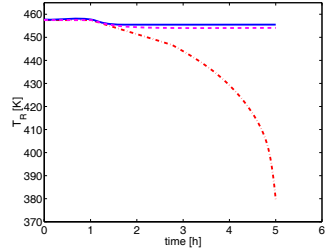
Independent of the specific control strategy, this type of disturbance leads to a drop in energy supplied to the reactor, and thus results in an immediate decrease of the reactor temperature. The further consequences of this disturbance, however, are very much control structure-specific:

Control structure CS1:

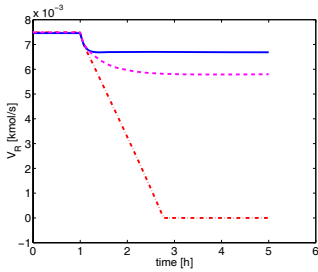
In the case of control structure CS1 (dashed-dotted lines in Fig. 5.3), where the reactor effluent stream (subfigure (a)) is manipulated in order to keep the reaction volume (subfigure (d)) constant, the decrease in reactor temperature (subfigure (b)) causes the reaction rate to decrease. Thus, less CO is consumed, resulting in an increase in x_{CO} and an additional decrease in temperature because of the self-inhibitory character of the reaction mechanism. Due to the material and energy integration with the flash, this effect is further amplified: The cold flash recycle increases as soon as the flash inlet temperature



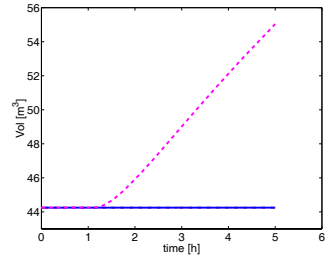
(a) Reactor liquid effluent stream



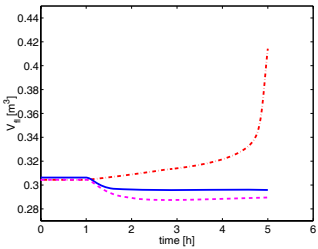
(b) Reactor temperature



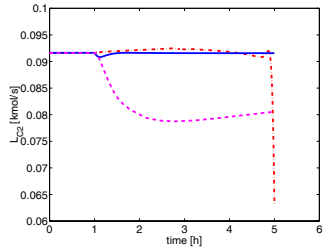
(c) Reactor vapor effluent stream



(d) Reactor volume



(e) Flash vapor effluent stream



(f) Bottoms stream column C2

Figure 5.3: Transients of the complete plant following a step-decrease of 30 K in methanol feed temperature for the three different control structures CS1 (dashed-dotted lines), CS2 (solid lines), and CS3 (dashed lines).

T_R drops. This larger and colder recycle decreases the reactor temperature even further and simultaneously increases the reactor effluent L_R . It is therefore identified as the origin of the **accumulation of flowrates in the coupled system**. Moreover, the decrease in temperatures is accompanied with a decrease of the vapor stream leaving the reactor (subfigure (c)) up to the point where it completely vanishes. From this point onwards the reactor is purely liquid-phase.

The increased flash feed naturally also leads to a rise in the flash vapor stream (subfigure (e)). As this flash vapor stream contains increasingly more unconverted reactants and less product due to the drop of the reaction rate, eventually also the bottoms product stream from column 2 (subfigure (f)), which is basically pure product acetic acid, collapses.

This dynamic behavior of the overall system is also reflected in its steady-state characteristics: The bifurcation diagram $L_R(T_{F,MeOH})$ with the feed temperature $T_{F,MeOH}$ as bifurcation parameter features an isola of steady states just as the bifurcation diagram $L_R(x_{Rh})$ in Fig. 5.2. The feed temperature disturbance of the original stable steady state leads to a region outside the isola where no steady state exists at all, and thus leads to the accumulation in the flowrates.

Control structure CS2:

In contrast to CS1, control structure CS2 (with the reactor effluent stream fixed and the distillate recycle stream from column 2 manipulated in order to keep the reaction volume constant, solid lines in Fig. 5.3), turns out to be far superior in terms of rejecting the given disturbance. This is because fixing the reactor effluent decouples the flash to some degree from the reactor. In particular, the flash is only subject to a slight disturbance in composition and temperature, as opposed to the large flowrate disturbance encountered for CS1. As a consequence, a further amplification of the self-inhibitory character of the reaction mechanism is prevented and the system can easily settle to a new steady state close to its initial state before the disturbance.

Control structure CS3:

Just like for the other two control strategies, the drop in reactor temperature and reaction rate leads to an increase in liquid flash recycle to the reactor also for control structure CS3 (dashed lines in Fig. 5.3). However, as the reaction volume is not controlled with CS3,

and as all other reactor feeds as well as the reactor effluent stream are fixed, the increase in flash recycle leads to an undesired **accumulation of the reaction volume**.

Thus, only control structure CS2 turns out to be capable of handling the given disturbance without additional control.

5.2.2 Load changes

Load changes are performed whenever a changing market situation requires either an increase or a decrease of a plant's production rate. For the given acetic acid production plant, the production rate is set within the reaction system. More precisely, as the reactants are flow-controlled into the system, the respective set points determine the eventual production rate. However, the operator has no direct handle to exactly set the desired product flow rate.

It is important to note that the respective set point changes are disturbances to the separation system that propagate both downstream and again upstream via the recycles. The effects of both a 10% load increase and a 10% load decrease on the plant for the given three control strategies are investigated in what follows (see Fig. 5.4).

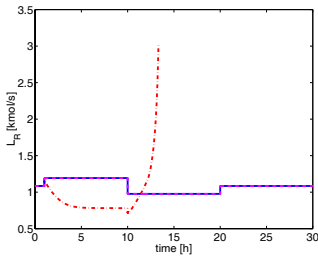
Control structure CS1:

After one hour of standard operation, both reactant feed rates are **increased by 10%**. This leads to an increase in reactant mole fractions and reaction rate, which in turn causes the reactor temperature and the vapor flow rates to rise.

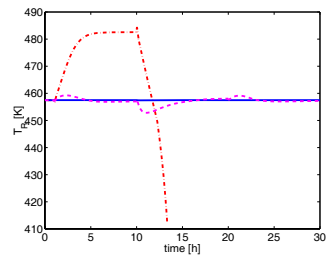
It is particularly interesting to observe the wrong-way behavior of the reactor effluent stream: The step-increase in reactant feeds initially causes the reactor effluent stream to rise accordingly. However, the higher reactor temperature leads to a higher evaporation rate in the flash. Thus, the liquid flash recycle stream to the reactor decreases and finally leads to a net decrease of the reactor effluent stream required to control the reaction volume to setpoint.

Overall, control structure CS1 can perform the desired positive load change and actually reaches a new steady state that entails a bottoms product stream increase of nearly 10%, although at the expense of a considerably higher reaction temperature.

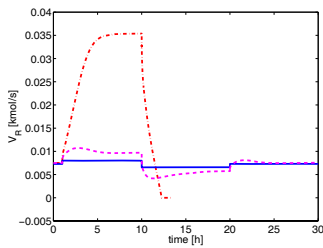
However, a follow-up load decrease by 20% after 10 hours of operation, corresponding to a **10% decrease** with respect to the initial operating conditions, can not be handled by



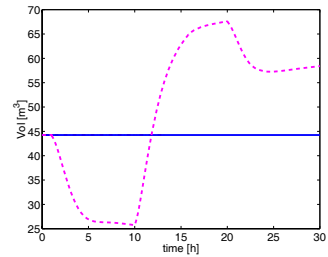
(a) Reactor effluent stream



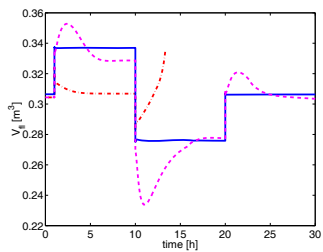
(b) Reactor temperature



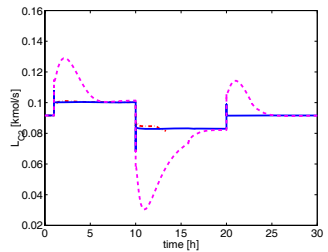
(c) Reactor vapor effluent stream



(d) Reactor volume



(e) Flash vapor effluent stream



(f) Bottoms stream column C2

Figure 5.4: Load changes of $\pm 10\%$ for the three different control structures CS1 (dashed-dotted lines), CS2 (solid lines), and CS3 (dashed lines).

control structure CS1. The reason is obvious: The decrease in reactant feeds leads to a decrease in both reactant mole fractions and in reaction temperature. Thus, it has the same effects as the negative feed temperature disturbance discussed in the previous example, i.e., again an accumulation in liquid streams occurs, with the explanations of the behavior from the previous subsection completely carrying through.

Control structure CS2:

Also in case of control structure CS2 the interpretation of the system's behavior from the previous example suffices to explain why this control strategy manages to effectively perform both aspired load changes (+10% after 1h, -10% after 10h, and back to initial conditions after 20h). In particular, it is again thanks to the partial decoupling of the reactor and the flash that no undesired accumulation of any kind occurs.

Note that for CS2 it is possible to change the reactor flow rate according to the given load change, which was not possible for CS1, where the reactor effluent stream was the manipulated variable to control the reaction volume. Apart from initial overshoots in the production rate, the system operated by means of control structure CS2 does approach the desired new steady states in an extremely short amount of time and is subject only to very small variations in reactor temperature (hardly visible in Fig. 5.4).

Control structure CS3:

As can be seen from Fig. 5.4, performing the load changes as described above for the plant operated with control structure CS3 is not possible in a satisfactory way. Although also for this control structure a setpoint change of the flow-controlled reactor effluent stream corresponding to the desired load change is possible, the system's transient is characterized by huge strides in some states, most obviously in the reaction volume. And although the aspired load change is approximately achieved within a couple of hours, further actions would be required to stabilize the system near this new operating point. Otherwise, it would slowly drift away again (within a time horizon not displayed in Fig. 5.4) due to the mechanisms explained for the previous example of a feed temperature disturbance.

Thus, also CS3 is unacceptable in terms of performing load changes.

5.3 Summary

The main results of the numerical simulations presented in this chapter are twofold:

On one hand, it has been shown that the acetic acid production plant's reaction system dominates the overall plant behavior to such an extent that the influence of downstream recycles on the overall plant behavior is almost negligible.

On the other hand, dynamic simulation studies that investigate the overall plant's response to an external disturbance and its capability to perform load changes have revealed that only control structure CS2 out of the three control structures extensively studied within this thesis can effectively handle the given tasks. This is because control structure CS2 manages to avoid accumulation in internal recycle streams thanks to fixing the reactor effluent stream, and also prevents accumulation of material in the reactor thanks to the reactor level-control via the downstream recycle from the second distillation column.

Moreover, it is not only its dynamic responses to the above scenarios, but also its steady-state characteristics with the lack of undesirable isolated solution branches which render control structure CS2 most attractive for operating the given production plant. However, one might argue that also control structure CS2 in combination with the adiabatic flash still has some shortcomings, as its region with stable steady states is limited (though not small), and because uniqueness of steady states could not be established.

Recalling the analytical results from Sections 4.1 and 4.2, it might therefore be interesting to consider **an alternative plantwide control structure** for the acetic acid production plant relying on control structure CS2 in combination with a flash with constant vapor flowrate, as this was the most attractive combination in the case of an ideal binary system. The final investigations in the following chapter will study exactly this type of system.

Chapter 6

Alternative plantwide control structures

Employing an adiabatic flash has the great advantages that it is both cheap and easy to operate, and it is therefore often used in practice. However, certain other types of flash control may be advantageous in the context of plantwide control, as indicated by the results for simple binary systems in Chapter 4.

For a system where the reactant is the light boiling component, the studies within this thesis have revealed that an isothermal flash operation is not suitable in terms of stability of the reactor-separator system's steady states. In contrast, the control structure combining flow-control of the reactor effluent stream with fixing the flash vapor flowrate has been deemed attractive as it leads to an integrated system featuring a unique stable steady state for the majority of practically interesting physical systems (see Sections 4.1.4 and 4.2.2). The following investigations of this particular control structure applied to the acetic acid production plant conclude the analysis of integrated chemical processes within this thesis.

6.1 Alternative control structure I

Figure 6.1 depicts the control structure for the industrial case study where the vapor flowrate is controlled by means of manipulating the heat input to the flash drum. Moreover, the reactor effluent stream is flow-controlled, while the recycle stream is used to control the reactor level, corresponding to what has so far been termed control structure CS2. The steady-state characteristics of this system for variations in the reactor effluent stream are captured in Fig. 6.2. It is most remarkable that the reactor-separator system operated with this new control structure features up to five coexisting steady states in a

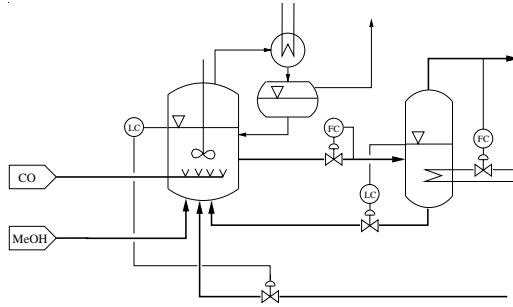


Figure 6.1: Control structure CS2 with level-control via the recycle and fixed vapor flow rate.

certain, yet small region of flow rate values. To better understand the origin of this double hysteresis, it is again particularly helpful to consider the evolution of the integrated system's features from those of the isolated reactor by means of sequentially closing the

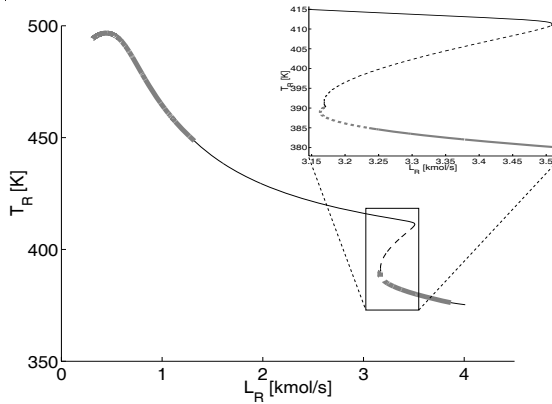


Figure 6.2: Steady-state characteristics of the system depicted in Fig. 6.1. Up to five steady states are feasible in a small region of the continuation parameter (the reactor effluent stream L_R).

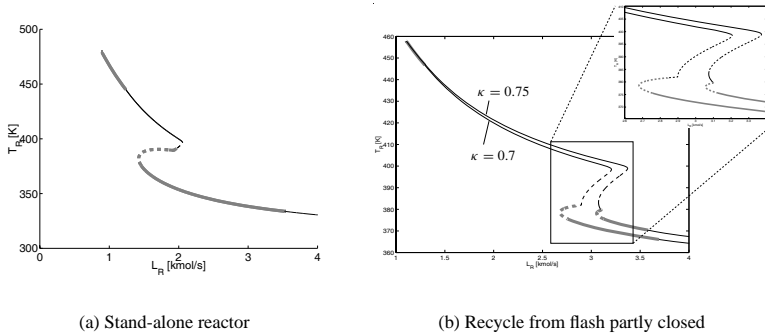


Figure 6.3: Evolution of the steady-state characteristics during a sequential closing of the flash recycle for the system from Fig. 6.1.

recycle from the flash to the reactor, as introduced in Section 4.3. This evolution is shown in Fig. 6.3. Obviously, the stand-alone reactor exhibits the well-known hysteresis (Fig. 6.3 (a)) attributable to the inhibitory reaction mechanism, and the only difference to the results obtained for a continuation in x_{Rth} is the region of single-phase steady states on the high conversion branch of stationary solutions. The exact origin of this partial switch from the two-phase to the one-phase regime is not further covered within this thesis and should rather be the topic of future research.

Much more interesting in the given context is to observe how the second hysteresis develops while the recycle from the flash to the reactor is being closed (three steady states for $\kappa = 0, 7$, five steady states for $\kappa = 0, 75$). Thus, this small second hysteresis is clearly caused by recycle effects, and this example shows that indeed a combination of reactor and recycle effects may give rise to more than just the three coexisting steady states found in all previous investigations within this thesis.

This remarkable result in terms of highly complex nonlinear behavior is, however, undesired for a smooth operation of the plant over a wide range of operating conditions. A more attractive plantwide control structure featuring a unique steady state for all values of L_R is introduced in the following section.

6.2 Alternative control structure II

The control structure depicted in Fig. 6.4 with fixed vapor flowrate via manipulation of the flash heating rate is also of the type referred to as control structure CS2 throughout this thesis, i.e., the reactor effluent stream is flow-controlled and the reactor level is fixed. However, in contrast to the control strategies presented so far, reactor level-control is now achieved by means of an advanced ratio control scheme:

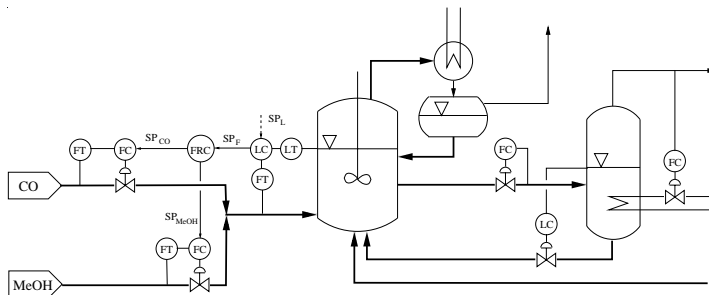


Figure 6.4: Control structure CS2 with level-control via the feed and fixed vapor flowrate. For simplicity, the two reactant feeds are drawn to be mixed before entering the reactor. Obviously, they can as well be fed to the reactor individually.

The overall feed flowrate is manipulated to control the reactor level to setpoint (SP_L), and in order to maintain the stoichiometry of the reactant feed conditions prevailing under standard operating conditions, $r = \frac{F_{CO}}{F_{MeOH}}|_{soc}$, the individual feed flowrates are adjusted accordingly by means of the cascade ratio controller. To be more precise, the master level-controller determines the setpoint (SP_F) for the slave flow-controller, which in turns guarantees that the individual reactants are ratioed into the system according to the standard stoichiometry ($SP_{CO} = \frac{r}{1+r}SP_F$, $SP_{MeOH} = \frac{1}{1+r}SP_F$).

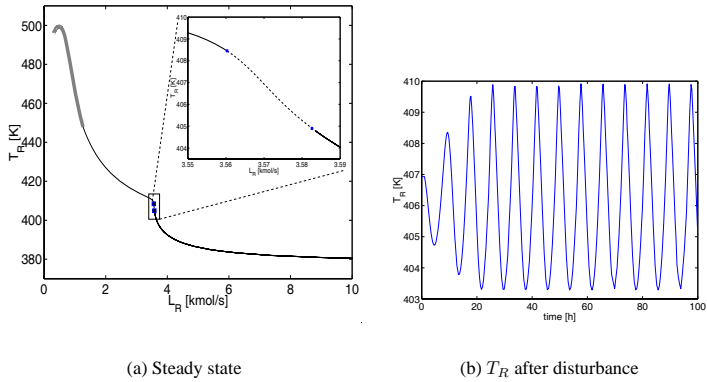


Figure 6.5: (a) Unique steady state of the system depicted in Fig. 6.4, with a small region of instability between two Hopf points, and (b) transient to temperature oscillations corresponding to a stable limit cycle after a disturbance of the unstable focus between the two supercritical Hopf points.

6.2.1 Steady-state characteristics of the reaction system

The steady-state characteristics of the reaction system with the given specific ratio control scheme are shown in Fig. 6.5 (a). As can be seen, this system exhibits a unique steady state for all values of the reactor effluent stream, and this steady state is stable except for a tiny range of L_R -values, for which the steady state is an unstable focus. Fig. 6.5 (b) shows a transient of the system to a stable oscillation after a disturbance of the unstable steady state, i.e., in a phase portrait, the unstable focus is surrounded by a stable limit cycle.

Once again, a sequential closing of the recycle from the flash to the reactor proves most illustrative for elucidating the integrated system's behavior: Fig. 6.6 (a) shows the usual hysteresis of the stand-alone reactor. It is worth noting that for the new control structure, the isolated reactor is single-phase for small values of L_R . This is because decreasing reactor effluent flowrates require a reduction of the feed provided, such that more of the supplied CO is consumed, resulting in a decrease of the boiling point temperature up to the point where the vapor phase disappears.

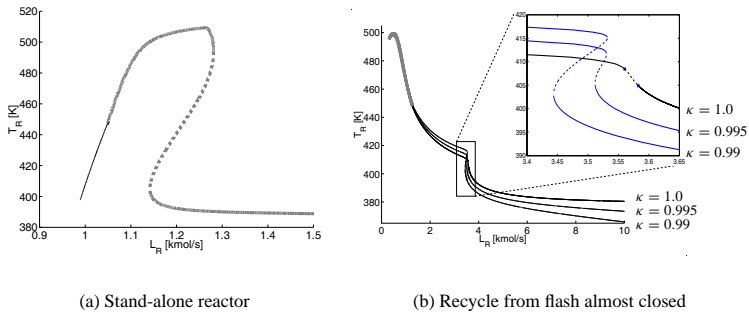


Figure 6.6: Evolution of the steady-state characteristics during a sequential closing of the flash recycle for the system from Fig. 6.4.

Fig. 6.6 (b) captures the system’s steady-state characteristics for almost completely closed recycle (κ very close to 1). Clearly, the hysteresis is by far less pronounced compared to the stand-alone reactor, and due to the effect of the recycle it has moved to the single-phase regime. Eventually, once the recycle is completely closed ($\kappa = 1, 0$), the steady-state multiplicity disappears¹.

More details concerning the exact nature of the evolution of the closed system’s characteristics from those of the stand-alone reactor are of minor interest here. Instead, the important conclusion from the above investigations is the finding that for the given control structure, the combination of effects attributable to the stand-alone reactor and to the presence of the recycle yield an integrated system that is most advantageous in terms of uniqueness and stability of operation. And this fact is by no means impaired by the existence of the tiny operating region featuring stable oscillations with comparatively small amplitudes.

Moreover, in contrast to the original control structure CS2 with an adiabatic flash, i.e. the most attractive control strategy for operating the acetic acid plant investigated within this thesis so far, operation of the new control structure CS2 with fixed flash vapor flowrate is not limited to a certain range of reactor effluent values (compare Figs. 4.23 and 6.5).

To further support the new control structure’s suitability in terms of plant operation, the following section studies the response of the overall acetic acid production plant oper-

¹I.e., the hysteresis point has a value of κ somewhere between 0,995 and 1.

ated with the new control structure² to the dynamic simulation scenarios first presented in Section 5.2.

6.2.2 Dynamics of the overall plant

Dynamic simulation studies along the lines of the disturbance and load changes introduced in the previous chapter reveal that the new control structure can easily handle both of the two scenarios.

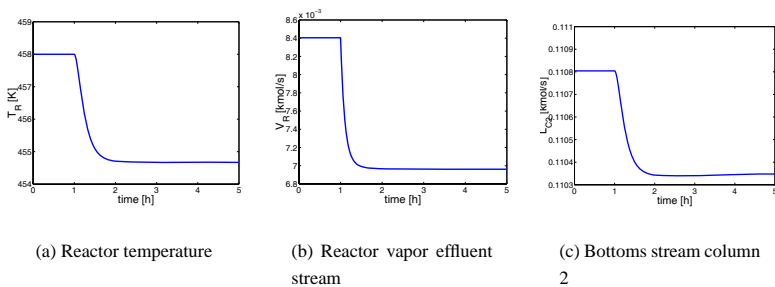


Figure 6.7: Transient of the system from Fig. 6.4. after a 30 K step-decrease in methanol feed temperature.

In Fig. 6.7, three representative states indicate the system's smooth transient to a nearby steady state after the 30 K step-decrease in methanol feed temperature.

Figure 6.8 shows the system's dynamics while performing the prescribed $\pm 10\%$ load changes. Note that for the given new control structure, these load changes are realized by adjusting the setpoints for the reactor effluent stream and for the flash vapor stream directly.

Like in the case of the 'classical' control structure CS2 with an adiabatic flash, these load changes are readily accomplished.

However, there remain some differences: Most obviously, an initial wrong-way behavior in the temperature dynamics of the new control structure can be observed. This is due to

²Here, in contrast to the 'original' control structure CS2, the distillate stream from column 2 is again flow-controlled as indicated for the basecase in Fig. 2.1.

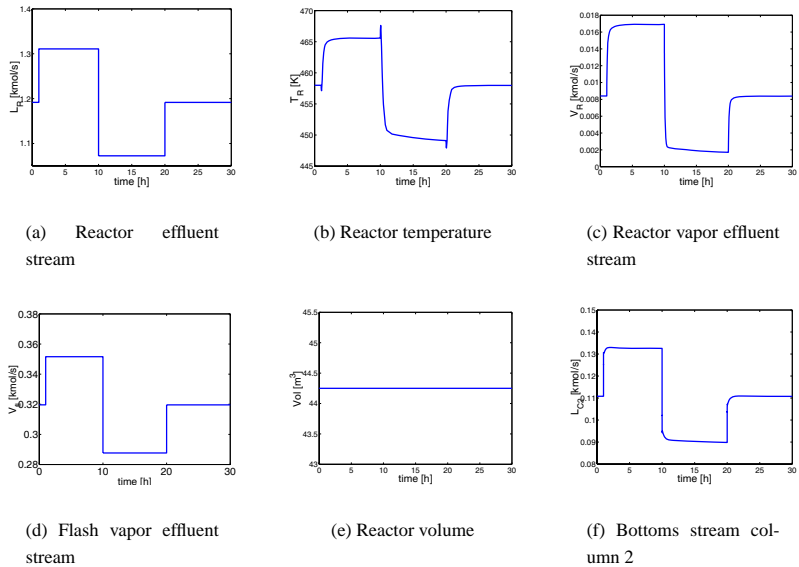


Figure 6.8: Transients of the system from Fig. 6.4 while performing load changes of $\pm 10\%$.

the well-known effects of the dissolved CO on the boiling point temperature: Considering for example the initial $+10\%$ load change, the reactor volume controller immediately increases the feed streams accordingly, which leads to an initial increase in reactant mole fractions in the reactor and inversely to the decrease of the reactor's boiling point temperature. Simultaneously, the reaction rate starts increasing due to the larger amount of reactants, and thus the reactants start being consumed to a higher degree. This leads to the decrease in x_{CO} and results in the observed rise of the reactor temperature up to a new steady state. Obviously, the explanation for the system's inverse response in T_R for the other load changes is analogous.

The big advantage of the new control structure is the direct handle of the production rate of the plant's reaction system. However, this does not necessarily mean that also the overall production rate, i.e. the bottoms stream from the second column, reaches exactly the desired value. An accurate adjustment of the plant's overall production rate would,

indeed, require a modification of the second column's control structure involving some type of bottoms flow-control.

6.3 Summary

The analytical results derived in Chapter 4 for ideal binary model systems of reactor-separator networks had suggested that an operation of the acetic acid plant based on a combination of control structure CS2 and flow-control of the flash vapor flowrate should be most advantageous in terms of uniqueness and stability of the plant's stationary behavior. And indeed, the numerical studies of both the steady-state characteristics and the dynamics of the industrial case study operated with this new control structure confirm this recommendation.

In this context, the investigations within this chapter have shown the importance of an appropriate realization of control structure CS2. To be more precise, it is not sufficient to simply control the reactor volume *somehow* by means of one of the reactor feeds, but the *proper choice* of a suitable feed stream is quintessential. A common rule of thumbs suggests that the largest available stream acting directly and without delay should be used to control liquid levels [73], and the results from this section confirm this recommendation, as reactor level control by means of the larger reactant feed stream has been shown to be superior in comparison to reactor level control via the smaller recycle stream.

The new plantwide control structure proposed in this chapter involves the control of the vapor flowrate via manipulation of the flash heating rate, and an advanced ratio control scheme to maintain the reactor level at its setpoint. Obviously, such a control configuration requires both additional equipment and energy supply, and is thus more expensive compared to the 'original' control structure CS2 currently used to operate the plant. Therefore, if it is clear in advance that the production plant is to be operated only near the standard operating point and that no large load changes are to be expected, then the 'original' control structure CS2 may actually be sufficient and economically favorable.

However, as soon as situations are conceivable which require plant operations further apart from the standard operating conditions, the 'original' control structure CS2 is likely to run into problems.

In such cases, it should be most appropriate to operate the production plant on basis of the new control structure derived and presented within this thesis.

Chapter 7

Conclusions

Research devoted to finding a suitable plantwide control structure for an integrated chemical production process involving material and energy recycles has witnessed a tremendous increase in attention from the process control community during the last decade. This is primarily to be attributed to the paramount importance a plantwide control structure has for the safe, reliable, and economically favorable operation of large-scale production plants.

For the control engineer confronted with the problem of deriving an efficient control strategy for an entire plant, this task poses a formidable creative challenge. This has been captured exceptionally well by S. Skogestad, one of the leading experts in the field of process control, when he remarks that “...since the issue of finding good controlled variables is a structural problem, then we often find that a good control structure obtained for a particular case, also works well on another similar process case with different parameter values. Thus, if we can actually find a self-optimizing structure for a process, then it is almost like an invention which may probably be patented.” [75]

The particular case study extensively investigated within this thesis is the Monsanto process for the production of acetic acid via methanol carbonylation. This process may be regarded as prototypical for the general class of processes involving an evaporatively cooled reactor and a separation system with a large number of nested recycles to the reactor.

By means of a systematic study, a suitable plantwide control structure for the given industrial case study has been derived, and the way to come up with this new control strategy has been **a clearly structured investigation of the nonlinear dynamics** that characterize the given production process:

Focussing first on the behavior of the **stand-alone synthesis reactor** as the core of the

overall process, a new source for the occurrence of multiple steady states in two-phase reactors operated under boiling conditions has been found. Thanks to an abstraction from the specifics of the methanol carbonylation reaction, it has been possible to show that the self-inhibition of the reaction mechanism is the general origin of potential steady-state multiplicities in all systems where an increase in the amount of light-boiling reactant reduces the reaction rate because of its decreasing effect on the reaction temperature.

The next step towards an understanding of the overall plant dynamics has been the study of the nonlinear behavior exhibited by **reactor-separator systems involving a single recycle**. Again, the recourse to simple model systems lending themselves to an analytical investigation has been particularly helpful to elucidate some general features typical for integrated systems. Most notably, the enormous influence the choice of a specific control structure has on the plant dynamics has been demonstrated, and it has been shown how the presence of recycles may cause the occurrence of steady-state multiplicities or limit cycles in the integrated plant even though the individual units are all characterized by uniqueness and stability of their respective stationary behavior. Moreover, it could be shown by means of numerical simulation studies of the industrial production process that the combination of stand-alone unit and recycle effects may give rise to very complex nonlinear behavior like the presence of up to five coexisting steady states, the existence of isolas of steady states, or the occurrence of relaxation oscillations and even deterministic chaos in the integrated system.

Further numerical studies of the **overall plant with its nested recycles** have revealed that the behavior of the Monsanto process is completely dominated by the behavior of its reaction system. Thus, it has been possible to conceive a suitable plantwide control structure for the acetic acid production plant on the basis of the analytical results obtained for simple model systems with just one recycle.

This result also supports the assertion that the use of appropriate simple model systems is most helpful for establishing insight into fundamental patterns of behavior of more complex systems.

The methods for investigating an integrated plant's behavior employed within this thesis in addition to standard dynamic simulations are basically the tools offered by bifurcation theory. Here, a word of caution seems appropriate: Without any doubt, it is a formidable task to investigate a large system's behavior in terms of all relevant operating parameters by means of bifurcation studies, as complexity increases drastically with increasing dimension of the parameter space. Nevertheless, the studies within this thesis should give valuable hints at what might in general be expected in terms of an integrated plant's non-

linear characteristics, and should thus be of great help for the design of control strategies.

The criterium determining a control structure's suitability for overall plant operation within this thesis has been the stability and uniqueness of the integrated system's steady states, and thus the prospect of safe and reliable operation over a wide range of operating conditions. In addition, sensitivity to disturbances and load changes has been checked exemplarily by means of dynamic simulation studies.

Future work should also take into account the economic aspects of plant operation. Conversely, approaches that so far focus on conceiving plantwide control structures that minimize operating costs or maximize profit by some type of (typically linear) optimization procedure should also consider the effects of nonlinearities as investigated within this thesis.

In the end, it is to be expected that any plantwide control structure will eventually have to compromise between optimizing steady-state economics and dynamic controllability issues.

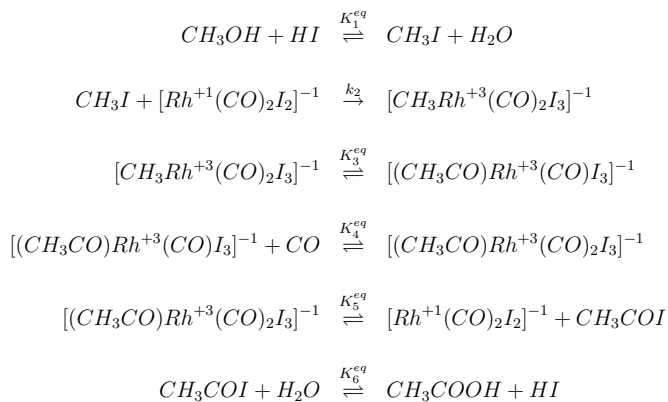
Appendix A

Modeling details and parameter values

This appendix supplies additional information related to the numerical simulation studies, which were not included in the main part of the text. In particular, details of the reaction mechanism and all physical property correlations along with the corresponding parameters required to reproduce all simulation results are summarized.

A.1 Kinetics of the methanol carbonylation reaction

In one of the most recent studies related to the methanol carbonylation reaction, a group of researchers from Sheffield [49] present details of the rhodium based reaction mechanism as depicted in Fig. A.1 It is made up of six separate stoichiometric reactions:



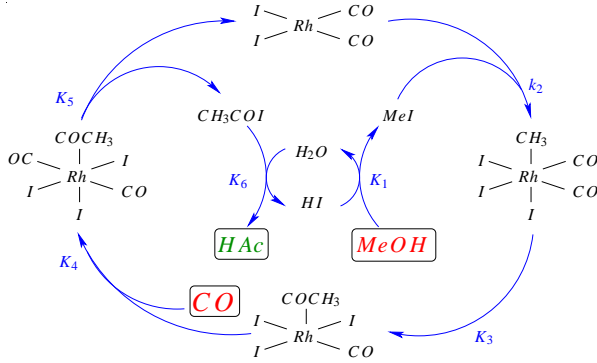
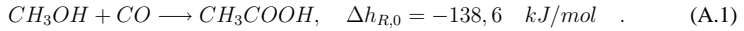


Figure A.1: The cycle of the rhodium-catalysed reaction mechanism

These reactions link to form the cycle that results in the brutto reaction



In compliance with former studies [27, 69], the oxidative addition of MeI to $[Rh^{+1}(CO)_2I_2]^{-1}$ is identified as the rate-determining step. Therefore, the reaction is approximately first order with respect to both the promoter MeI and the catalyst Rh . Based on the assumption that the reaction equilibrium constants $K_3^{eq}, K_6^{eq} \gg 1$ and that the associated reactions are very fast, and supposing that all reactions except for the rate-determining step are in equilibrium, a detailed analysis reveals that the above mechanism is of shifting order in the reactant $MeOH$. This is in line with the general fact that even reactions that are of zeroth order in the reactants over a wide range of reactant concentrations show a first order dependence on the reactants in the limit of very small reactant concentrations $c_i < c_i^*$ [42]. It also corresponds to the findings in [27], where the reaction rate is discerned as independent of the educt $MeOH$ for $c_{MeOH} > c_{MeOH}^* = 0.5 \text{ mol/l}$. Such a shifting order mechanism in a reactant i may be described by means of the expression $\frac{K_i^* c_i}{1 + K_i^* c_i}$, which is formally of Langmuir-Hinshelwood type (see also Fig. A.2), although the kinetic constant K_i^* in this case obviously is no adsorption constant as in classical Langmuir-Hinshelwood kinetics but instead a lumped parameter that follows from the above reaction equilibrium assumptions and accounts for the shift in reaction order.

In case of $MeOH$, the specific value of $c_{MeOH}^* = 0.5$ corresponds to a kinetic constant of approximately $K_{MeOH}^* \approx 50$.

Moreover, the reaction rate is identified to be independent of CO for CO partial pressures above 2 bar. At standard operating conditions of about 30 bar, plant data reveal a K-value relating the vapor mole fraction of CO to the liquid mole fraction of the dissolved CO of about $K_{CO} = y_{CO}/x_{CO} \approx 200$. Thereby, a partial pressure of CO of about 2 bar corresponds to a CO -concentration of about $c_{CO}^* = 0.007$ mol/l, below which the reaction rate does depend on CO and is of first order in c_{CO} . The corresponding kinetic constant is $K_{CO}^* \approx 1000$.

Taking the values of the reaction rate constant and the activation energy from the plant operator's manual [5] (which are very similar to those in [27]), the rate law of the reaction mechanism is given as

$$\begin{aligned} r_0 &= k_0 e^{-\frac{E}{R} \left(\frac{1}{T_R} - \frac{1}{T_{ref}} \right)} c_{MeI}^{1.05} \cdot c_{Rh}^{0.99} \cdot \frac{K_{MeOH}^* \cdot c_{MeOH}}{1 + K_{MeOH}^* \cdot c_{MeOH}} \cdot \frac{K_{CO}^* \cdot c_{CO}}{1 + K_{CO}^* \cdot c_{CO}} \\ &= 0.4986 \cdot e^{-7830 \left(\frac{1}{T_R} - \frac{1}{443} \right)} c_{MeI}^{1.05} \cdot c_{Rh}^{0.99} \cdot \frac{50 \cdot c_{MeOH}}{1 + 50 \cdot c_{MeOH}} \cdot \frac{1000 \cdot c_{CO}}{1 + 1000 \cdot c_{CO}} \end{aligned}$$

Hjortkjaer et al. [27] do note that extrapolations of this rate expression “*may be very hazardous because a possible shift in mechanism or rate-determining step will lead to another dependence on temperature and concentrations*”. In addition, the values of the kinetic constants K_{MeOH}^* and K_{CO}^* are obviously rather crude estimates of the real conditions.

Nevertheless, they enable the description of the complex shifting-order reaction mechanism. And moreover, as explained in Section 2.5, at least under standard operating conditions the reactor model based on this rate law shows good agreement with real plant data.

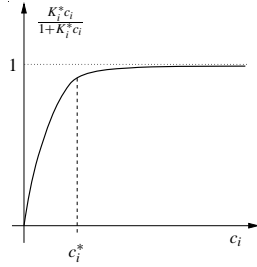


Figure A.2: Shifting-order reaction mechanism: approximately first order for $c_i < c_i^*$ and zeroth order for $c_i > c_i^*$.

A.2 Physical property correlations, parameter values, and operating data

In this part of the appendix, all the physical property correlations along with the respective parameters as required for the acetic acid plant model and the simple model systems are compiled.

In order to keep the presentation compact, details concerning the origin of the various volumetric and calorimetric correlations, their range of validity or interpretations of the parameters' physical meanings are not given here, as such information can easily be found in standard references like [64].

A.2.1 Acetic acid system

The parameters for the components water, methanol, acetic acid, and methyl iodide are all from the Dortmund Data Base *Detherm* ([15], see Table A.1), except for the Uniquac parameters employed for modeling the ternary liquid-liquid equilibrium between water, acetic acid, and methyl iodide in the decanter. The respective parameters A_{ij} required in this context have been identified based on measurements of the miscibility gap given in [30].

Moreover, the supercritical reactant CO requires specific treatment as described below.

- **Saturation pressures according to Antoine:**

$$p_{i,S}[Pa] = 133,2895 \cdot 10 \left(A_i - \frac{B_i}{\vartheta[^\circ C] + C_i} \right), \quad (\text{A.2})$$

with $\vartheta[^\circ C] = T[K] - 273,15 K$.

- **Molar volume liquid phase according to Cavett:**

$$v_i' \left[\frac{m^3}{kmol} \right] = \xi_i' (5,7 + 3 T_{r,i}) \quad (\text{A.3})$$

with $\xi_i' = \frac{v_{0,i}'}{5,7 + 3 T_{r,0,i}}$, $T_{r,i} = \frac{T}{T_{crit,i}}$, $T_{r,0,i} = \frac{T_0}{T_{crit,i}}$, $T_0 = 298,15 K$.

Parameter	Water	Methanol	Acetic Acid	Methyl Iodide
General:				
$T_{crit,i}$ [K]	647,3	512,6	594,4	528,0
$p_{crit,i}$ [Pa]	$220,483 \cdot 10^5$	$80,9587 \cdot 10^5$	$57,8566 \cdot 10^5$	$65,8613 \cdot 10^5$
$v'_{0,i}$ [m ³ /kmol]	0,0180742	0,0407323	0,0575357	0,0626694
Antoine:				
A_i	8,07131	8,08097	7,55960	6,98803
B_i	1730,630	1582,271	1644,048	1146,34
C_i	233,426	239,726	233,524	236,674
Enthalpies:				
$h_{0,i}$ [kJ/kmol]	-241951	-201137	-434925	-233997
$h_{A,i}$ [(°C) ⁻¹]	7,8580	9,8460	15,060	9,9430
$h_{B,i}$ [(°C) ⁻²]	0,001378	0,01056	0,01925	0,009124
$h_{C,i}$ [(°C) ⁻³]	$-0,1884 \cdot 10^{-7}$	$-0,2391 \cdot 10^{-7}$	$-0,7108 \cdot 10^{-7}$	$-0,251 \cdot 10^{-7}$
Watson:				
$\Delta h_{V,SN,i}$ [kJ/kmol]	40660	35280	23693	26960
$T_{SN,i}$ [K]	373,15	337,85	391,05	315,55
UNIQUAC:				
r_i [-]	0,9200	1,4311	2,2024	2,1654
q_i [-]	1,4000	1,4320	2,0720	1,8400

Table A.1: Pure component parameters

- **Molar volume vapor phase v_i'' $\left[\frac{m^3}{kmol}\right]$ and v'' $\left[\frac{m^3}{kmol}\right]$ implicitly from Redlich-Kwong (with $p, p_{i,S}$ [Pa]):**

$$p = \frac{RT}{v'' - B} - \frac{A}{v''(v'' + B) \cdot \sqrt{T}} \quad (A.4)$$

$$p_{i,S} = \frac{RT}{v_i'' - b_i} - \frac{a_i}{v_i''(v_i'' + b_i) \cdot \sqrt{T}} \quad (A.5)$$

with

$$a_i = \Omega_a \cdot R^2 \cdot \frac{T_{crit,i}^{2,5}}{p_{crit,i}}, \quad b_i = \Omega_b \cdot R \cdot \frac{T_{crit,i}}{p_{crit,i}}, \quad A = \left(\sum_{i=1}^{NC} y_i \cdot \sqrt{a_i} \right)^2,$$

$$B = \sum_{i=1}^{NC} y_i \cdot b_i, \quad \Omega_a = 0,42748, \quad \Omega_b = 0,08664, \quad R = 8,3145 \left[\frac{kJ}{kmolK} \right].$$

\	H_2O	$MeOH$	HAc	MeI
H_2O	0	631,7369	504,4811	0
$MeOH$	-378,4130	0	-127,8987	45,2061
HAc	-501,8032	-142,4038	0	37,2990
MeI	0	1238,3729	472,1011	0

Parameters A_{ij} for the VLE.

\	H_2O	HAc	MeI
H_2O	0	-23084,0	4286,0
HAc	146,0	0	1390,0
MeI	6671,0	-20815,0	0

Parameters A_{ij} for the LLE.

Table A.2: UNIQUAC Parameters for the four-component vapor-liquid equilibrium (VLE) and for the three-component liquid-liquid equilibrium (LLE).

• **Activity coefficients according to UNIQUAC:**

$$\gamma_i = \exp \left\{ \ln \frac{\psi_i}{x_i} + \frac{z}{2} q_i \ln \frac{\vartheta_i}{\psi_i} + l_i - \frac{\psi_i}{x_i} \sum_{j=1}^{NC} x_j l_j \right. \\ \left. + q_i \left[1 - \ln \left(\sum_{j=1}^{NC} \vartheta_j \tau_{ji} \right) - \sum_{j=1}^{NC} \frac{\vartheta_j \tau_{ij}}{\sum_{k=1}^{NC} \vartheta_k \tau_{kj}} \right] \right\}$$

with

$$z = 10 \quad , \quad l_i = \frac{z}{2}(r_i - q_i) - (r_i - 1) \quad , \quad \psi_i = \frac{x_i r_i}{\sum_{j=1}^{NC} x_j r_j}$$

$$\vartheta_i = \frac{x_i q_i}{\sum_{j=1}^{NC} x_j q_j} \quad , \quad \tau_{ji} = \exp \left[\frac{-A_{ij}}{RT} \right]$$

The adjustable parameters A_{ij} are given in Table A.2. As already mentioned, the parameters for the vapor-liquid equilibrium are from [15], while those for describ-

ing the liquid-liquid equilibrium in the decanter have been obtained by means of a parameter identification on the basis of data from [30], using least-squares optimization algorithms in MATLAB [81].

Due to a lack of data, the UNIQUAC parameters for the vapor-liquid equilibrium of the binary pair water – methyl iodide have been set to zero, which corresponds to the assumption of ideal mixing with respect to these two components.

- **Molar enthalpies of vaporization according to WATSON:**

$$\Delta h_{i,V} \left[\frac{kJ}{kmol} \right] = \Delta h_{i,V,SN} \left(\frac{1 - T_{r,i}}{1 - T_{r,i,SN}} \right)^{0,38}, \quad T_{r,i,SN} = \frac{T_{i,SN}}{T_{crit,i}} \quad (\text{A.6})$$

- **Molar enthalpies:**

$$h_i'' \left[\frac{kJ}{kmol} \right] = h_{0,i} + [h_{A,i}(\vartheta - \vartheta_0) + h_{B,i}(\vartheta^2 - \vartheta_0^2) + h_{C,i}(\vartheta^3 - \vartheta_0^3)] \cdot \zeta, \\ \zeta = 4,186 \left[\frac{kJ}{kmol} \right], \quad \vartheta_0 = 25^\circ C \quad (\text{A.7})$$

$$h_i' \left[\frac{kJ}{kmol} \right] = h_i'' - \Delta h_{i,V} \quad (\text{A.8})$$

Due to a lack of data it is assumed that the molar enthalpy of CO in both phases is given by its standard energy of formation, i.e., $h'_{CO} = h''_{CO} = h_{0,CO}$.

- **Fugacity coefficients according to Redlich-Kwong:**

$$\varphi_{0,i,S}'' = \exp \left\{ \ln \frac{v_{0,i}''}{v_{0,i}'' - b_i} + \frac{b_i}{v_{0,i}'' - b_i} - \ln \frac{p_{i,S} v_{0,i}''}{RT} - \frac{a_i}{RT^{1,5} \cdot b_i} \cdot \left(\ln \frac{v_{0,i}'' + b_i}{v_{0,i}''} - \frac{b_i}{v_{0,i}'' + b_i} \right) \right\} \quad (\text{A.9})$$

$$\varphi_i'' = \exp \left\{ \ln \frac{v''}{v'' - B} + \frac{b_i}{v'' - B} - \ln \frac{p \cdot v''}{RT} + \frac{A \cdot b_i}{RT^{1,5} \cdot B^2} \cdot \left(\ln \frac{v'' + B}{v''} - \frac{B}{v'' + B} \right) - 2 \cdot \frac{\sum_{j=1}^{NC} y_j a_{i,j}^*}{RT^{1,5} \cdot B} \cdot \ln \frac{v'' + B}{v''} \right\} \quad (\text{A.10})$$

with $a_{i,j}^* = \sqrt{a_i \cdot a_j}$.

- Throughout, it is assumed that the pure component molar quantities coincide with the respective partial molar quantities, $\bar{\sigma}_i = \sigma_i$. Thus, the mixture quantities σ are given by

$$\sigma = \sum_{i=1}^{NC} x_i \sigma_i \quad , \quad \sigma \in \{v', h', h''\} \quad . \quad (\text{A.11})$$

In the computation of v' , the contribution of the two components CO and rhodium catalyst has been neglected as they both are very small, and also the contribution of rhodium to the liquid phase enthalpy h' is not considered.

Physical properties of CO

As already mentioned above, the reactant CO with a critical pressure of $p_{CO,crit} = 35$ bar and a critical temperature of $T_{CO,crit} = 132,9$ K is supercritical under standard operating

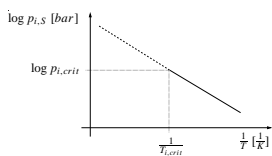


Figure A.3: Vapor pressure of component i ; linear extrapolation to the hypothetical state beyond the critical point denoted by dashed lines.

conditions. For the description of a supercritical component's gas solubility, Prausnitz suggests the concept of *ideal gas solubility* [59], with the vapor pressure of the gaseous solute at conditions beyond the component's critical point following from an extrapolation on a linear plot of $\log p_{i,s}$ vs. $\frac{1}{T}$ (see Fig. A.3). The ideal gas solubility neglects all gas-phase nonidealities, the Poynting correction and any nonidealities due to solute-solvent interactions. It is therefore independent of the nature of the

solvent and corresponds to Raoult's law, for CO

$$y_{CO} p = x_{CO} p_{CO,S} \quad . \quad (\text{A.12})$$

According to [59], this model usually gives correct order-of-magnitude results provided the partial pressure of the gas is not large and provided the solution temperature is well below the critical temperature of the solvent and not too excessively above the critical temperature of the gaseous solute.

Below the critical point, the vapor pressure of CO is calculated according to a correlation given in [64],

$$p_{CO,S} = p_c \cdot e \left(\frac{1}{1-x} (ax + bx^{1.5} + cx^3 + dx^6) \right) \quad , \quad (\text{A.13})$$

with $x = 1 - \frac{T}{T_{CO,crit}}$ and $a = -6, 20798$, $b = 1, 27885$, $c = -1, 34533$, $d = -2, 56842$ for CO . Note that this saturation pressure under supercritical conditions may also be interpreted as the component's Henry coefficient, $p_{CO,S} = H_{CO}$.

The only other pure CO property used within the models in the main part of this thesis is the standard enthalpy of formation $h_{0,CO} = -110590$ kJ/kmol. It is assumed that the enthalpy of CO for all temperatures and pressures is given by this standard enthalpy of formation and deviations from it are neglected.

All other physical properties of CO like activity or fugacity coefficients are not calculated and set equal one instead ($\gamma_{CO} = 1$, $\varphi''_{CO} = 1, \dots$), corresponding to the assumption of ideal behavior of CO .

A.2.2 Model Systems

Parameter values for simulation studies in Section 2.6.1 (Figs. 2.7 and 2.8):

Operating parameters		Physical properties	
n_R	100 mol	$T_{SN,A}$	300.0 K
n_{fl}	20.0 mol	$T_{SN,B}$	420.0 K
p	1.013 bar	$\Delta h_{V,A}$	25080 J/mol
F	1.84 mol/s	$\Delta h_{V,B}$	35080 J/mol
$x_{A,F}$	1.0	c_P	209.836 J/(K mol)
T_R	320.0 K	k_0	1.0e+05 1/s
		E_A	40000 J/mol

In addition, the following operating parameters have been chosen:

- For Fig. 2.7: $Q_{fl} = 4.373 \cdot 10^4$ W for system S1,
and $Q_{fl} = 2.58 \cdot 10^5$ W for system S2.
- For Fig. 2.8(a): $F = 1.84$ mol/s and $Q_{fl} = 1.25 \cdot 10^5$ W.
- For Fig. 2.8(b): $L_R = 5.0$ mol/s and $Q_{fl} = 1.25 \cdot 10^5$ W.

Parameter values for simulation studies in Section 4.1:

For Fig. 4.7:

Operating parameters		Physical properties	
n_R	100 mol	$T_{SN,A}$	300.0 K
n_{fl}	20.0 mol	$T_{SN,B}$	400.0 K
p	1.013 bar	c_P	209.836 J/(K mol)
$x_{A,F}$	1.0	E_A	40000 J/mol
T_R	320.0 K		
Q_{fl}	$2.5 \cdot 10^5$ W		
F	1.0 mol/s		

In addition, the following operating parameters have been chosen:

- For Fig. 4.7(a): $\Delta h_{V,A} = 25080$ J/mol, $\Delta h_{V,B} = 100000$ J/mol, and $k_0 = 1.0 \cdot 10^5$.
- For Fig. 4.7(b): $\Delta h_{V,A} = 100000$ J/mol, $\Delta h_{V,B} = 25080$ J/mol, and $k_0 = 5.0 \cdot 10^5$.

For Fig. 4.8:

Operating parameters		Physical properties	
L_R	21.53 mol/s	$T_{SN,A}$	300.0 K
n_{fl}	20.0 mol	$T_{SN,B}$	400.0 K
p	1.013 bar	c_P	209.836 J/(K mol)
$x_{A,F}$	1.0	E_A	40000 J/mol
T_R	320.0 K	k_0	$1.0 \cdot 10^6$
Q_{fl}	$1.4 \cdot 10^6$ W		

- For Fig. 4.8(a): $\Delta h_{V,A} = 85900$ J/mol, $\Delta h_{V,B} = 65000$ J/mol.
- For Fig. 4.8(b): $\Delta h_{V,A} = 65000$ J/mol, $\Delta h_{V,B} = 85900$ J/mol.

Appendix B

Mathematical supplements

B.1 Some facts on the stability of dynamical systems

This section briefly summarizes some basic results concerning the stability of dynamical systems, and introduces the notion of *static stability*. The concept of static stability is frequently used in engineering applications and throughout this thesis, as it enables a very intuitive interpretation of a system's stability features *based on steady-state arguments only*. However, in spite of its frequent use, a general derivation is hardly found in literature. Instead, usually examples form the basis for the derivation of problem-specific static stability conditions, like for the classical first order exothermic reaction in a CSTR (see also Chapter 3 and e.g. [84]).

In what follows, the static stability condition is derived for general first order systems, the condition for static stability of second order systems is presented, and the link between the static stability condition and the potential for real bifurcations in nonlinear systems is commented on.

B.1.1 First order systems and the concept of static stability

Consider the general nonlinear first order dynamical system

$$\dot{x} = f(x), \quad x \in \mathbb{R}, \quad f : \mathbb{R} \rightarrow \mathbb{R}, \quad (\text{B.1})$$

and suppose f is continuously differentiable. The steady states $x_{S,j}$ of (B.1) follow from $f(x_{S,j}) = 0$. Fig. B.1 helps to illustrate the concept of *static stability* for the given

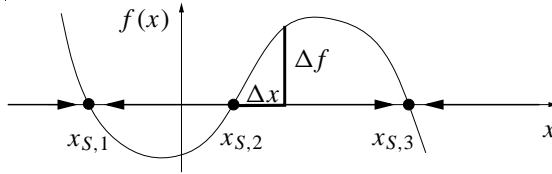


Figure B.1: Illustration of the concept of *static stability* for the scalar system $\dot{x} = f(x)$: The steady state $x_{S,2}$ is statically unstable, as a small $\Delta x > 0$ implies $\Delta f > 0$. In contrast, both $x_{S,1}$ and $x_{S,3}$ are statically stable, as they comply with the general static stability condition (B.2).

scalar system. Interpreting the right hand side f of the differential equation as the driving force acting on the dynamic state x , then the concept of static stability is based on the idea, that for an equilibrium $x_{S,j}$ to be statically stable, f must act as a restoring force that counteracts any small deviation $\Delta x := x - x_{S,j}$ from that steady state. In other words, for a steady state $x_{S,j}$ to be statically stable, it must hold that the restoring force $\Delta f := f(x_{S,j} + \Delta x) - f(x_{S,j})$ must ‘drive x back to the equilibrium’, which is fulfilled for $\Delta f < 0$ in case of $\Delta x > 0$, and for $\Delta f > 0$ in case of $\Delta x < 0$. This can be summarized to the static stability condition

$$\frac{\Delta f}{\Delta x} < 0, \quad (\text{B.2})$$

which is the well-known so-called *slope condition*. Note that in case of a scalar system, static stability of an equilibrium coincides with the rigorous dynamic stability that determines an equilibrium as locally asymptotically stable if and only if its eigenvalue is negative, $\lambda := \frac{\partial f}{\partial x}|_{f=0} < 0$.

B.1.2 Static vs. dynamic stability and local bifurcations of second order systems

Consider the general second order dynamical system

$$\dot{x}_1 = f_1(x_1, x_2), \quad (\text{B.3})$$

$$\dot{x}_2 = f_2(x_1, x_2). \quad (\text{B.4})$$

A steady state of this system is locally asymptotically stable if and only if both eigenvalues of the Jacobian J , evaluated at the equilibrium, have negative real parts, or, in a different notation, if and only if

$$\det(J) > 0 \quad \text{and} \quad (\text{B.5})$$

$$\text{tr}(J) < 0 \quad . \quad (\text{B.6})$$

Here, both conditions together mark the *dynamic stability* of the system (B.3, B.4), while the first condition (B.5) alone is often referred to as the *static stability condition*, indicating that from a steady-state perspective there is a restoring force counteracting any deviation from equilibrium.

It is important to bear in mind that *static stability is only necessary, but not sufficient for rigorous asymptotic stability of a second order system*. In fact, a statically stable equilibrium may still be dynamically unstable if $\text{tr}(J) > 0$:

E.g., suppose a branch of statically stable steady-state solutions with $\det(J) > 0$ has lost its dynamic stability as parameter variations have caused a pair of complex eigenvalues to cross the imaginary axis, such that $0 < \text{tr}(J) < \sqrt{4\det(J)}$. In this case, the statically stable but dynamically unstable fixed point is an unstable focus, and the outspiraling trajectories caused by a disturbance of the unstable steady state may converge to a stable limit cycle (see also Fig. B.2). In the case of the afore-mentioned CSTR example, such a situation would correspond to the occurrence of phase-shifted oscillations in temperature and concentration (see, e.g. [20]). Note, moreover, that the stability of the limit cycle is not guaranteed, but has to be established by means of more advanced tools from nonlinear dynamics (see, e.g., [25]).

On the other hand, it holds that *static instability implies dynamic instability, and obviously dynamic stability implies static stability*.

Finally, it is worth noting that the static stability condition is closely linked to the potential for real, i.e. static bifurcations of equilibria in nonlinear systems. In fact, the boundary between static stability and instability given by $\det(J) = 0$ exactly marks the necessary, but not sufficient condition for a real bifurcation.

Figure B.2 summarizes the topological behavior of general linear and nonlinear systems ‘near their equilibria’ in terms of the trace and the determinant of the systems’ Jacobians. Note that in case of nonlinear systems, all phase portraits are valid only locally in a sufficiently small neighborhood of the steady states. Accordingly, also the indicated bifurcations are only local bifurcations, i.e. bifurcations occurring in the neighborhood of a fixed point [92].

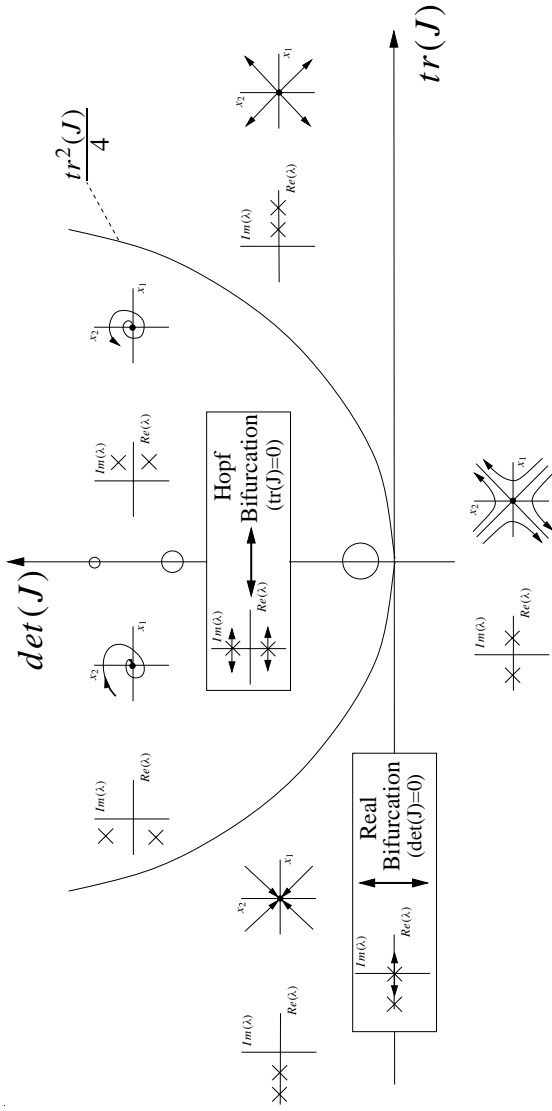


Figure B.2: Topological classification of equilibria in \mathbb{R}^2 in terms of the trace and the determinant of a system's Jacobian. For all the different regions, the location of eigenvalues and a schematic phase plot of the linearized system in the neighborhood of the steady state is shown. Degenerate cases like the phase portraits in the neighborhood of non-hyperbolic fixed points and on the boundaries of the various regions are not depicted. The circles on the positive ordinate indicate the oscillations a linear system with purely imaginary eigenvalues would display, with larger radii of the circles indicating larger periods of the oscillations. For $\det(J) = 0$ and $\text{tr}(J) \neq 0$, locally only real bifurcations of equilibria, i.e. stationary bifurcations, are possible. Similarly, $\text{tr}(J) = 0$ and $\det(J) \neq 0$ marks the necessary condition for Hopf bifurcations, which give birth to limit cycles, corresponding to a distinguished dynamic behavior of the system in form of permanent oscillations.

B.1.3 Stability of linear third order systems

In general, the stability of fixed points in dynamical systems of order $n \geq 3$ may be determined relying on the Routh-Hurwitz criterion (see e.g. [93]).

In case of a third order dynamical system for which the characteristic equation of its linearization around an equilibrium is given by

$$q(s) = a_3s^3 + a_2s^2 + a_1s + a_0 = 0 \quad , \quad (\text{B.7})$$

it holds that the equilibrium is asymptotically stable if and only if the inequalities

$$a_0 > 0, \quad a_2 > 0, \quad a_3 > 0, \quad a_1a_2 - a_0a_3 > 0 \quad (\text{B.8})$$

are fulfilled [93].

B.2 Uniqueness of the steady state for the system from Section 4.1.2

To understand the relevance of this section, it has to be noted that stability of all potential steady-state solutions alone is not sufficient to guarantee uniqueness, as there could, e.g., exist unstable limit cycles separating multiple stable steady-state solutions. However, it is shown here that for a second order system with bounded solutions, $\text{tr}(J) < 0$ and $\text{det}(J) > 0$ are indeed sufficient for stability *and* uniqueness.

To establish this result, the well-known Bendixson criterion (see [35]) is required. Consider the dynamical second order system $\dot{x} = f(x)$,

$$\dot{x}_1 = f_1(x_1, x_2) \quad , \quad (\text{B.9})$$

$$\dot{x}_2 = f_2(x_1, x_2) \quad , \quad (\text{B.10})$$

where $f(x)$ is continuously differentiable on a simply connected and compact region D .

Bendixson criterion: *If, on a simply connected region D of the phase plane, the expression $\frac{\partial f_1}{\partial x_1} + \frac{\partial f_2}{\partial x_2}$ is not identically zero and does not change sign, then the second order system (B.9), (B.10) has no periodic orbits lying entirely in D .* \diamond

For a proof, see e.g. [35].

Based on this result, the following Lemma can be established:

Lemma: Consider the second order system (B.9), (B.10), and suppose its solutions are bounded. Then it holds that this system exhibits a unique and stable steady state if $tr(J) < 0$ and $det(J) > 0$, where J is the Jacobian matrix of the system. \diamond

Proof: From $tr(J) < 0$ and $det(J) > 0$ it follows that each steady state of the second order system is exponentially stable. This implies that the system exhibits no heteroclinic or homoclinic orbits. Moreover, from $tr(J) < 0$ and Bendixson's criterion, it follows that the system exhibits no periodic orbits. Therefore, any bounded trajectory of the system must tend towards the only remaining possible limit set, which is a stable steady state. \square

In other words: There are no thresholds that might separate the regions of attraction of two or more stable steady states. As it is topologically impossible that two or more stable steady states do coexist without such thresholds, and as any bounded solution in \mathbb{R}^2 must eventually approach a limit set, there can be only one unique and stable steady state.

This Lemma is sufficient to show that the binary system as given in Section 4.1.2 with $\Delta h_{V,A} < \Delta h_{V,B}$ and $T_R > T_{fl}$ has a unique and stable steady state. Both $tr(J) < 0$ and $det(J) > 0$ are already established, and it is straightforward to show boundedness of solutions. In this regard, bear in mind that thermodynamic consistency requires that at steady state $x_{A,R} = 0$ implies $x_{A,fl} = 0$ (and also $y_{A,fl} = 0$), and vice versa, corresponding to infinitely fast reaction. Equivalently, $x_{A,R} = 1$ implies $x_{A,fl} = 1$ (and also $y_{A,fl} = 1$), and vice versa, corresponding to no reaction. Then it is easily shown that for $F > F_{min}$, the set $S = \{(x_{A,R}, x_{A,fl}) \mid 0 \leq x_{A,R} \leq 1, 0 \leq x_{A,fl} \leq 1\}$ is positively invariant, as $\frac{dx_{A,R}}{dt}|_{x_{A,R}=0} > 0$, $\frac{dx_{A,R}}{dt}|_{x_{A,R}=1} < 0$, $\frac{dx_{A,fl}}{dt}|_{x_{A,fl}=0} > 0$, $\frac{dx_{A,fl}}{dt}|_{x_{A,fl}=1} = 0$. Therefore, no solution can leave the unit square of feasible solutions, i.e., any solution is bounded.

B.3 Stability of individual process units

The **isothermal stand-alone reactor** from Section 4.1, described by equations (4.1) and (4.2), has a steady state for $F + L_{fl} - L_R = 0$ only. In this case, the eigenvalue of the governing scalar linear differential equation (4.2) is guaranteed to be negative, i.e., the given isolated reactor is always stable.

A **binary (p,T)-flash with constant holdup** as treated in Section 4.1.1 is a purely static system and therefore cannot be unstable.

As explained in [95], the stability of a **constantly heated binary flash** follows from the sign of the element J_{22} of the Jacobian (4.34). Inserting $\frac{dV_{fl}}{dx_{A,fl}}$ from (4.33) yields

$$J_{22} = -\frac{1}{n_{fl}} \left(\underbrace{(L_R - V_{fl})}_{>0} + L_R c_p \underbrace{\frac{x_{A,fl} - y_{A,fl}}{\Delta h_{V,fl}}}_{<0} \underbrace{\frac{dT_{fl}}{dx_{A,fl}}}_{<0} \right) \underbrace{\hspace{10em}}_{>0} \begin{matrix} \text{for A light} \\ \text{for A heavy} \end{matrix} + V_{fl} \underbrace{\frac{dy_{A,fl}}{dx_{A,fl}}}_{>0} \underbrace{\left(1 + \frac{x_{A,fl}(\Delta h_{V,A} - \Delta h_{V,B})}{\Delta h_{V,fl}} - \frac{y_{A,fl}(\Delta h_{V,A} - \Delta h_{V,B})}{\Delta h_{V,fl}} \right)}_{:=g} \right).$$

With $\Delta h_{V,fl} = y_{A,fl}\Delta h_{V,A} + (1 - y_{A,fl})\Delta h_{V,B}$, it holds that

$$\begin{aligned} g &= \frac{\Delta h_{V,fl} + (x_{A,fl} - y_{A,fl})(\Delta h_{V,A} - \Delta h_{V,B})}{\Delta h_{V,fl}} \\ &= \frac{1}{\Delta h_{V,fl}} ((1 - x_{A,fl})\Delta h_{V,B} + x_{A,fl}\Delta h_{V,A}) > 0 \quad . \end{aligned}$$

Thus,

$$J_{22} < 0 \quad ,$$

which means that the stand-alone flash with Q_{fl} fixed is always stable, independent of the boiling sequence or specific values of $\Delta h_{V,A}$ and $\Delta h_{V,B}$.

The **binary flash with V_{fl} fixed** is a special case of the systems treated in [16], where it is shown that any nonideal multicomponent mixture on a single column stage with constant molar overflow does possess a unique stable node for all sets of thermodynamically and physically feasible parameters. In particular, this implies that a binary flash with fixed vapor flowrate has a unique stable equilibrium, independent of the boiling sequence.

Bibliography

- [1] V.H. Agreda and J.R. Zoeller. *Acetic Acid and its derivatives*. Marcel Dekker, Inc., New York, 1993.
- [2] A. Arbel, I.H. Rinard, and R. Shinnar. Dynamics and control of fluidized catalytic crackers 3, designing the control system: Choice of manipulated and measured variables for partial control. *Ind. Engng. Chem. Res.*, pages 2215–2233, 1996.
- [3] R. Aris. On stability criteria of chemical reaction engineering. *Chem. Engng. Sci.*, pages 149–169, 1969.
- [4] Y. Arkun and G. Stephanopoulos. Studies in the synthesis of control structures for chemical processes, Part IV: Design of steady-state optimizing control structures for chemical process units. *AIChE J.*, 26:975–991, 1980.
- [5] AZOT. *Acetic Acid Production Process – Internal manual*, 1983.
- [6] A. Bahrami. *Object Oriented System Development*. Irwing/McGraw-Hill, 1999.
- [7] V. Balakotaiah and D. Luss. Global analysis of the multiplicity features of multi-reaction lumped-parameter systems. *Chem. Engng. Sci.*, 39:865–881, 1984.
- [8] P. Balasubramanian, M.R. Kosuri, S. Pushpavanam, and A. Kienle. Effect of delay on the stability of a coupled reactor-separator system. *Ind. Engng. Chem. Res.*, pages 3758–3764, 2003.
- [9] A. Banerjee and Y. Arkun. Control Configuration Design applied to the Tennessee Eastman Plant-Wide Control Problem. *Comp. Chem. Engng.*, 19:453–480, 1995.
- [10] C.S. Bildea, A.C. Dimian, and P.D. Iedema. Nonlinear behavior of reactor-separator-recycle systems. *Comp. Chem. Engng.*, 24:209–215, 2000.

- [11] P. Buckley. *Techniques of Process Control*. Wiley, New York, 1964.
- [12] H.B. Callen. *Thermodynamics and an Introduction to Thermostatistics*. John Wiley and Sons, Inc., New York, second edition, 1985.
- [13] S.K. Chodavarapu and A. Zheng. Control system design for recycle systems. *J. Proc. Cont.*, 11:459–468, 2001.
- [14] A.R. Ciric and P. Miao. Steady state multiplicities in an ethylene glycol reactive distillation colum. *Industrial & Engineering Chemistry Research*, 33:2738–2748, 1994.
- [15] DDBST. *DDB-Predict*. DDBST Software & Separation Technology GmbH, Oldenburg, 1993.
- [16] M.F. Doherty and J.D. Perkins. On the dynamics of distillation processes - iv. Uniqueness and stability of the steady state in homogeneous continuous distillations. *Chem. Engng. Sci.*, 37:381–392, 1982.
- [17] J.M. Douglas. *Conceptual Design of Chemical Processes*. McGraw-Hill, 1988.
- [18] J.J. Downs and E.F. Vogel. A Plant-Wide Industrial Process Control Problem. *Comp. Chem. Engng.*, 17:245–255, 1993.
- [19] A.S. Foss. Critique of chemical process control theory. *AIChE J.*, 19:209–214, 1973.
- [20] E.D. Gilles and H. Hofmann. Bemerkung zu der Arbeit: “An analysis of chemical reactor stability and control”. *Chem. Engng. Sci.*, 15:328–331, 1961.
- [21] E.D. Gilles, A. Kienle, R. Waschler, V. Sviatnyi, A. Anoprienko, and V. Potapenko. Zur Entwicklung des Trainingssimulators einer großchemischen Anlage. In *Problems of Simulation and Computer Aided Design of Dynamic Systems*, pages 23–28, Donetsk, 2002. Donetsk State Technical University.
- [22] M. Golubitsky and D.G. Schaeffer. *Singularities and groups in bifurcation theory*. Springer, New York, 1985.
- [23] P. Gray and S.K. Scott. Autocatalytic reactions in the isothermal, continuous stirred tank reactor. *Chem. Engng. Sci.*, 38:29–43, 1983.

- [24] P. Gray and S.K. Scott. *Chemical Oscillations and Instabilities*. Oxford University Press, Oxford, 1994.
- [25] J. Guckenheimer and P. Holmes. *Nonlinear Oscillations, Dynamical Systems, and Bifurcations of Vector Fields*. Springer, New York, 1983.
- [26] A. Haynes, P.M. Maitlis, G.E. Morris, G.J. Sunley, H. Adams, P.W. Badger, C.M. Bowers, D.B. Cook, P.I.P. Elliott, T. Ghaffar, H. Green, T.R. Griffin, M. Payne, J.M. Pearson, M.J. Taylor, P.W. Vickers, and R.J. Watt. Promotion of iridium-catalyzed methanol carbonylation: Mechanistic studies of the cativa process. *Journal of the Am. Chem. Soc.*, 126:2847–2861, 2004.
- [27] J. Hjortkjaer and V.W. Jensen. Rhodium complex catalyzed methanol carbonylation. *Industrial & Engineering Chemistry Process Design and Development*, 15:46–49, 1976.
- [28] P. Holl. *Entwicklung und Einsatz eines dynamischen Simulators für verfahrenstechnische Prozesse*. PhD thesis, Universität Stuttgart, 1994.
- [29] P. Holl, W. Marquardt, and E.D. Gilles. DIVA – A powerful tool for dynamic process simulation. *Comp. Chem. Engng.*, 12:421–425, 1988.
- [30] S. Horiba. *Mem. Coll. Sci. Eng. Kyoto Imp. Univ.*, 3:63, 1911.
- [31] E.W. Jacobsen. Effect of Recycle on the Plant Zero Dynamics. *Comp. Chem. Engng.*, 21:279–284, 1997.
- [32] E.W. Jacobsen. On the dynamics of integrated plants – non-minimum phase behavior. *J. Proc. Cont.*, 9:439–451, 1999.
- [33] E.W. Jacobsen and M. Berezowski. Chaotic dynamics in homogeneous tubular reactors with recycle. *Chem. Engng. Sci.*, 53:4023–4029, 1997.
- [34] D.V. Jorgensen and R. Aris. On the dynamics of a stirred tank with consecutive reactions. *Chem. Engng. Sci.*, 38:45–53, 1983.
- [35] H.K. Khalil. *Nonlinear Systems*. Prentice-Hall, Upper Saddle River, third edition, 2002.
- [36] A. Kienle, G. Lauschke, V. Gehrke, and E.D. Gilles. On the dynamics of the circulation loop reactor - numerical methods and analysis. *Chem. Engng. Sci.*, 50:2361–2375, 1995.

- [37] A.A. Kiss, C.S. Bildea, A.C. Dimian, and P.D. Iedema. State multiplicity in CSTR-separator-recycle polymerization systems. *Chem. Engng. Sci.*, pages 535–546, 2002.
- [38] R. Köhler. *Preprocessing Tool for Method-of-Lines Discretization of Process Models in the Simulation Environment DIVA*. PhD thesis, Universität Stuttgart, 2002.
- [39] M.V. Kothare, R. Shinnar, I. Rinard, and M. Morari. On Defining the Partial Control Problem: Concepts and Examples. *AIChE J.*, 46:2456–2474, 2000.
- [40] A. Kröner, P. Holl, W. Marquardt, and E.D. Gilles. DIVA – An open architecture for dynamic simulation. *Comp. Chem. Engng.*, 14:1289–1295, 1990.
- [41] T. Larsson and S. Skogestad. Plantwide control: A review and a new design procedure. *Modeling, Identification and Control*, 21:209–240, 2000.
- [42] O. Levenspiel. *Chemical reaction engineering*. Wiley, New York, second edition, 1972.
- [43] D. Liberzon. *Switching in Systems and Control*. Birkhäuser, Boston, 2003.
- [44] D. Luss. Steady-state multiplicity features of chemically reacting systems. *Chemical Engineering Education*, pages 12–56, 1986.
- [45] W.L. Luyben. Snowball effect in reactor/separator processes with recycle. *Ind. Engng. Chem. Res.*, 33:299–305, 1994.
- [46] W.L. Luyben. Temperature control of autorefrigerated reactors. *Journal of Process Control*, 9:301–312, 1999.
- [47] W.L. Luyben. *Plantwide Dynamic Simulators in Chemical Processing and Control*. Marcel Dekker, New York, 2002.
- [48] W.L. Luyben, B.D. Tyreus, and M.L. Luyben. *Plantwide Process Control*. McGraw-Hill, New York, 1999.
- [49] P.M. Maitlis, A. Haynes, G.J. Sunley, and M.J. Howard. Methanol carbonylation revisited: thirty years on. *J. Chem. Soc., Dalton Trans.*, pages 2187–2196, 1996.
- [50] M. Mangold, O. Angeles-Palacios, M. Ginkel, R. Waschler, A. Kienle, and E.D. Gilles. Computer-Aided Modeling of Chemical and Biological Systems: Methods, Tools, and Applications. *Ind. Engng. Chem. Res.*, 44, 2005. In press.

- [51] M. Mangold, A. Kienle, E.D. Gilles, and K.D. Mohl. Nonlinear computation in DIVA - methods and applications. *Chem. Engng. Sci.*, 55:441–454, 2000.
- [52] T.J. McAvoy and N. Ye. Base Control for the Tennessee Eastman Problem. *Comp. Chem. Engng.*, 18:383–413, 1994.
- [53] I.S. Metcalfe. *Chemical Reaction Engineering*. Oxford University Press, Oxford, 1997.
- [54] K.D. Mohl, A. Spieker, E. Stein, and E.D. Gilles. DIVA—Eine Umgebung zur Simulation, Analyse und Optimierung verfahrenstechnischer Prozesse. In A. Kuhn, editor, *Simulationstechnik, 11. ASIM-Symposium in Dortmund, 1997*, pages 278–283, Braunschweig/Wiesbaden, 1997. Vieweg Verlag.
- [55] M. Morari, G. Stephanopoulos, and Y. Arkun. Studies in the synthesis of control structures for chemical processes, Part I: formulation of the problem. Process decomposition and the classification of the control task. Analysis of the optimizing control structures. *AIChE J.*, 26:220–232, 1980.
- [56] J. Morud and S. Skogestad. Dynamic behaviour of integrated plants. *J. Proc. Cont.*, 6:145–156, 1996.
- [57] J.H. Nielsen, J. Villadsen, and G. Lidén. *Bioreaction engineering principles*. Kluwer Academic/Plenum Publishers, New York, second edition, 2003.
- [58] A. S. Parker. Preparation of alkylene glycol, 1958. U.S. Patent 2 839 588.
- [59] J.M. Prausnitz, R.N. Lichtenthaler, and E.G. de Azevedo. *Molecular Thermodynamics of fluid–phase equilibria*. Prentice–Hall, Englewood Cliffs, N.J., 1986.
- [60] S. Pushpavanam and A. Kienle. Nonlinear behavior of an ideal reactor separator network with mass recycle. *Chem. Engng. Sci.*, 56:2837–2849, 2001.
- [61] I. Ramos Ramos. Development, implementation, and nonlinear analysis of a model family for reactor separator networks using ProMoT/DIVA. Diploma thesis, Otto-von-Guericke University, Magdeburg, 2004.
- [62] S. Räumerschüssel, A. Gerstlauer, E.D. Gilles, and M. Zeitz. Ein Präprozessor für den verfahrenstechnischen Simulator DIVA. In G. Kampe and M. Zeitz, editors, *Simulationstechnik, 9. ASIM-Symposium in Stuttgart, 1994*, pages 177–182, Braunschweig/Wiesbaden, 1994. Vieweg Verlag.

- [63] L.F. Razon and R.A. Schmitz. Multiplicities and instabilities in chemically reacting systems – a review. *Chemical Engineering Science*, 42:1005–1047, 1987.
- [64] R.C. Reid, J.M. Prausnitz, and T.K. Sherwood. *The Properties of Gases and Liquids*. McGraw-Hill, New York, 1977.
- [65] N.L. Ricker. Decentralized control of the Tennessee Eastman Challenge Process. *J. Proc. Cont.*, 6:205–221, 1996.
- [66] N.L. Ricker and J.H. Lee. Nonlinear model predictive control of the Tennessee Eastman Challenge Process. *Comp. Chem. Engng.*, 19:961–981, 1995.
- [67] I.E. Rodriguez, A. Zheng, and M.F. Malone. The stability of a reactive flash. *Chemical Engineering Science*, 56:4737–4745, 2001.
- [68] I.E. Rodriguez, A. Zheng, and M.F. Malone. Parametric dependence of solution multiplicity in reactive flashes. *Chem. Engng. Sci.*, 59:1589–1600, 2004.
- [69] J.F. Roth, J.H. Craddock, A. Hershman, and F.E. Paulik. Low pressure process for acetic acid via carbonylation. *Chem Tech*, pages 600–605, 1971.
- [70] A.A. Sagale and S. Pushpavanam. A comparison of control strategies for a nonlinear reactor-separator network sustaining an autocatalytic isothermal reaction. *Ind. Engng. Chem. Res.*, pages 2005–2012, 2002.
- [71] W.C. Salmon. *Logic*. Prentice-Hall, Englewood Cliffs, N.J., second edition, 1973.
- [72] J.D. Seader and E.J. Henley. *Separation Process Principles*. John Wiley & Sons, New York, 1998.
- [73] D.E. Seborg, T.F. Edgar, and D.A. Mellinchamp. *Process Dynamics and Control*. Wiley Series in Chemical Engineering. John Wiley & Sons, New York, 1989.
- [74] S. Skogestad. Plantwide control: the search for the self-optimizing control structure. *J. Proc. Cont.*, 10:487–507, 2000.
- [75] S. Skogestad. Control structure design for complete chemical plants. *Comp. Chem. Engng.*, 28:219–234, 2004.
- [76] S. Skogestad and I. Postlethwaite. *Multivariable feedback control – Analysis and design*. John Wiley & Sons, Chichester, 1996.

- [77] K. Stephan and F. Mayinger. *Thermodynamik, Band 2: Mehrstoffsysteme*. Springer, Berlin, 14. edition, 1999.
- [78] G. Stephanopoulos and C. Ng. Perspectives on the synthesis of plant-wide control structures. *J. Proc. Cont.*, 10:97–111, 2000.
- [79] K. Sundmacher. *Reaktivdestillation mit katalytischen Füllkörpern – ein neuer Prozeß zur Herstellung der Kraftstoffkomponente MTBE*. PhD thesis, Technische Universität Clausthal, 1995.
- [80] K. Sundmacher and A. Kienle, editors. *Reactive Distillation – Status and Future Trends*, Weinheim, 2003. Wiley-VCH.
- [81] The MathWorks, Inc. *Using Matlab, Version 6*. Natick, MA, USA, 2000.
- [82] A. Uppal, W.H. Ray, and A.B. Poore. On the dynamic behavior of continuous stirred tank reactors. *Chem. Engng. Sci.*, 29:967–985, 1974.
- [83] A. Uppal, W.H. Ray, and A.B. Poore. The classification of the dynamic behavior of continuous stirred tank reactors – influence of reactor residence time. *Chem. Engng. Sci.*, 31:205–214, 1976.
- [84] C. van Heerden. Autothermic processes, properties and reactor design. *Ind. Engng. Chem.*, 45:1242–1247, 1953.
- [85] A. Varma, M. Morbidelli, and H. Wu. *Parametric Sensitivity in Chemical Systems*. Cambridge University Press, Cambridge, Uk, 1999.
- [86] E.M. Vasbinder and K.A. Hoo. Decision-Based Approach to Plantwide Control Structure Synthesis. *Ind. Engng. Chem. Res.*, 42:4586–4598, 2003.
- [87] R. Waschler. Entwicklung einer Modellfamilie für die Destillation/Rektifikation. Studienarbeit, Institut für Systemdynamik und Regelungstechnik, Universität Stuttgart, 1996.
- [88] R. Waschler, O. Angeles-Palacios, M. Ginkel, and A. Kienle. Flexible Modellierung großchemischer Anlagen mit dem Modellierungswerkzeug ProMoT. In R. Hohmann, editor, *Simulationstechnik, 17. Symposium, ASIM 2003*, pages 173–178, Erlangen, 2003. SCS Publishing House.

- [89] R. Waschler, O. Angeles-Palacios, M. Ginkel, and A. Kienle. Object-oriented modeling of large-scale chemical engineering processes with ProMoT. *Mathematical and Computer Modelling of Dynamical Systems*, 2005. Accepted for publication.
- [90] R. Waschler, S. Pushpavanam, and A. Kienle. Multiple steady states in two-phase reactors under boiling conditions. *Chem. Engng. Sci.*, 58:2203–2214, 2003.
- [91] K. Weissermel and H.-J. Arpe. *Industrial Organic Chemistry*. Wiley-VCH, Weinheim, fourth edition, 2003.
- [92] S. Wiggins. *Introduction to Applied Nonlinear Dynamical Systems and Chaos*. Springer, New York, 1990.
- [93] L.A. Zadeh and C.A. Desoer. *Linear System Theory - The State Space Approach*. Robert E. Krieger Publishing Company, New York, 1979.
- [94] K.-P. Zeyer, M. Mangold, T. Obertopp, and E.D. Gilles. The iron-(iii)-catalyzed oxidation of ethanol by hydrogen peroxide: A thermokinetic oscillator. *J. Phys. Chem. A*, 103:5515–5522, 1999.
- [95] K.-P. Zeyer, S. Pushpavanam, and A. Kienle. Nonlinear behavior of reactor-separator networks: Influence of separator control structure. *Ind. Engng. Chem. Res.*, 42:3294–3303, 2003.
- [96] K.P. Zeyer, M. Mangold, T. Obertopp, and E.D. Gilles. An oscillating liquid-gas reaction with periodic evaporation: nonlinear analysis and experimental results. *Chem. Engng. Sci.*, 54:4845–4851, 1999.
- [97] A. Zheng, R.V. Mahajanam, and J.M. Douglas. Hierarchical Procedure for Plantwide Control System Synthesis. *AIChE J.*, 45:1255–1265, 1999.